

NACA RM L9H18a



3 9 FEB 1950

~~TOP SECRET~~
~~SECRET~~
65-21-112

NACA

RESEARCH MEMORANDUM

MAXIMUM LIFT AND LONGITUDINAL STABILITY

CHARACTERISTICS AT REYNOLDS NUMBERS UP TO 7.8×10^6 OF A
35° SWEEP FORWARD WING EQUIPPED WITH HIGH-LIFT AND STALL-
CONTROL DEVICES, FUSELAGE, AND HORIZONTAL TAIL

By Albert P. Martina and Owen J. Deters

Langley Aeronautical Laboratory
Langley Air Force Base, Va.

CLASSIFICATION CANCELLED

Authority J. A. C. ... Date 12/26/53
E. O. 12812
By R. F. 1640

CLASSIFIED DOCUMENT

This document contains classified information affecting the National Defense of the United States within the meaning of the Espionage Act, USC 50:31 and 32. Its transmission or the revelation of its contents in any manner to an unauthorized person is prohibited by law. Information so classified may be imparted only to persons in the military and naval services of the United States, appropriate civilian officers and employees of the Federal Government who have a legitimate interest therein, and to United States citizens of known loyalty and discretion who if necessary must be informed thereof.

NATIONAL ADVISORY COMMITTEE
FOR AERONAUTICS

WASHINGTON
February 9, 1950

RESTRICTED

UNCLASSIFIED

~~RESTRICTED~~
UNCLASSIFIED

NATIONAL ADVISORY COMMITTEE FOR AERONAUTICS

RESEARCH MEMORANDUM

MAXIMUM LIFT AND LONGITUDINAL STABILITY
CHARACTERISTICS AT REYNOLDS NUMBERS UP TO 7.8×10^6 OF A
35° SWEEPFORWARD WING EQUIPPED WITH HIGH-LIFT AND STALL-
CONTROL DEVICES, FUSELAGE, AND HORIZONTAL TAIL

By Albert P. Martina and Owen J. Deters

SUMMARY

An investigation was conducted in the Langley 19-foot pressure tunnel of a 35° sweptforward wing of aspect ratio 5.8, having a taper ratio of 0.39, and incorporating NACA 65-210 airfoil sections. Included in the investigation were three leading-edge stall-control devices, extensible-nose flaps, slats, and drooped-nose flaps; three high-lift devices, split, single, and double slotted trailing-edge flaps; midwing fuselage; and horizontal tail.

Extension of either the extensible-nose flaps or slats over the inboard 41 percent of the span prevented leading-edge separation over the portions of the span covered by the leading-edge devices and minimized the unstable pitching-moment changes of the basic wing in the high-lift range. Deflection of trailing-edge flaps caused undesirable changes in stability that were dependent on both the types and spanwise locations of flaps.

A midwing fuselage increased the basic wing maximum lift coefficient from 0.96 to 1.21.

Stability was obtained throughout the lift range with the tail located 0.11 semispan below the wing-chord plane extended for all model configurations investigated and with the tail located 0.11 semispan above the wing-chord plane with trailing-edge flaps neutral. Instability occurred in the high-lift range with the other tail positions investigated.

The maximum trimmed lift coefficient obtained with a stable tail arrangement and with nose and trailing-edge flaps deflected was 1.85.

~~RESTRICTED~~
UNCLASSIFIED

The lift-drag ratio at 0.85 of the maximum lift coefficient (approx. 110 percent of the stalling speed) for the configuration with flaps deflected was 7.3, while the maximum lift-drag ratio with flaps neutral was 14.6.

INTRODUCTION

Theory and experiment have shown that sweepback and sweepforward are parallel means of increasing the force divergence Mach number of wings employing subsonic airfoil sections. Low maximum lift coefficients are experienced in either case as a result of early tip stalling when the wing panels are swept back and root stalling when the wing panels are swept forward.

Numerous low-speed investigations on sweptback wings (for example, see references 1 to 3) have shown that the undesirable stalling characteristics could be improved by proper use of leading-edge stall-control devices with resultant increases in maximum lift coefficient and improvement of the longitudinal stability while flap effectiveness has been found to be low. Still other investigations (references 3 to 5) have shown that the stabilizing influence of the horizontal tail in the vicinity of maximum lift depends rather critically upon the vertical location of the tail.

In order to examine the aerodynamic characteristics of a swept-forward wing, an investigation was conducted in the Langley 19-foot pressure tunnel to determine:

- (1) The extent to which stalling could be controlled by various leading-edge stall-control devices
- (2) Effects of vertical location of the horizontal tail on the stability characteristics of the wing-fuselage combination
- (3) Aerodynamic characteristics of the wing with various high-lift devices
- (4) Lateral-control characteristics.

The results of (1), (2), and (3) are presented herein, while reference 6 presents the results of the lateral-control investigation.

COEFFICIENTS AND SYMBOLS

The data are referred to the wind axes with the origin at 25 percent of the mean aerodynamic chord and are reduced to standard NACA nondimensional coefficients defined as follows:

C_L	lift coefficient	$\left(\frac{\text{Lift}}{qS}\right)$
C_D	drag coefficient	$\left(\frac{\text{Drag}}{qS}\right)$
C_m	pitching-moment coefficient	$\left(\frac{\text{Pitching moment}}{qSc}\right)$
ΔC_L	increment in C_L	due to flap deflection
ΔC_m	increment in C_m	due to flap deflection
$C_{D_{pe}}$	effective profile-drag coefficient	$(C_D - C_{D_i})$
S	wing area,	square feet
q	dynamic pressure,	pounds per square foot $\left(\frac{\rho V^2}{2}\right)$
V	velocity,	feet per second
ρ	mass density of air,	slugs per cubic foot
R	Reynolds number	$\left(\frac{\rho V \bar{c}}{\mu}\right)$
μ	coefficient of viscosity,	slugs per foot second
M	Mach number	(V/a)
a	sonic velocity,	feet per second
\bar{c}	wing mean aerodynamic chord (M.A.C.),	feet $\left(\frac{2}{b} \int_0^{b/2} c^2 dy\right)$
c	local wing chord, parallel to plane of symmetry,	feet
c'	chord normal to reference line,	feet (see fig. 1)
y	lateral distance parallel to y-axis,	feet

b	span, feet
z	vertical distance from root-chord line extended to 0.25 point of tail mean aerodynamic chord, feet
α	angle of attack of root chord, degrees
i_t	incidence of tail chord plane with respect to wing root chord; positive in same sense as α , degrees
δ	flap deflection measured in planes normal to flap hinge line, degrees
$C_{m_{i_t}}$	tail-effectiveness parameter, increment in pitching-moment coefficient per degree change of tail incidence $\left(\frac{dC_m}{di_t}\right)$
ϵ	effective downwash angle, degrees
Λ	angle of sweep of 0.25c line, degrees

Subscripts:

max	maximum
t	tail
f	trailing-edge flap
n	leading-edge device
s	sinking
i	induced

MODEL AND APPARATUS

The wing had 35.3° sweepforward at the 0.25c line, an aspect ratio of 5.79, and incorporated NACA 65-210 airfoil sections in planes perpendicular to the 22.50-percent-chord line. The model was of solid steel and was provided with a smooth finish. Complete wing details are shown in figure 1.

Leading-edge stall-control devices investigated included the following:

- (1) Drooped-nose flaps
- (2) Retractable slats
- (3) Extensible-nose flaps

The effects of upper-surface fences in conjunction with each of the leading-edge devices were also included. Details of the leading-edge devices and upper-surface fences are given in figure 2; and, as shown therein, the drooped-nose flaps formed the airfoil contour in the neutral position. The retractable-slat assemblies, which were interchangeable with the drooped-nose flaps, were of machined dural, while the extensible-nose flaps were of steel.

Three types of trailing-edge flaps were investigated and are briefly summarized in the following table:

Type	c'_f/c'	δ_f (deg)
Split	0.20	60
Split	.55	28
Split	.77	23
Slotted	.25	45
Double slotted	.31	50

The positioning of the slotted and double slotted flaps which were nearly the two-dimensional optimums are shown in figure 3. Also shown therein are the spanwise variations, although only one span of each of the 0.55- and 0.77-chord split flaps was investigated.

Leading-edge roughness was simulated on the basic wing by means of No. 60 (approx. 0.01 in.) carborundum grains sprayed onto a freshly shellacked strip applied to the forward 8 percent of the upper and lower airfoil surfaces along the entire span.

Fuselage effects were determined for the midwing position. The fuselage, a body of revolution, had a maximum diameter of 12 percent of the wing span and was of laminated mahogany. The wing and wing with fuselage were mounted on the two-support system as shown in figure 4. The three-support system was used for tail-on tests with the third support located slightly behind the wing trailing edge on the fuselage underside. Figure 5 shows the location of the three support points and fuselage details in addition to those of the horizontal tail.

Vertical positioning of the horizontal tail was achieved by mounting the tail on a streamlined strut which could be moved in a vertical slot in the fuselage afterbody. In order to minimize the strut overhang from the under surface of the fuselage, two strut lengths were used, one for the two upper positions, and one of very short length for the two lower positions. The vertical location of the tail was measured from the root-chord line extended because of wing washout which was a result of deriving the wing from one having uniform twist. It can be seen, however, that the twist at the wing station corresponding to the tip station of the tail was such that the difference between the local wing-chord and root-chord lines extended was negligible (0.009 semispan). Ensuing discussion, therefore, will refer to the vertical distance as being measured from the wing-chord plane extended.

TESTS

The tests were conducted in the Langley 19-foot pressure tunnel with the air compressed to about $2\frac{1}{3}$ atmospheres. All tests were conducted at constant values of Reynolds number which for the majority of the tests was 6.5×10^6 (based on the wing M.A.C.). The resulting values of Mach number and dynamic pressure were approximately 0.19 and 120 pounds per square foot, respectively. Because of structural limitations, the tail-on tests were conducted at a Reynolds number of 5×10^6 . Scale effect was determined in the range of Reynolds numbers from 1.85×10^6 to 7.80×10^6 with corresponding Mach numbers ranging from 0.06 to 0.24.

Lift, drag, and pitching-moment measurements for each configuration were taken through an angle-of-attack range extending from about -4° through maximum lift in most cases. Stall progressions were determined by observing the behavior of wool tufts attached to the wing upper surface.

CORRECTIONS TO DATA

All data were corrected for support tares and interference and for air-stream misalignment. For the tests with the tail, the tail-support tare was taken as the difference in coefficients between corresponding runs with and without the tail support and was quite small.

Jet-boundary corrections were determined by means of a method adapted from reference 7 and were as follows:

$$\Delta\alpha = 0.674C_L$$

$$\Delta C_m = 0.00391C_L \text{ (without tail)}$$

$$\Delta C_m = 0.0215C_L \text{ (with tail)}$$

$$\Delta C_D = 0.0106C_L^2$$

All corrections were added to the data.

RESULTS AND DISCUSSION

The force characteristics of the wing and wing with fuselage are given in figures 6 and 7, respectively. Figure 8 presents the effects of several leading-edge devices and upper-surface fences on the wing characteristics, and figures 9 to 11 present the characteristics of the wing and fuselage in combination with various leading-edge devices, upper-surface fences, and trailing-edge split flaps. Some of the more important stall diagrams are presented in figures 12 to 14. Figure 15 summarizes the effects of the leading-edge devices, and figures 16 to 26 present and summarize the effects of trailing-edge flap deflection. Figures 27 to 29 include the effects of a horizontal tail. All data are summarized in tables I to IV.

Basic wing. - The wing became longitudinally unstable at lift coefficients well below $C_{L_{max}}$ as a result of extensive leading-edge separation which occurred over the root sections. At a Reynolds number of 6.5×10^6 , initial separation began at the leading edge of the root section at a lift coefficient of about 0.5, spread rearward, and fanned out at the trailing edge as shown in the stall diagrams

(fig. 12(a)). The value of $\frac{dC_m}{dC_L}$ (fig. 15) was zero at this point but broke sharply negative at a lift coefficient of 0.7.

At a lift coefficient of 0.8 separation occurred at the leading edge over the inner 60 percent of the semispan and quickly spread to the trailing edge with increasing C_L , as a result of which the pitching moment incurred an abrupt unstable trend. The separated area extended to about 85 percent of the semispan at $C_{L_{max}}$.

The over-all wing characteristics were similar to those reported in reference 8 for a thin sweptforward wing which, notwithstanding the differences in plan form and sweep, allows by means of pressure distributions an explanation of the changes in loading associated with this type of stall progression.

The stabilizing trend in pitching moment prior to extensive leading-edge separation is believed to have resulted from rearward shifts in the loadings over the root sections in a manner similar to reference 8.

Reference 8, furthermore, shows that with the occurrence of extensive laminar separation over the inboard sections, the section maximum lifts were generally established. Further increases to the angle of attack, therefore, generally resulted in lift losses over the inboard sections and an outboard shift in spanwise loading, while the over-all lift of the wing continued to increase somewhat. This redistributed loading, defined by a progressive loss of lift over the inboard sections and an increase over the outboard sections, produced the large forward movement of the aerodynamic center.

Increasing the Reynolds number normally promotes a greater extent of turbulent boundary layer which, by virtue of its greater resistance to separation, permits the attainment of progressively higher angles of attack, higher leading-edge peak pressures and, consequently, a higher $C_{L_{max}}$ before the occurrence of separation. It would be expected then that a more severe and sudden separation of flow would occur with an increase of Reynolds number. Such effects are indicated in figure 6, although beyond a Reynolds number of 5×10^6 no significant changes were noted to 7.8×10^6 .

The delay in leading-edge separation, as would be expected, postponed the sudden increase in drag as shown in figure 6(c) and reduced the loss in lift-curve slope so that $C_{L_{max}}$ occurred approximately 6° to 8° earlier at and above 5×10^6 than it did at the lowest Reynolds number. The maximum lift of 0.96, however, was essentially unchanged in the range of Reynolds numbers from 1.85×10^6 to 7.8×10^6 and was not well defined by sudden losses. The value of $C_{L_{max}}$ was of the same order of magnitude as that of other thin sweptforward wings.

The effects of leading-edge roughness were determined throughout the Reynolds number range and were similar to those shown in figure 6 for a Reynolds number of 7×10^6 .

The high minimum drag values (fig. 6(c)) are believed to have resulted from four pairs of brackets which supported the flap panels in the neutral position and which protruded about 5 percent of the airfoil thickness from the lower surface. The brackets were oblique to the air stream and are visible in figure 4 near the trailing edge on either side of each support. Sealing and fairing the gaps on the upper and lower surfaces around the trailing-edge-flap panels (fig. 1, section A-A) caused no discernible changes in the aerodynamic characteristics.

In the low-lift range, the wing aerodynamic center was located at 29.3 percent of the mean aerodynamic chord which compared with 28.5 percent indicated by reference 9 (based on the Weissinger theory) for this plan form with no camber.

The lift-curve slopes obtained by means of reference 9 and the experimental results of reference 10 (reduced in accordance with simple sweep theory) agreed within 2 percent of the experimental value of 0.064.

Wing with fuselage.- A midwing fuselage increased $C_{l_{max}}$ appreciably although it promoted premature local leading-edge separation. Maximum lift was increased 0.25 over the basic wing and occurred at 8° higher angle of attack. Leading-edge separation occurred approximately 2° earlier than it did on the basic wing as shown in the fuselage on-off stall diagrams of figure 12. Consequently, the unstable pitching-moment break and rapid drag increase also occurred earlier as seen in figure 7. Instability after pitching-moment reversal was greatly reduced by the fuselage.

The unfavorable effect of the fuselage in promoting premature local leading-edge separation can be qualitatively explained to some extent from several investigations of unswept wings. References 11 and 12 indicate theoretically and experimentally that the fuselage-induced upwash appreciably increases the span-load distributions on the wing-fuselage combination over those of the wing without fuselage, particularly at high angles of attack. The effect extends 1.5 body diameters outward from the fuselage (reference 12).

This induced loading in addition to the fuselage boundary layer would favor early separation. Although not included in this investigation, it is possible that the favorable effects of a high-wing fuselage might reduce or eliminate the adverse effects of a midwing combination with respect to separation.

The aerodynamic center was located at 9 percent of the mean aerodynamic chord which represented a forward shift of 20.3 percent from that of the basic wing. This large shift is in reasonable agreement with the effects indicated in reference 13 and arose from both the large body length ahead of the wing and the greatly reduced loading across the portion of the wing covered by the fuselage.

Effects of Leading-Edge Stall-Control Devices

Wing.- The stall diagrams of the wing with 41-percent-span nose flaps extended are presented in figure 13(a). As shown therein, the

extensible-nose flaps delayed leading-edge separation over the flapped portions of the span. Initial leading-edge separation began at the outboard ends of the flaps at a lift coefficient of about 0.8 ($\alpha \approx 12^\circ$), while rough flow was noted behind and inboard of the separated areas. The pitching moment simultaneously incurred an unstable trend, as seen in figure 8(b). A definite stabilizing trend in pitching moment occurred at $C_L = 1.17$ ($\alpha \approx 21^\circ$), although rough flow was noted over the root sections. There is no obvious explanation evident from the tuft diagrams for such a stabilizing trend. Stalling occurred over the root sections at nearly 22° although the pitching moment did not incur an unstable trend until a somewhat higher angle of attack was reached.

The addition of fences at the 32-percent-semispan station limited the inboard stall progression (see fig. 14(a)) and slightly alleviated the unstable trend which began at a C_L of 0.8. Stalling occurred over the root sections, however, and progressed outboard to the fences, thereby rendering them ineffective past a lift coefficient of approximately 1.15.

Tuft studies indicated that an increase in the spans of the extensible-nose flaps resulted in stalling over the root sections at lower angles of attack with a greater degree of instability noted thereafter. (See fig. 8(b).)

Characteristics with slats extended were nearly identical to those with nose-flaps extended. A slight difference was noted between the 41-percent-semispan devices in that a more pronounced unstable trend in pitching moment occurred with slats extended at a lift coefficient of 0.8. (See fig. 8(b).)

The leading-edge stall-control devices effected an appreciable extension of the lift curves. (See fig. 8(a).) The longest span devices reached lift-coefficient values of 1.4 with no indication that maximum lift was being approached at the highest angles of attack reached during the tests. The shortest span devices reached maximum lift values of 1.20. As would be expected from the nature of the flow characteristics, the drags in the high-lift range decreased with increasing spans of leading-edge devices. (See fig. 8(c).)

Wing-fuselage combination.- Extension of 41-percent-span nose flaps on the wing-fuselage combination prevented leading-edge separation in a manner similar to that on the wing alone. Local leading-edge separation behind the nose flaps at the wing-fuselage juncture occurred at a lift coefficient of 0.63 (fig. 13(b)) although it was of little consequence because of its localized character, and would be expected in view of the previously explained body interference.

As shown in figure 15, the drooped-nose flaps were the least effective in reducing the large variations in $\frac{dC_m}{dC_L}$ experienced by the wing-fuselage combination, mainly because the development of separation behind the flaps as indicated by tuft studies was not greatly delayed. The combination with slats extended was unstable at $C_{L_{max}}$ (fig. 10(a)) and instability was also indicated with nose flaps extended (see fig. 15), although this was not definitely established since maximum lift was not reached.

Upper-surface fences at 32 percent of the wing semispan on the wing-fuselage combination with leading-edge devices extended produced effects similar to those with fuselage off in that they delayed the inboard stall progression and thereby alleviated slightly the unstable trend in pitching moments (figs. 9(a), 10(a), and 11(a)) and reduced the variations of $\frac{dC_m}{dC_L}$ for all cases except with drooped-nose flaps (fig. 15).

A maximum lift coefficient of 1.36 was reached with $0.41\frac{b}{2}$ slats extended at $\alpha = 25^\circ$. Nearly identical values of lift coefficient were obtained at the same angle of attack with the $0.41\frac{b}{2}$ nose flaps extended and with 57.5-percent-span drooped-nose flaps deflected 30° , although maximum lift was not attained with the latter two devices.

The lift-drag ratios in the high-lift range were considerably improved by extension of $0.41\frac{b}{2}$ nose flaps (fig. 25).

Effects of Trailing-Edge Flaps

All the configurations with trailing-edge flaps deflected exhibited unstable variations of $\frac{dC_m}{dC_L}$ in the vicinity of maximum lift, although the unstable variations occurred somewhat below maximum lift with either single slotted or double slotted flaps deflected on the wing-fuselage combination with $0.41\frac{b}{2}$ nose flaps extended (fig. 21(a)).

Figure 22 presents the increments in pitching moments due to flap deflection at $\alpha = -0.7^\circ$ ($C_L = 0$ with flaps neutral). As seen therein, the ratios of the incremental pitching-moment coefficients to the incremental lift coefficients $\frac{\Delta C_m}{\Delta C_L}$ for given flap spans were nearly constant for the three types of flaps investigated and were a minimum for flaps extending from $0.37\frac{b}{2}$ to $0.97\frac{b}{2}$.

Addition of the fuselage (plus extension of nose flaps) reduced the negative pitching-moment increments due to trailing-edge flap deflection, which reductions in the cases of split flaps appeared to be greatest for inboard located flaps. Figure 23 presents the pitching-moment variations with angle of attack for various split flaps to illustrate the aforementioned effects. The nonlinearity of the fuselage-on curves at low angles is believed to arise from the effects of the nose flaps, although it can be seen that the pitching-moment increments are not greatly altered by the nonlinearities.

The influence of the fuselage on the incremental pitching moments of inboard located flaps is believed to result from the flap-induced angle of attack on the fuselage and the change caused by the fuselage in the carry-over load between the inboard ends of the flaps. On the other hand, the influence of the fuselage on the outboard flaps was small.

Thin airfoil theory indicates that ΔC_m may be reduced by increasing the flap-wing-chord ratio, although for swept wings it is a much less effective means than varying the spanwise locations of the flaps. The effects of increasing the split-flap chords for the 43-percent-span flaps located from 37 to 80 percent of the semispan are shown in figure 17(a). It can be seen that the 55-percent-chord flaps were nearly self trimming, although little or no gain in maximum lift coefficient over that of basic wing was experienced.

The lift increments both in the linear range and at $C_{L_{max}}$ were nearly proportional to flap span as shown in figure 24, with those due to double slotted flaps about double those of split flaps. It is to be noted that figure 24 takes no account of spanwise-flap location so that only trends are indicated. The modified increments of a similarly flapped unswept wing (reference 10) are also shown in figure 24.

The increments of reference 10 were modified as follows:

$$(\Delta C_L)_\Lambda = (\Delta C_L)_{\Lambda=0} \cos^2 \Lambda \frac{\left(\frac{A}{A+2}\right)_\Lambda}{\left(\frac{A}{A+2}\right)_{\Lambda=0}}$$

Some agreement is shown. Addition of the fuselage and extension of leading-edge devices did not alter the lift increments in most cases.

It is indicated in figure 25 that high trimmed lift coefficients can be obtained with relatively high values of the lift-drag ratios. The differences in gliding speeds at minimum sinking speeds for the

various flaps were not over 10 percent, as shown by the glide sinking-speed envelope superimposed on figure 25; but deflection of either full-span single or double slotted flaps effected reductions in minimum sinking speeds in the order of 30 percent over those with either full-span split or partial-span double slotted flaps. Obviously, the lift-drag ratios omit the drag of the tail, landing gear, and parasite items which, if included, would reduce the values presented therein but would not alter the comparative trends.

An interesting illustration of the effects of sweep on the effective profile drag coefficient $C_{D_{pe}}$, for various flap arrangements is given in figure 26. The unswept values were obtained from the data of reference 10 with the best possible estimates of induced drag used in both cases. The induced drags for the sweptforward wing were calculated by means of reference 9 and were increased 10 percent as an estimate of the effects of the flap cut-out at the plane of symmetry. Substantial reductions ranging from 36 percent for the split flaps to approximately 50 percent for the single slotted flaps were shown and were at least as great as indicated by the cosine of the sweep angle, squared.

Effects of Horizontal Tail

Linear lift range.- In the range of tail positions investigated, -0.11 to 0.36 semispans from the wing-chord plane extended, the greatest stability in the linear lift range was generally obtained with the tail located at the higher positions as shown by the neutral points of figure 28. It can also be seen that deflection of trailing-edge flaps considerably reduced the stability of most configurations. The values of $\frac{d\epsilon}{d\alpha}$ are tabulated as follows:

Flaps and spans (percent semispan)		Tail positions $\frac{z}{b/2}$			
Nose	Trailing edge	0.361	0.252	0.114	-0.107
Neutral	Neutral	0.38	0.42	0.50	0.56
41	Neutral	.29	.32	.57	.70
41	50 double slotted	.58	.69	.80	.78
41	87 double slotted	.50	.47	.45	.79
41	87 single slotted	.48	.55	.68	.85

These values were constant throughout most of the linear lift-coefficient range except at the lowest tail positions. The values were obtained from the effective downwash calculated from pitching moments, tail on and off.

The values of tail-effectiveness parameter $C_{m_{it}}$ (obtained from two tail incidences) were constant in the linear lift-coefficient range for all tail positions except the lowest, at which slight increases with angle of attack were generally noted (figs. 27(a) and 27(b)). In the cases with trailing-edge flaps neutral, it is possible that interference from supports and support fairings would produce such effects. The tail effectiveness based on the isolated tail lift-curve slope of 0.0495 per degree (which was constant to $C_{L_{max}}$ of the tail and reported in reference 4) agreed with the experimental value of -0.0421 per degree obtained for the highest tail position with all flaps neutral. The values of tail effectiveness for all positions above the chord plane were from 10 to 15 percent lower with nose flaps extended than with nose flaps neutral (fig. 27(b)) and are believed to have resulted from consistent errors in measuring tail incidence.

Nonlinear lift range.- Large changes in stability were experienced at nearly all tail positions as evidenced by the pitching-moment variations given in figure 27. No changes were indicated at the $-0.11\frac{b}{2}$ position with nose flaps deflected and rather small changes at the $0.11\frac{b}{2}$ position with full-span single slotted flaps deflected. The stability changes with flaps neutral were stabilizing and occurred in the lower part of this range (moderate-lift range) at all positions below the $0.25\frac{b}{2}$ position, at which a destabilizing change occurred at a higher angle of attack in what may be considered the high-lift range. Deflection of nose flaps caused a stabilizing change to occur at the $0.11\frac{b}{2}$ position in the moderate-lift range, while destabilizing changes were noted for higher positions in the high-lift range.

With trailing-edge flaps deflected, all of the changes in stability were stabilizing in the moderate-lift range, although most of the trends subsequently reversed to unstable in the high-lift range.

In the cases with flaps neutral, abrupt losses in tail effectiveness were experienced at all positions above the chord plane simultaneously with the stability changes (fig. 27(a)). The losses resulted from the entry of the tail into the wakes emanating from the stalled root sections of the wing which were directly ahead of the tail. Consequently, it is believed that buffeting would occur and thus render operation in this region quite unlikely. While little change in tail

effectiveness occurred at the lowest position $(-0.11\frac{b}{2})$, the change in stability is attributed to the tail-off characteristics. The rather abrupt increases in tail effectiveness at the higher angles of attack indicate that the lower edges of the wakes moved up quite rapidly. This movement is borne out in reference 14, which shows that the lower edge of the wake at the plane of symmetry moved from below the chord plane at low angles of attack to between 0.15 and 0.25 semispan above at high angles.

Since extension of nose flaps prevented leading-edge separation, the wake dimensions were obviously reduced as indicated by the smaller losses in tail effectiveness at the higher positions and the nearly complete elimination of the losses at the lower positions (fig. 27(b)). Changes in $\frac{d\epsilon}{d\alpha}$ were also reduced at the lowest position and hence the stability changes were also minimized. The $0.11\frac{b}{2}$ position exhibited a strong stabilizing tendency ($\alpha \approx 12^\circ$, fig. 27(b)) and was believed to result from the loss in $\frac{d\epsilon}{d\alpha}$ arising from the onset of wing root stall.

The configurations with the tail located above $0.11\frac{b}{2}$ from the chord plane became unstable in the vicinity of 14° angle of attack. It is not certain whether or not sufficient stall warning would develop to preclude the possibility of operating in the unstable range. Abrupt and severe losses in tail effectiveness and rather large losses in $\frac{d\epsilon}{d\alpha}$ were experienced at all tail positions concurrent with the stability changes with trailing-edge flaps deflected. The losses in tail effectiveness eventually predominated, causing the subsequent unstable trends. It is believed, however, that the likelihood of buffeting would make operation into or past the stable regions unlikely.

From the foregoing considerations it appears that reasonable values of lift coefficient can be obtained with a tail-stabilized configuration. The orders of magnitude of trimmed lift coefficients believed to be attainable on the wing fuselage with $0.41\frac{b}{2}$ nose flaps extended were taken from figure 25 and are tabulated as follows, together with the L/D values:

Flaps	C_L	L/D
Full-span split	1.4	5.1
Full-span single slotted	1.5	6.6
Partial-span double slotted	1.5	4.8
Full-span double slotted	1.7	6.2

The lift coefficients correspond approximately to the regions where large stability changes occurred as indicated by the abrupt variations in the calculated values of the horizontal tail incidence required for trim (fig. 29), except, the value given for split flaps which was based on an estimate inasmuch as no tail tests were conducted with split flaps deflected. The maximum trimmed lift coefficient obtained with a stable tail arrangement and with nose and full-span double slotted flaps deflected was 1.85. The lift-drag ratio for this configuration was 7.3 at $0.85C_{L_{max}}$ (approx. 110 percent of the stalling speed), while the maximum lift-drag ratio with flaps neutral was 14.6.

CONCLUDING REMARKS

A wind-tunnel investigation at Reynolds numbers ranging from 1.85×10^6 to 7.8×10^6 of a 35° sweptforward wing of aspect ratio 5.79 including high-lift and stall-control devices, midwing fuselage, and horizontal tail indicated the following results:

1. The wing became longitudinally unstable at lift coefficients well below maximum lift as a result of extensive leading-edge separation which occurred over the root sections. The maximum lift coefficient of 0.96 was essentially unchanged throughout the Reynolds number range.

2. A midwing fuselage increased the basic-wing maximum lift coefficient to 1.21, caused premature local leading-edge separation, and reduced the magnitudes of the basic-wing stability changes. The combined effects of adding the fuselage and extensible nose flaps in the linear lift range were to decrease the negative pitching-moment increments due to trailing-edge-flap deflection.

3. Extension of either the extensible nose flaps or slats over the inboard 41 percent of the span prevented leading-edge separation over the portions of the span covered by the leading-edge devices and minimized the unstable pitching-moment trends of the basic wing in the high-lift range. Unstable pitching-moment variations were indicated near maximum lift, however, on the wing-fuselage combination. The shortest span devices were found to be the most satisfactory from the stability standpoint in the range investigated from 41 to 75 percent of the semispan. Drooped-nose flaps were the least effective of the three leading-edge devices.

4. Deflection of trailing-edge flaps on the wing-fuselage combination caused undesirable changes in stability which were dependent on both the types and locations of flaps. High lift coefficients appear to be attainable with relatively high values of the lift-drag ratios.

5. Stability was obtained throughout the lift range with the tail located 0.11 semispan below the wing chord plane extended for all model configurations investigated and with the tail located 0.11 semispan above the wing chord plane with trailing-edge flaps neutral. Stability was obtained to moderately high lift coefficients for all other positions up to 0.36 semispan above the wing-chord plane extended with instability indicated at high lift coefficients. It is believed, however, in the majority of these cases, that the probability of tail buffeting would provide adequate stall warning and thus render operation into the unstable range unlikely.

6. The orders of magnitude of trimmed lift coefficients believed to be attainable on the wing-fuselage combination with 41-percent-span nose flaps were as follows: 1.5 with either full-span single slotted or partial-span double slotted flaps and 1.7 with full-span double slotted flaps. Lift-drag ratios ranging from 4.8 to 6.6 existed at these lift coefficients. The maximum trimmed lift coefficient obtained with a stable tail arrangement and with nose and trailing-edge flaps deflected was 1.85. The lift-drag ratio for this configuration was 7.3 at $0.85C_{L_{max}}$ (approx. 110 percent of the stalling speed), while the maximum lift-drag ratio with flaps neutral was 14.6.

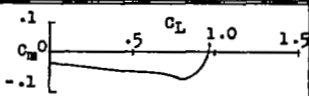
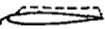
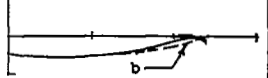
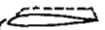
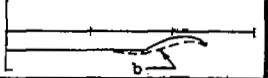
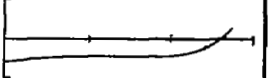
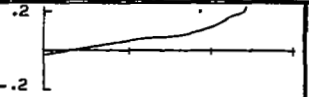
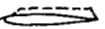
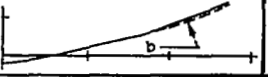
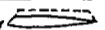
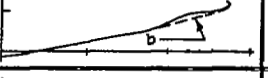
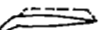
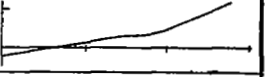
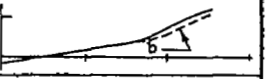
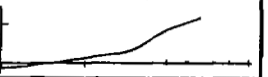
Langley Aeronautical Laboratory
National Advisory Committee for Aeronautics
Langley Air Force Base, Va.

REFERENCES

1. Conner, D. William, and Neely, Robert H.: Effects of a Fuselage and Various High-Lift and Stall-Control Flaps on Aerodynamic Characteristics in Pitch of an NACA 64-Series 40° Swept-Back Wing. NACA RM L6L27, 1947.
2. Koven, William, and Graham, Robert R.: Wind-Tunnel Investigation of High-Lift and Stall-Control Devices on a 37° Sweptback Wing of Aspect Ratio 6 at High Reynolds Numbers. NACA RM L8D29, 1948.
3. Foster, Gerald V., and Fitzpatrick, James E.: Longitudinal-Stability Investigation of High-Lift and Stall-Control Devices on a 52° Sweptback Wing with and without Fuselage and Horizontal Tail at a Reynolds Number of 6.8×10^6 . NACA RM L8I08, 1948.
4. Spooner, Stanley H., and Martina, Albert P.: Longitudinal Stability Characteristics of a 42° Sweptback Wing and Tail Combination at a Reynolds Number of 6.8×10^6 . NACA RM L8E12, 1948.
5. Woods, Robert L., and Spooner, Stanley H.: Effects of High-Lift and Stall-Control Devices, Fuselage, and Horizontal Tail on a Wing Swept Back 42° at the Leading Edge and Having Symmetrical Circular-Arc Airfoil Sections at a Reynolds Number of 6.9×10^6 . NACA RM L9B11, 1949.
6. Graham, Robert R.: Lateral-Control Investigation at a Reynolds Number of 5,300,000 of a Wing of Aspect Ratio 5.8 and Swept-forward 32° at the Leading Edge. NACA RM L9H18, 1949.
7. Eisenstadt, Bertram J.: Boundary-Induced Upwash for Yawed and Swept-Back Wings in Closed Circular Wind Tunnels. NACA TN 1265, 1947.
8. McCormack, Gerald M., and Cook, Woodrow L.: A Study of Stall Phenomena on a 45° Swept-Forward Wing. NACA TN 1797, 1949.
9. DeYoung, John: Theoretical Additional Span Loading Characteristics of Wings with Arbitrary Sweep, Aspect Ratio, and Taper Ratio. NACA TN 1491, 1947.
10. Sivells, James C., and Spooner, Stanley H.: Investigation in the Langley 19-Foot Pressure Tunnel of Two Wings of NACA 65-210 and 64-210 Airfoil Sections with Various Type Flaps. NACA TN 1579, 1948.

11. Multhopp, H.: Aerodynamics of the Fuselage. NACA TN 1036, 1942.
12. Lochmann: Druckverteilungsmessungen an einem Mitteldecker bei symmetrischer Anströmung. FB Nr. 1710/2, Deutsche Luftfahrtforschung (Braunschweig), 1943.
13. Schlichting, H.: Calculation of the Influence of a Body on the Position of the Aerodynamic Centre of Aircraft with Sweptback Wings. TN No. Aero. 1879, British R.A.E., March 1947.
14. Hoggard, H. Page, Jr., and Hagerman, John R.: Downwash and Wake behind Untapered Wings of Various Aspect Ratios and Angles of Sweep. NACA TN 1703, 1948.

TABLE I
SUMMARY OF 35° SWEEPFORWARD WING CHARACTERISTICS WITH VARIOUS
LEADING-EDGE DEVICES EXTENDED. $R = 6.5 \times 10^6$.

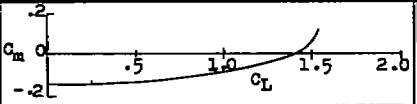
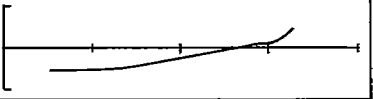
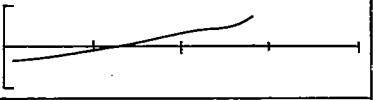
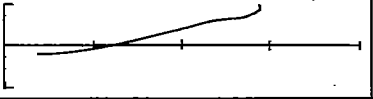
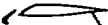
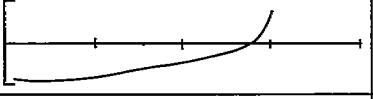
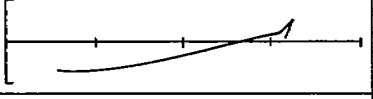
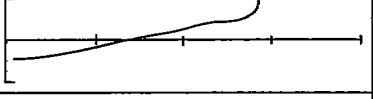
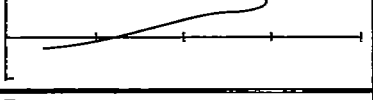
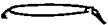
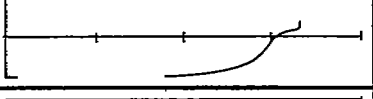
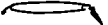
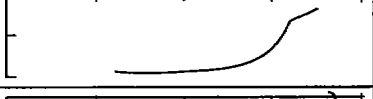
Device	b_D/b	C_{Lmax}	α at C_{Lmax}	ΔC_m at $\alpha = 0^\circ$	L/D at $.85 C_{Lmax}$	$C_m - C_L$	Fig.
 Basic wing	—	0.96	18.7	—	8.15		
 Extensible nose flaps	0.41	1.20	24.8	-.018	5.83		8
	0.58	1.28 ^a	28.9	-.028	7.21		
	0.75	1.40 ^a	29.0	-.045	8.82		
 Retractable slats	0.41	1.20	25.9	-.018	5.83		9
	0.58	1.26 ^a	26.1	-.024	7.09		
	0.75	1.33 ^a	25.9	-.031	8.55		
Wing-Fuselage Combination							
 Flaps Neutral	—	1.21	26.0	—	3.86		9
 Nose flaps	0.41	1.35 ^a	26.0	-.011	3.66		10
 Slats	0.41	1.36	25.0	-.017	3.86		11
 Drooped nose flaps	0.58 $\delta_n = 30^\circ$	1.37 ^a	26.0	-.020	3.94		11
	0.41 $\delta_n = 30^\circ$	1.28 ^a	26.1	-.016	3.70		
	0.41 $\delta_n = 40^\circ$	1.20 ^a	26.0	-.005	3.58		

^a C_{Lmax} not obtained at highest α

^b fences at $0.52b/2$



TABLE II
 SUMMARY OF 35° SWEEPFORWARD WING-FUSELAGE CHARACTERISTICS WITH 41-PERCENT-SEMI-SPAN
 LEADING-EDGE DEVICES AND VARIOUS TRAILING-EDGE FLAPS. $R = 6.5 \times 10^6$.

L. E. Device	T. E. Flaps	Span c_r/b	Location percent $b/2$	C_{Lmax}^a	α at C_{Lmax}	ΔC_m at $\alpha = 0^\circ$	L/D at $0.85 C_{Lmax}$	$C_m - C_L$	Fig.
 Nose flaps	0.20c' split	50	10 - 60	1.54 ^b	23.2	-.110	4.75		9
		87	10 - 97	1.61	18.2	-.068	5.27		
		43	37 - 80	1.39 ^b	20.0	-.020	5.37		
		60	37 - 97	1.46	21.6	.012	5.41		
 Slats	0.20c' split	50	10 - 60	1.51 ^b	23.2	-.142	5.29		10
		87	10 - 97	1.60	18.7	-.094	5.52		
		43	37 - 80	1.42	21.0	-.026	5.27		
		60	37 - 97	1.46	18.8	.016	5.16		
 Nose flaps	0.25c' single slotted	87	10 - 97	1.67	19	-.158	8.25		21
 Nose flaps	0.31c' double slotted	50	10 - 60	1.77 ^b	21.3	-.353	5.68		
		87	10 - 97	1.86	17.0	-.242	7.73		

^b C_{Lmax} not attained at highest α

^a untrimmed



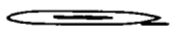
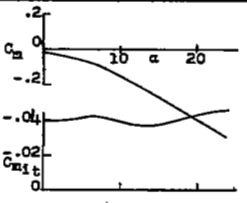
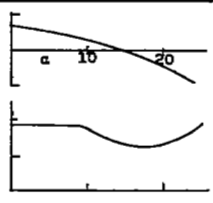
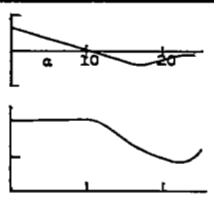
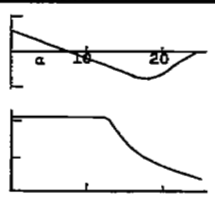
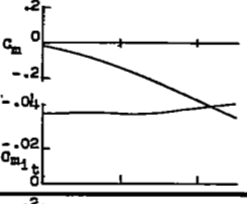
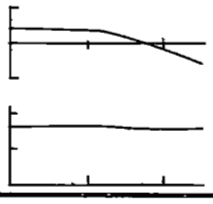
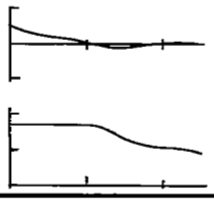
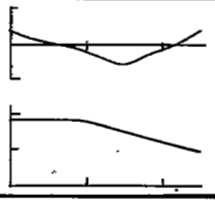
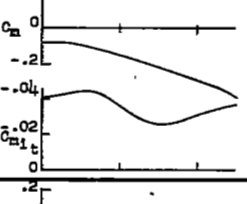
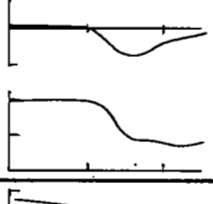
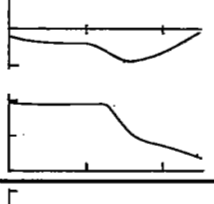
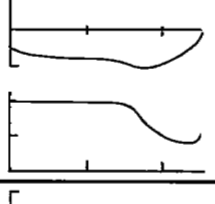
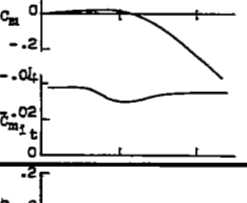
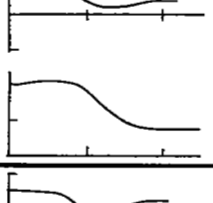
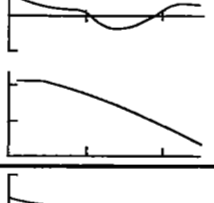
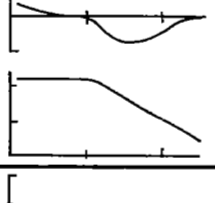
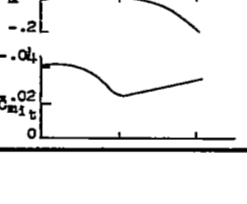
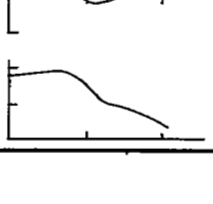
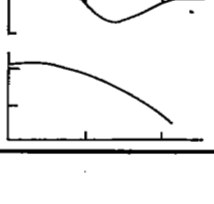
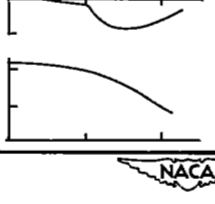
TABLE III
SUMMARY OF CHARACTERISTICS OF 35° SWEEPFORWARD WING WITH
VARIOUS TRAILING-EDGE FLAPS DEFLECTED

T.E. flap location (b/2)		0.10 to 0.60			0.10 to 0.97			0.37 to 0.80			0.37 to 0.97			Fig.
Flaps		a $C_{L_{max}}$	α at $C_{L_{max}}$	ΔC_m at $\alpha = 0$	a $C_{L_{max}}$	α at $C_{L_{max}}$	ΔC_m at $\alpha = 0$	a $C_{L_{max}}$	α at $C_{L_{max}}$	ΔC_m at $\alpha = 0$	a $C_{L_{max}}$	α at $C_{L_{max}}$	ΔC_m at $\alpha = 0$	
Trailing edge	Nose													
0.20c' split	Neutral	1.20	18	-.204	1.31	18	-.155	1.10	17	-.035	1.11	18	-.002	16
0.55c' split		--	--	---	--	--	---	1.01	15	-.003	--	--	---	17
0.77c' split		--	--	---	--	--	---	.98	16	.008	--	--	---	17
Single-slotted		1.24	18	-.287	1.38	9	-.193	1.14	10	-.053	1.20	8.9	.005	18
Double-slotted		1.36	18	-.366	1.57	7	-.263	1.20	10	-.067	1.32	8	.004	19
0.20c' split	0.75b/2	1.39	15.0	-.082	1.59	14.2	-.062	1.41	16.0	-.022	1.37	17.0	.037	20
Single-slotted		--	--	---	--	--	---	1.49	15.2	-.031	--	--	---	20
Double-slotted		--	--	---	--	--	---	1.63	15.2	-.022	--	--	---	20

^a untrimmed



TABLE IV
 SUMMARY OF CHARACTERISTICS WITH HORIZONTAL TAIL LOCATED
 AT SEVERAL VERTICAL POSITIONS. $R = 5.0 \times 10^6$

Tail Pos. $\frac{x}{b/2}$		-0.107	0.114	0.252	0.361	Ref.
Flaps						Fig.
Nose	T.E.					
Neutral	Neutral					27a
0.41b/2	Neutral					27b
0.41b/2	Partial span double-slotted					27c
0.41b/2	Full-span single-slotted					27d
0.41b/2	Full-span double-slotted					27e



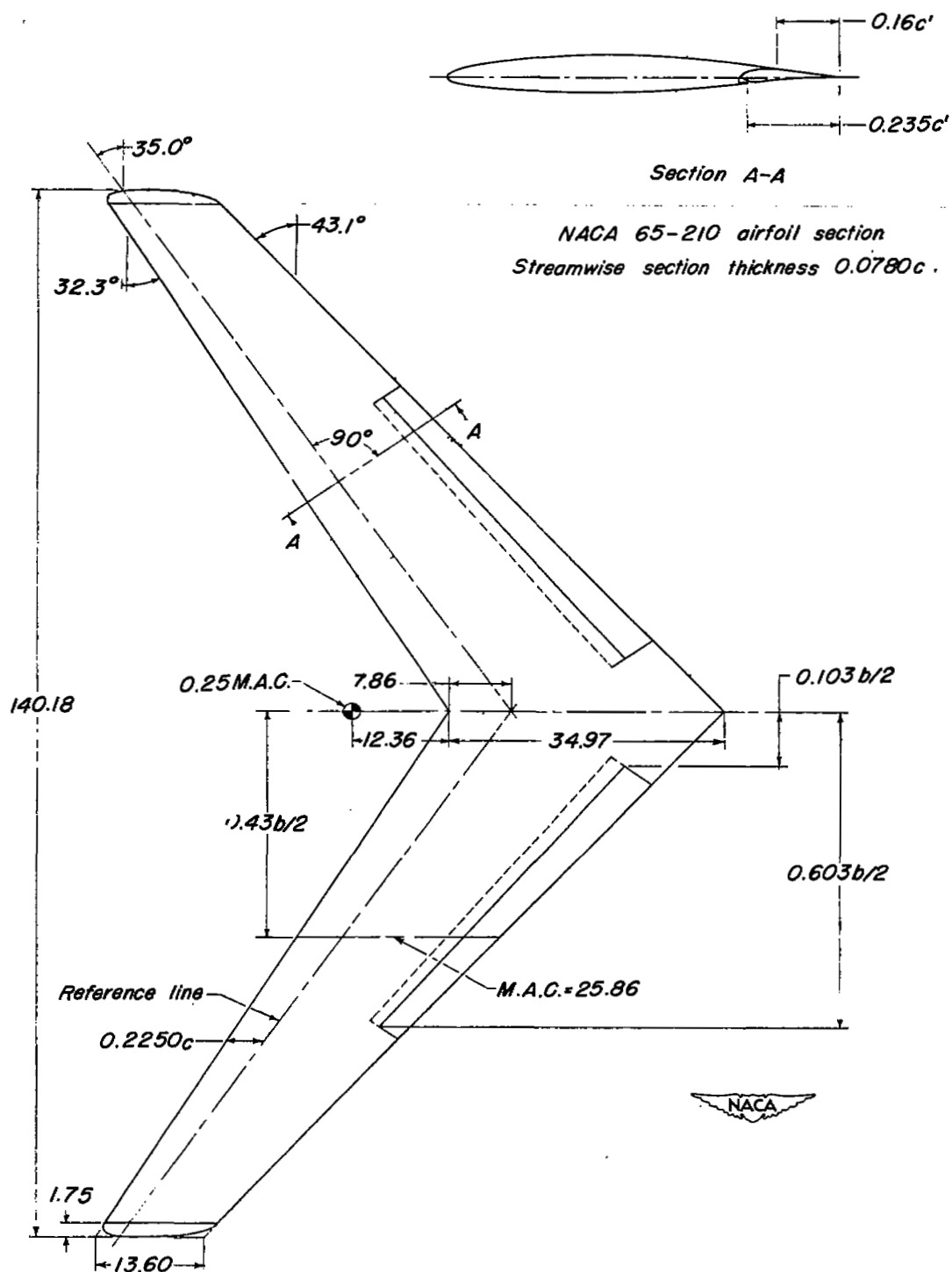


Figure 1.- Basic wing details. Aspect ratio, 5.79; taper ratio, 0.389; area, 23.58 square feet; washout, 1.8°; no dihedral at reference line. Linear dimensions in inches unless noted.

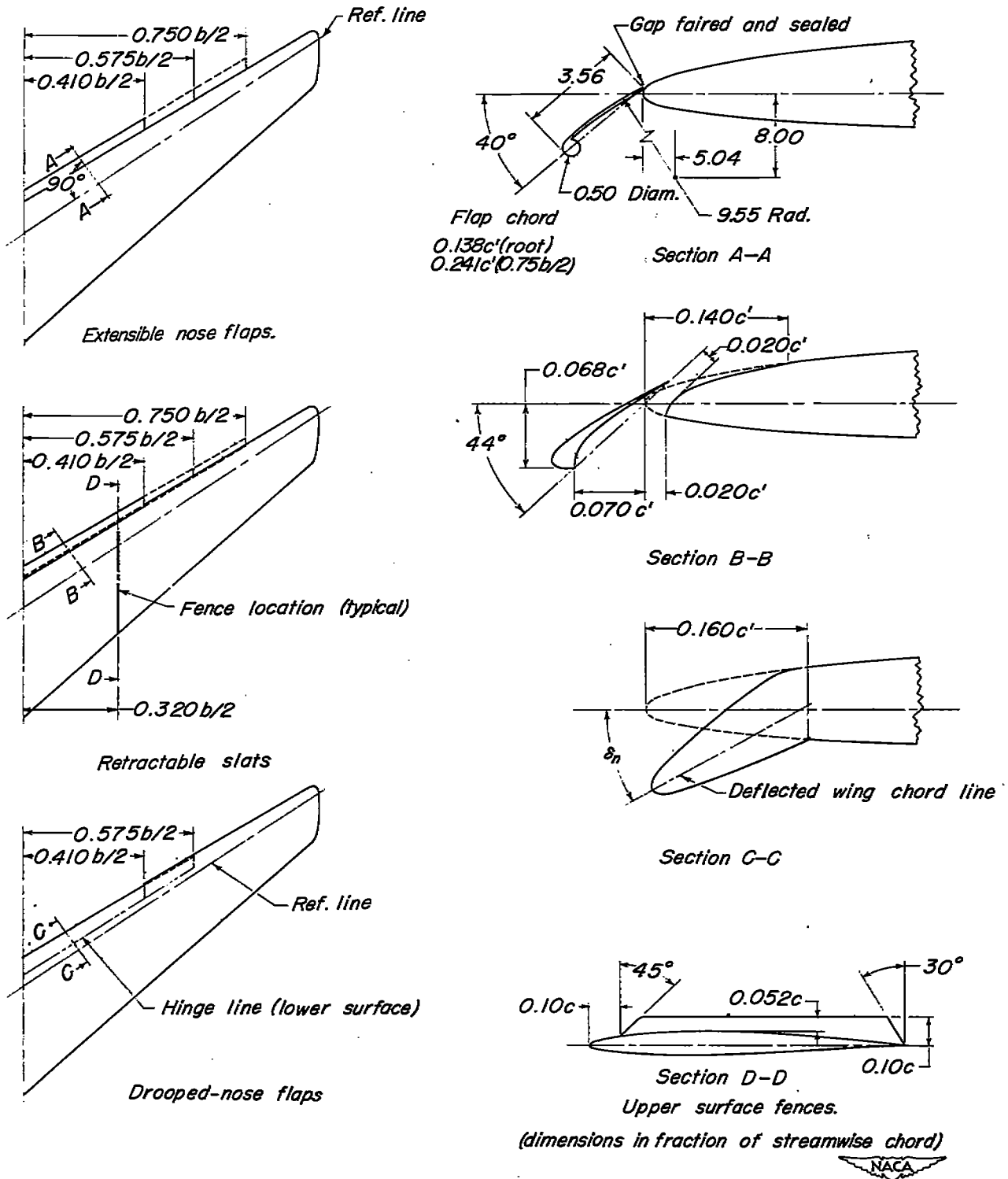
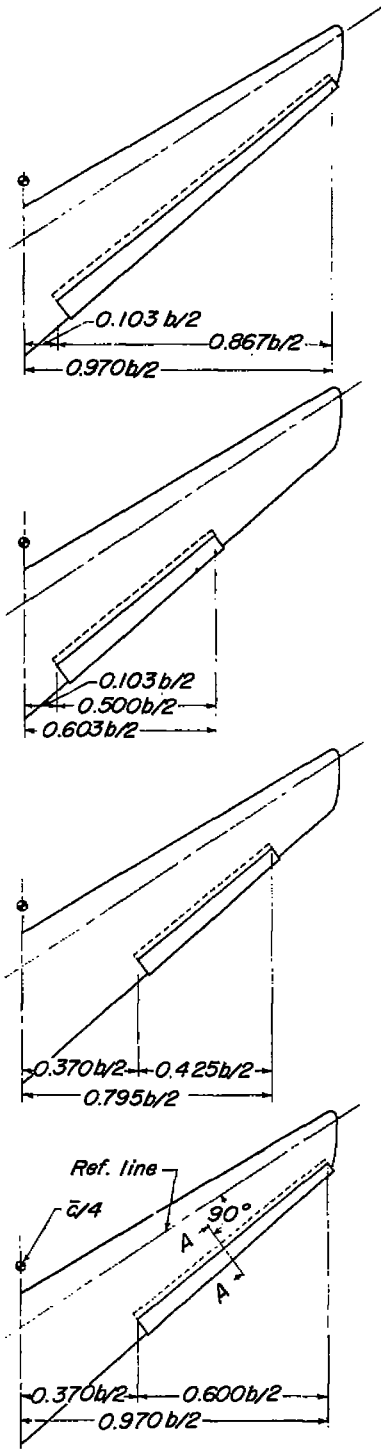
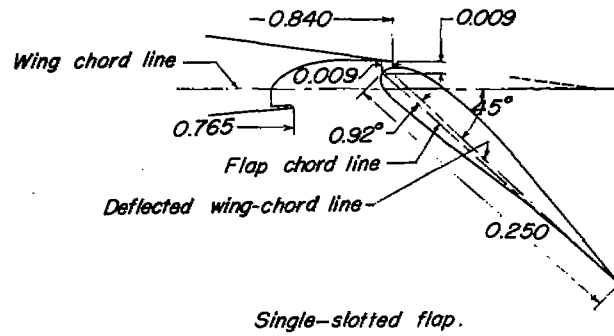
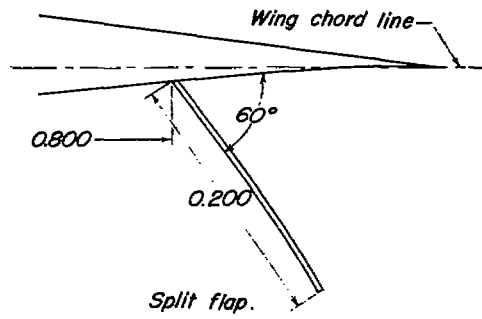


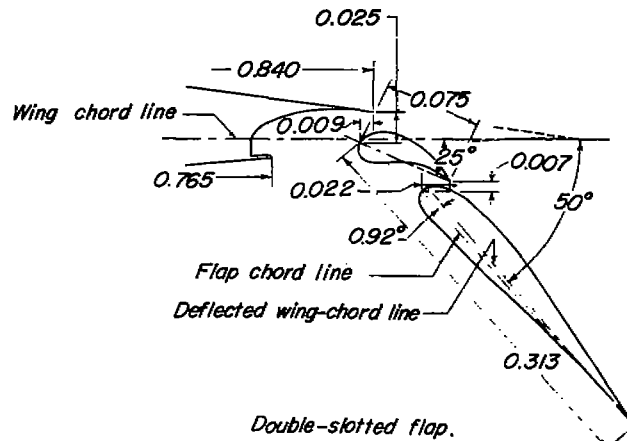
Figure 2.- Details of leading-edge stall-control devices and upper-surface fences. Linear dimensions in inches unless noted.



Spans and spanwise locations of trailing-edge flaps. (Single-slotted flaps shown)



Single-slotted flap.



Double-slotted flap.

Typical sections A-A through flaps. Dimensions in fraction of chord normal to reference line.



Figure 3.- Trailing-edge flap details.

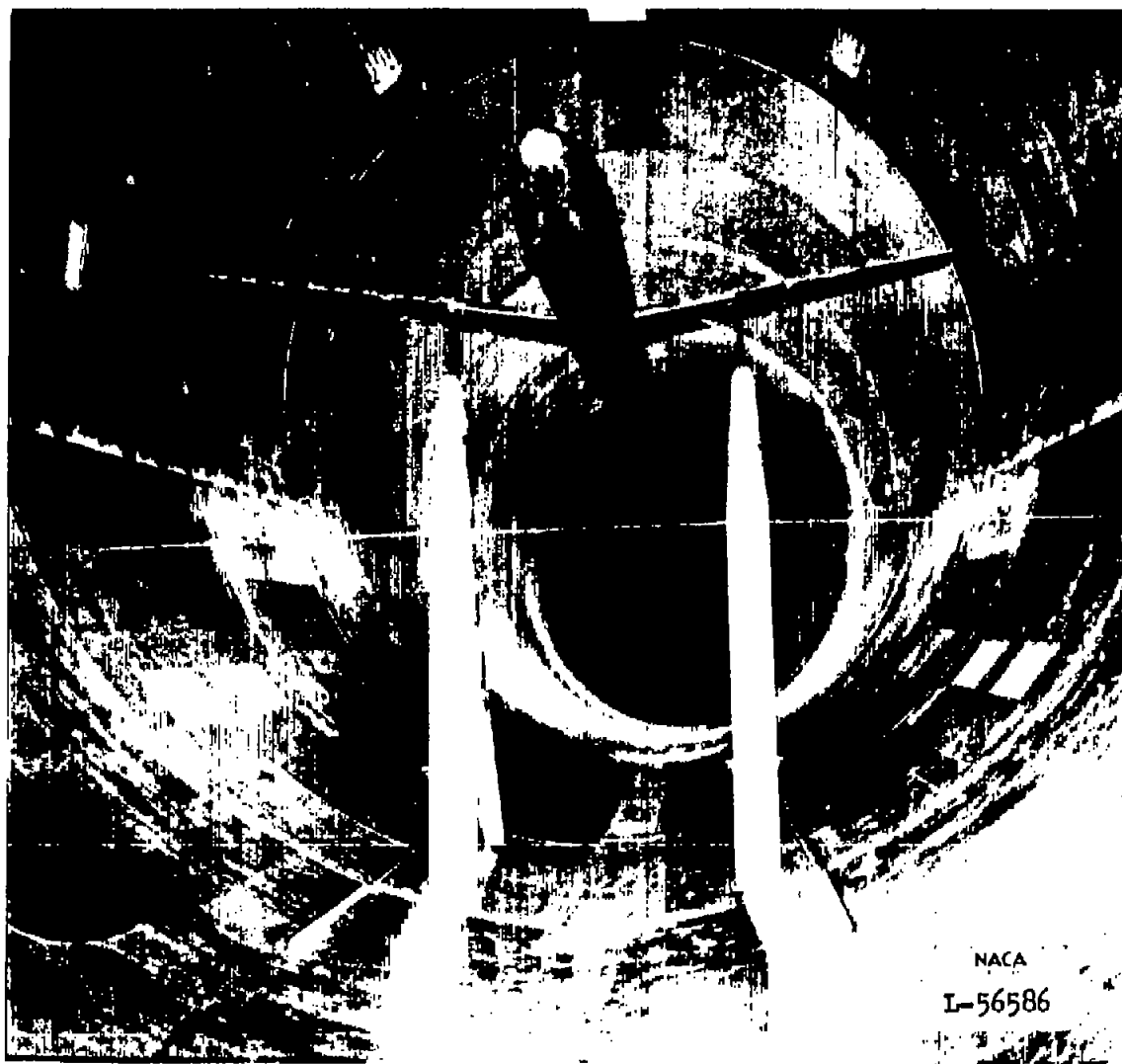
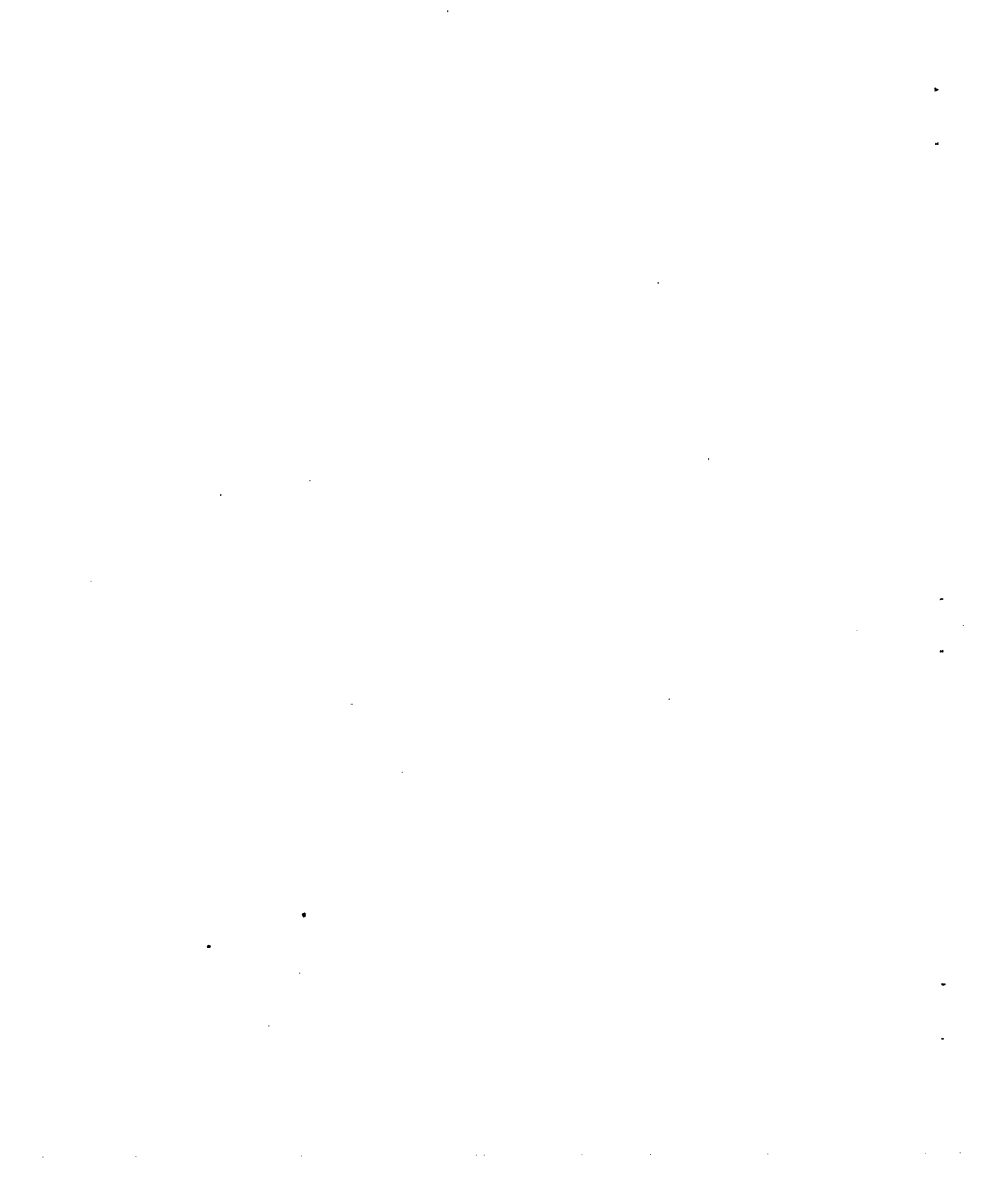


Figure 4.- The 35° sweptforward wing with fuselage as tested in the Langley 19-foot pressure tunnel.



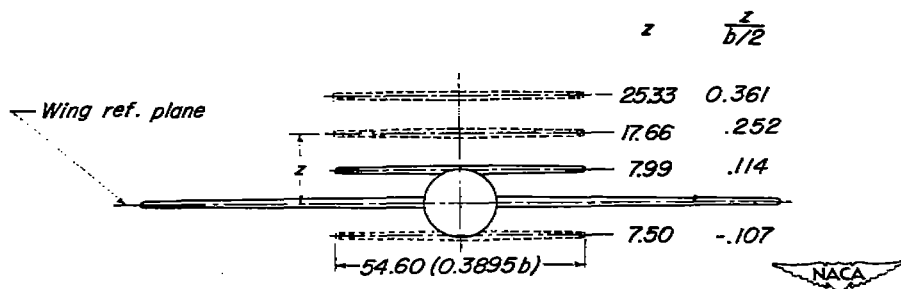
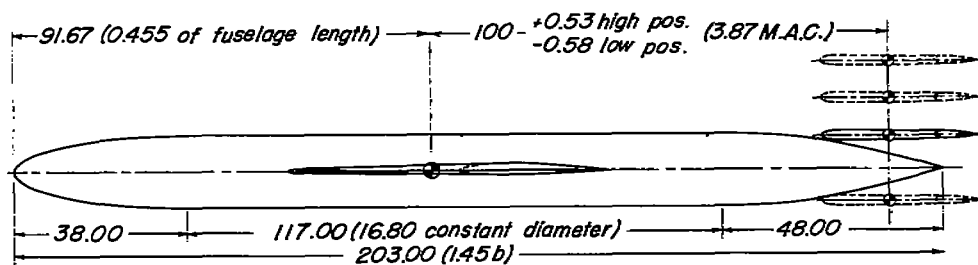
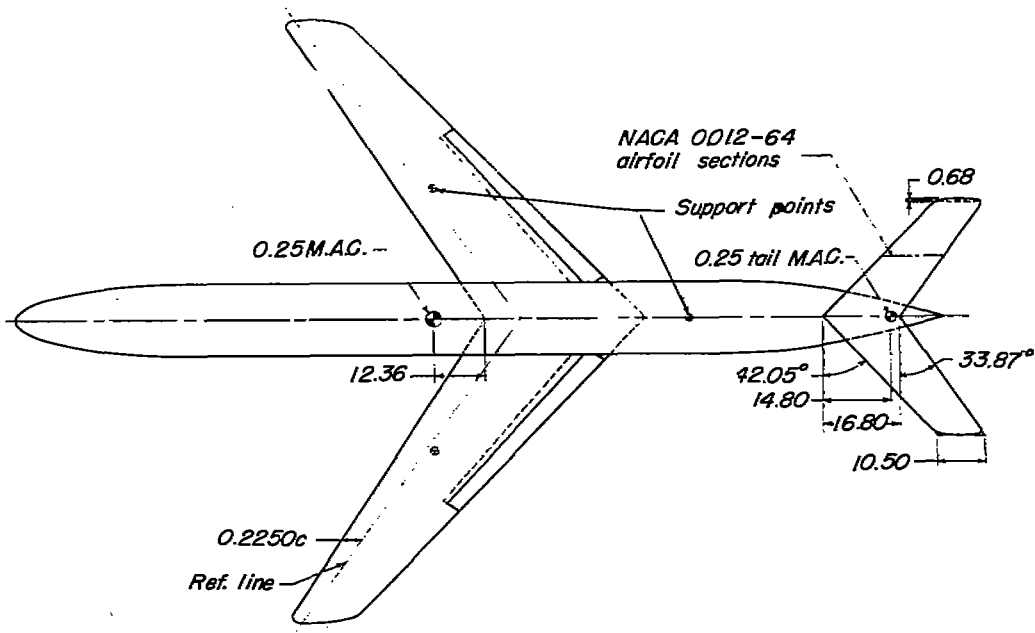
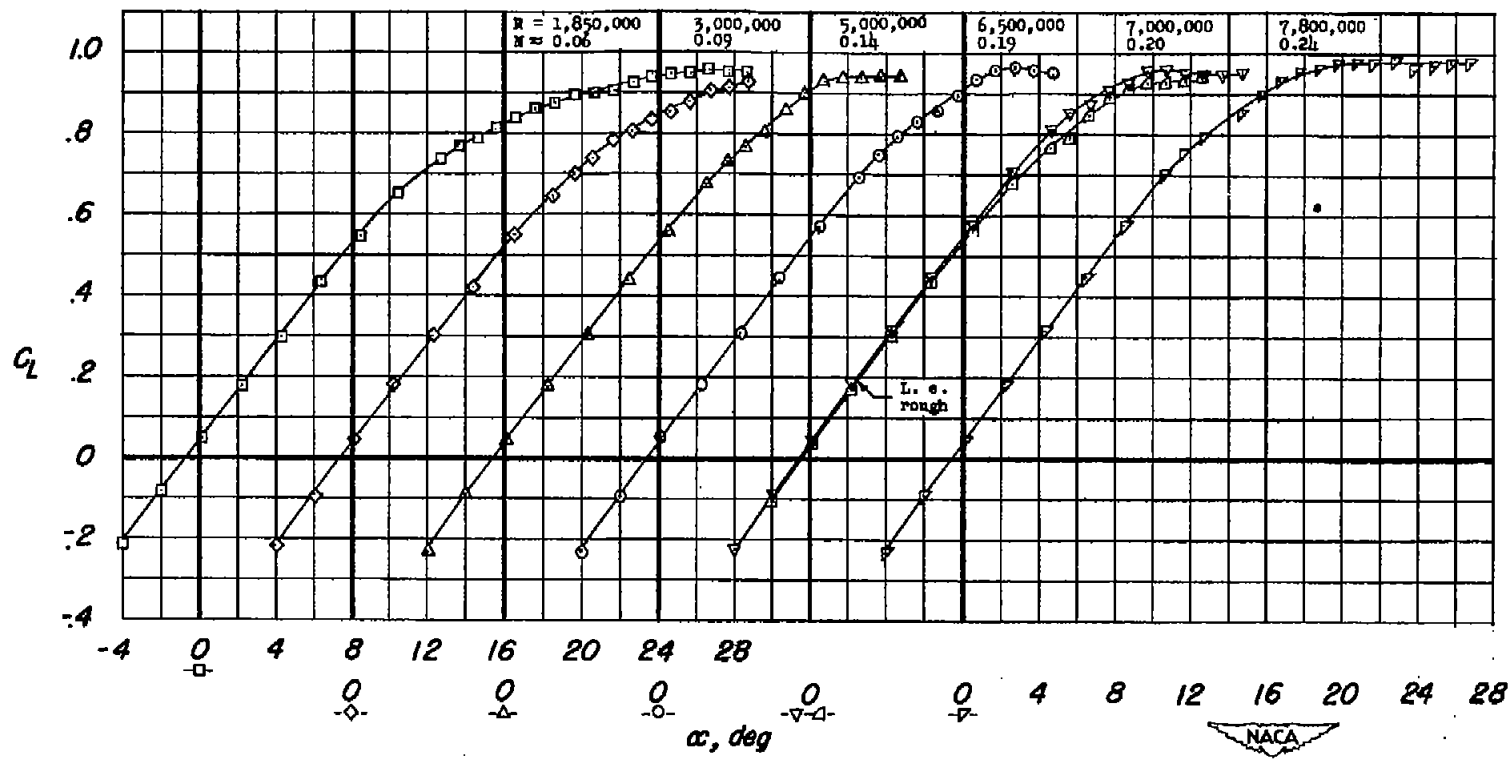
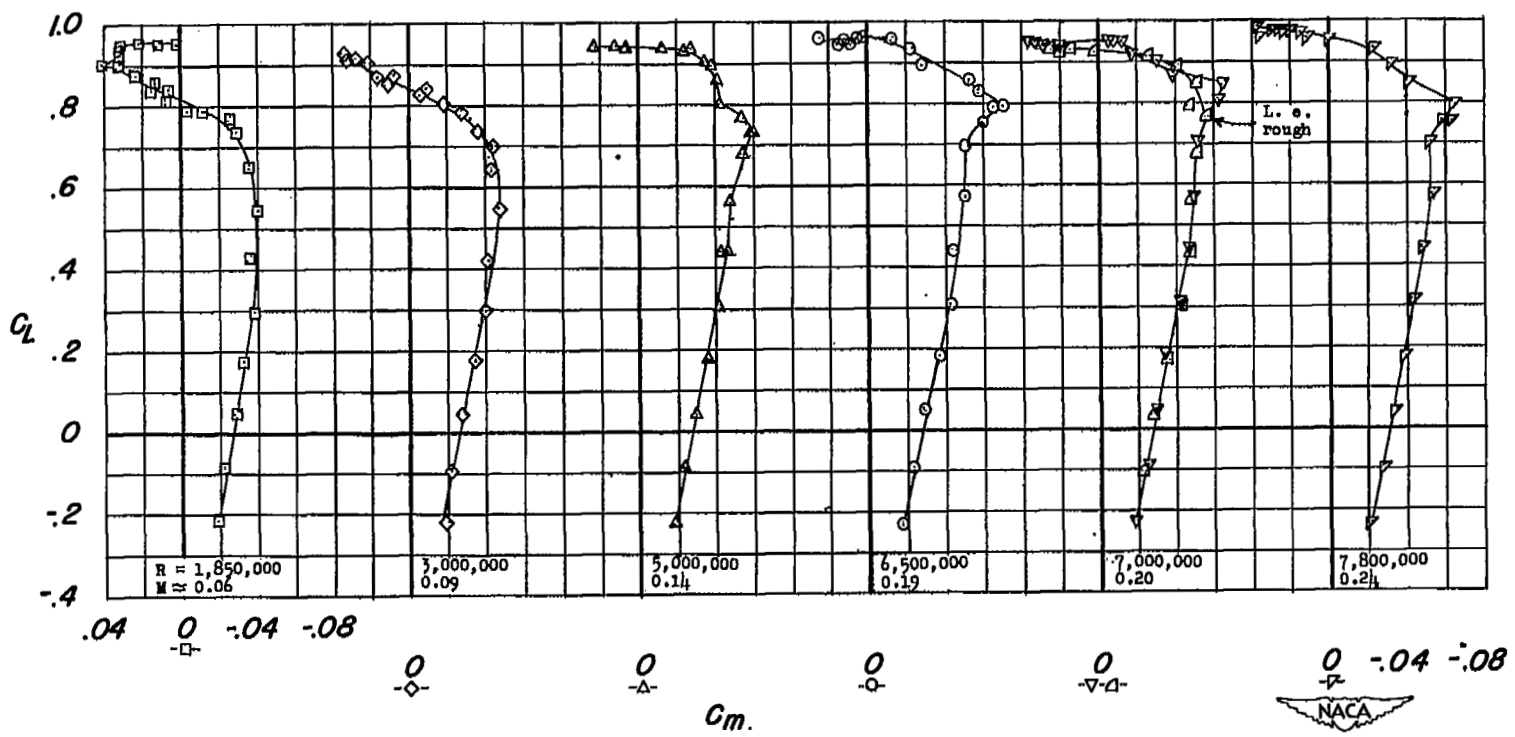


Figure 5.- Fuselage and horizontal tail details. Wing reference plane passes through root chord and 0.2250c line. Fuselage fineness ratio, 12:1; no incidence. Tail aspect ratio, 4.01; taper ratio, 0.625; M.A.C., 13.85; $S_t = 5.16$ square feet (0.2198). Linear dimensions in inches unless noted.

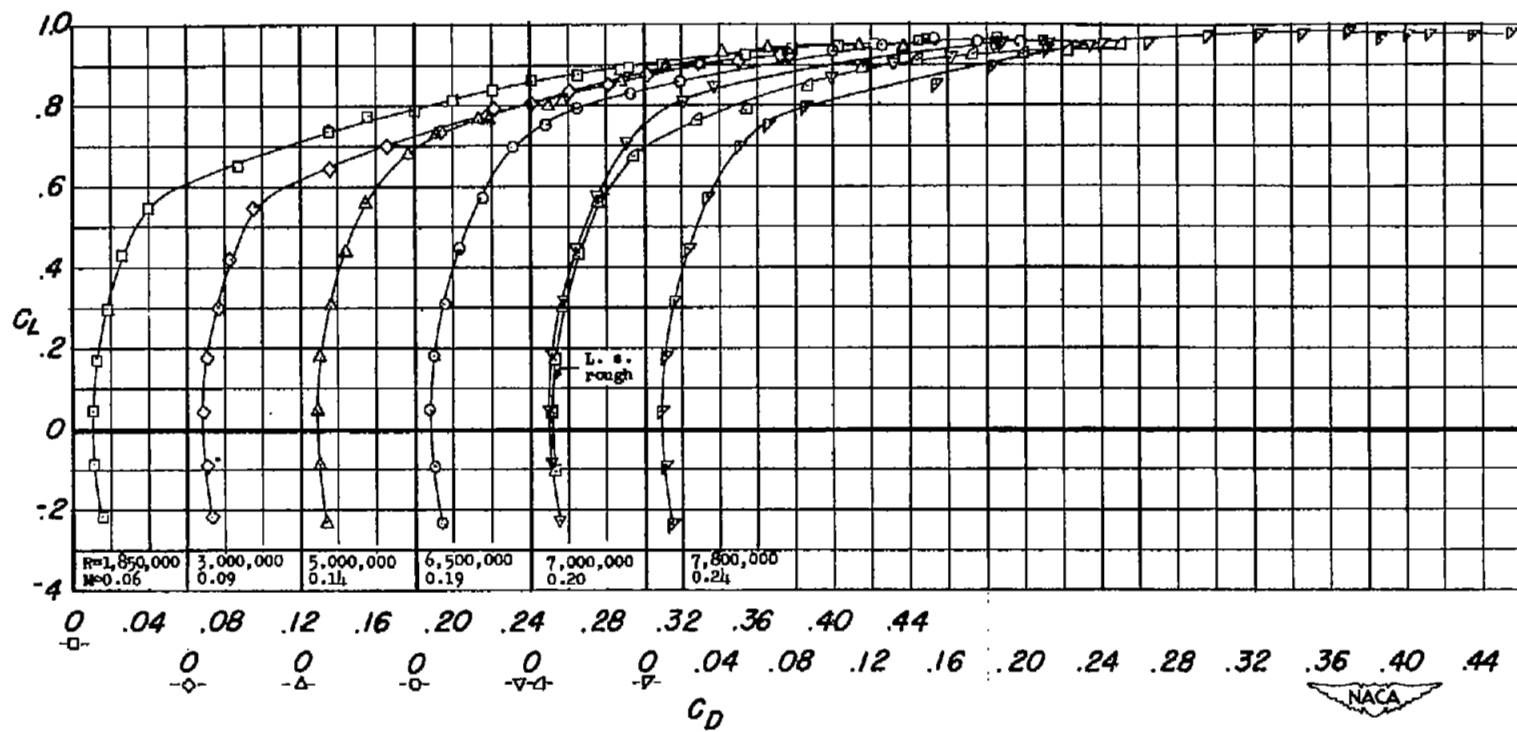


(a) C_L against α .

Figure 6.- Aerodynamic characteristics of basic wing at several values of Reynolds number.



(b) C_L against C_m .
 Figure 6.- Continued.



(c) C_L against C_D .

Figure 6.- Concluded.

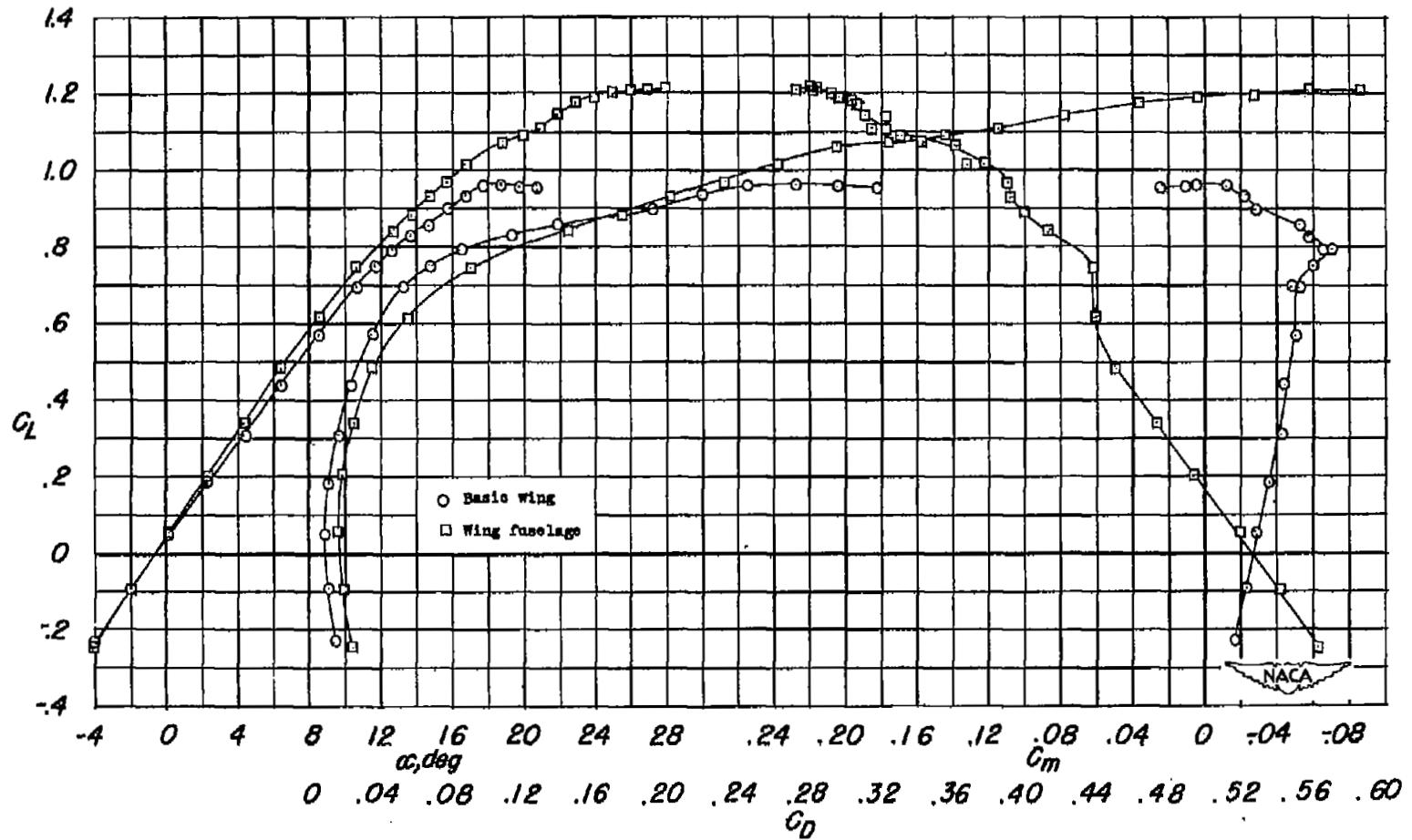
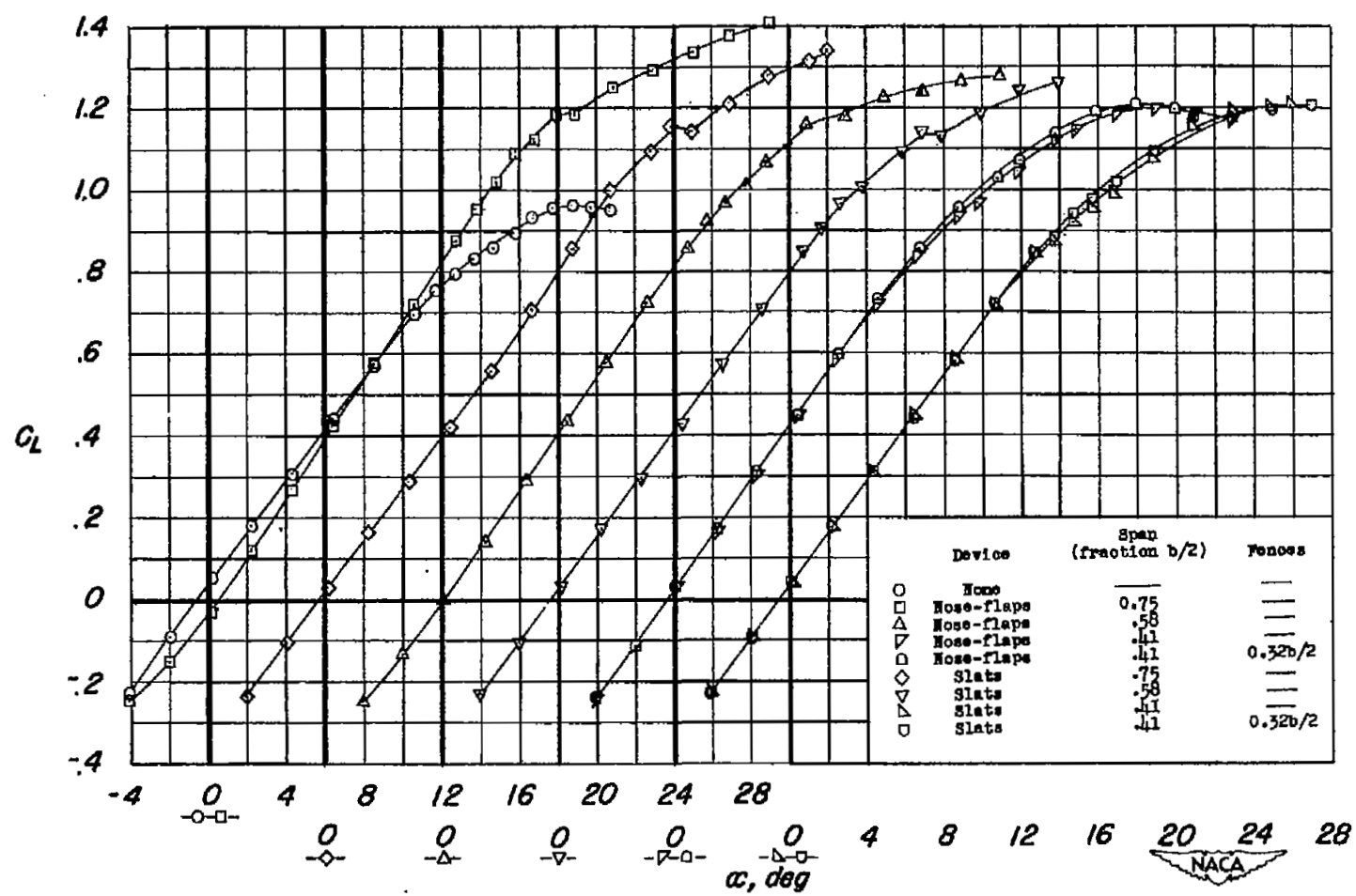
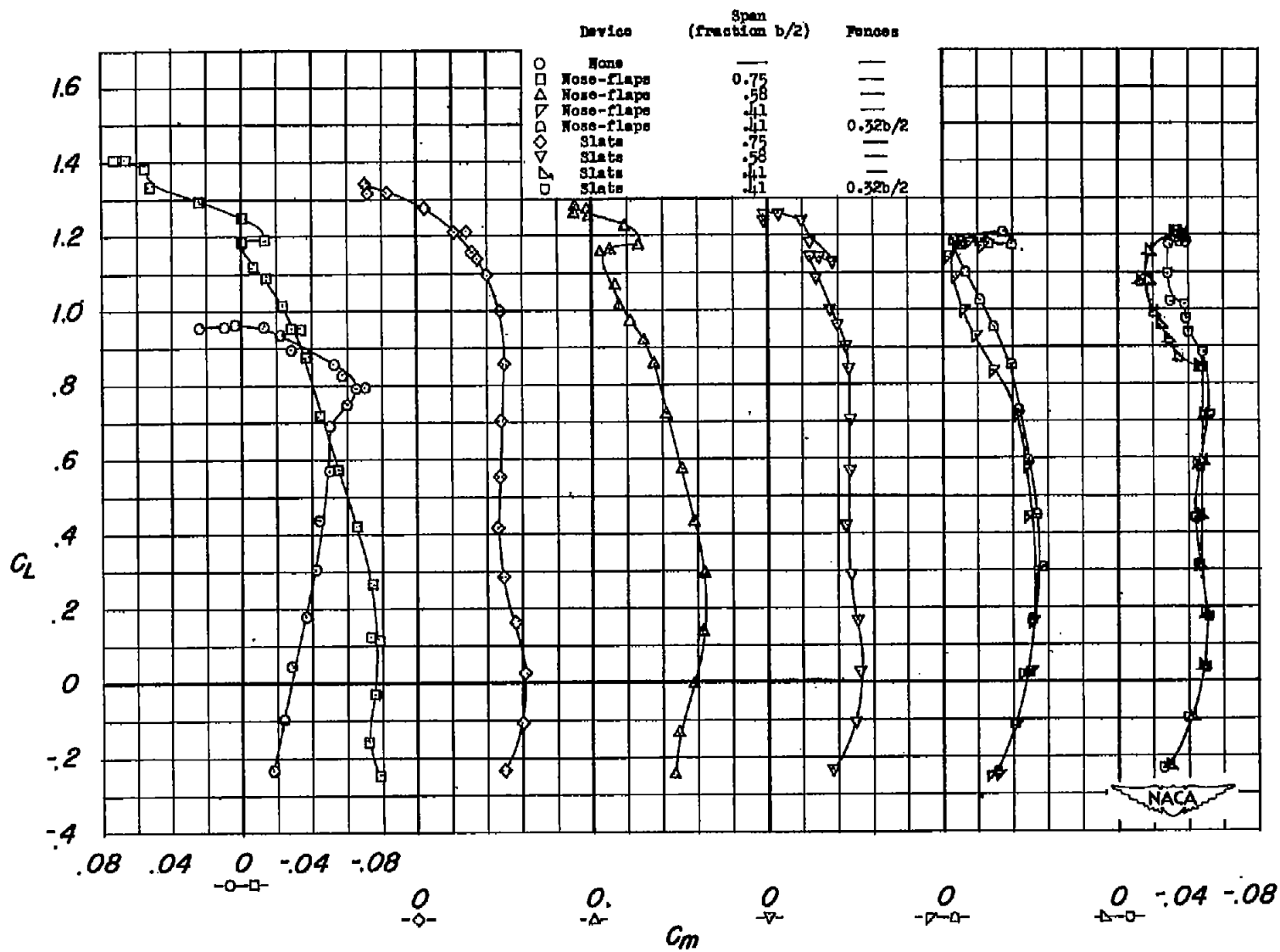


Figure 7.- Effects of a midwing fuselage on wing characteristics; $R = 6.5 \times 10^6$.



(a) C_L against α .

Figure 8.- Effects of various span leading-edge stall-control devices on aerodynamic characteristics of basic wing. $R = 6.5 \times 10^6$.



(b) C_L against C_m .

Figure 8.- Continued.

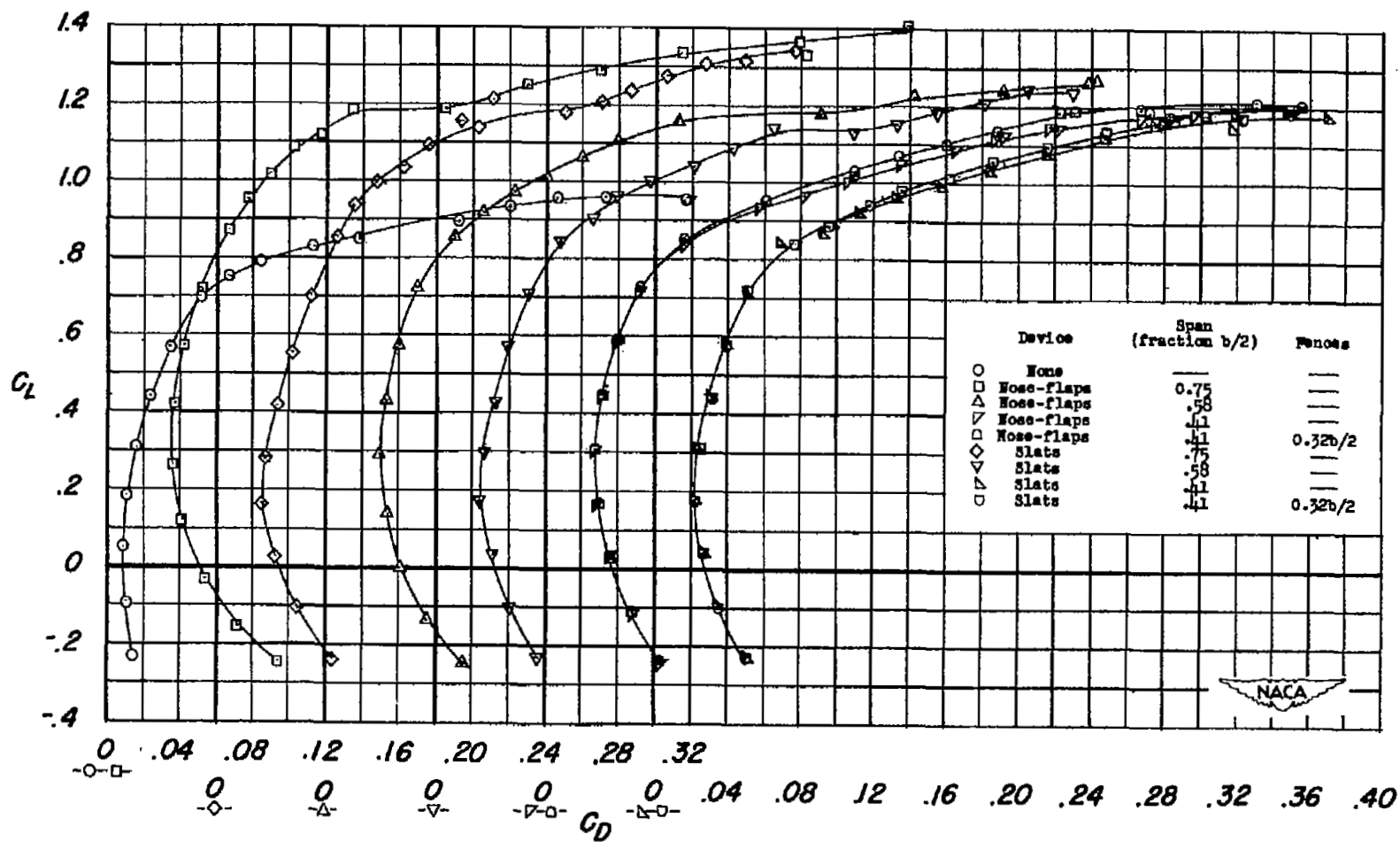
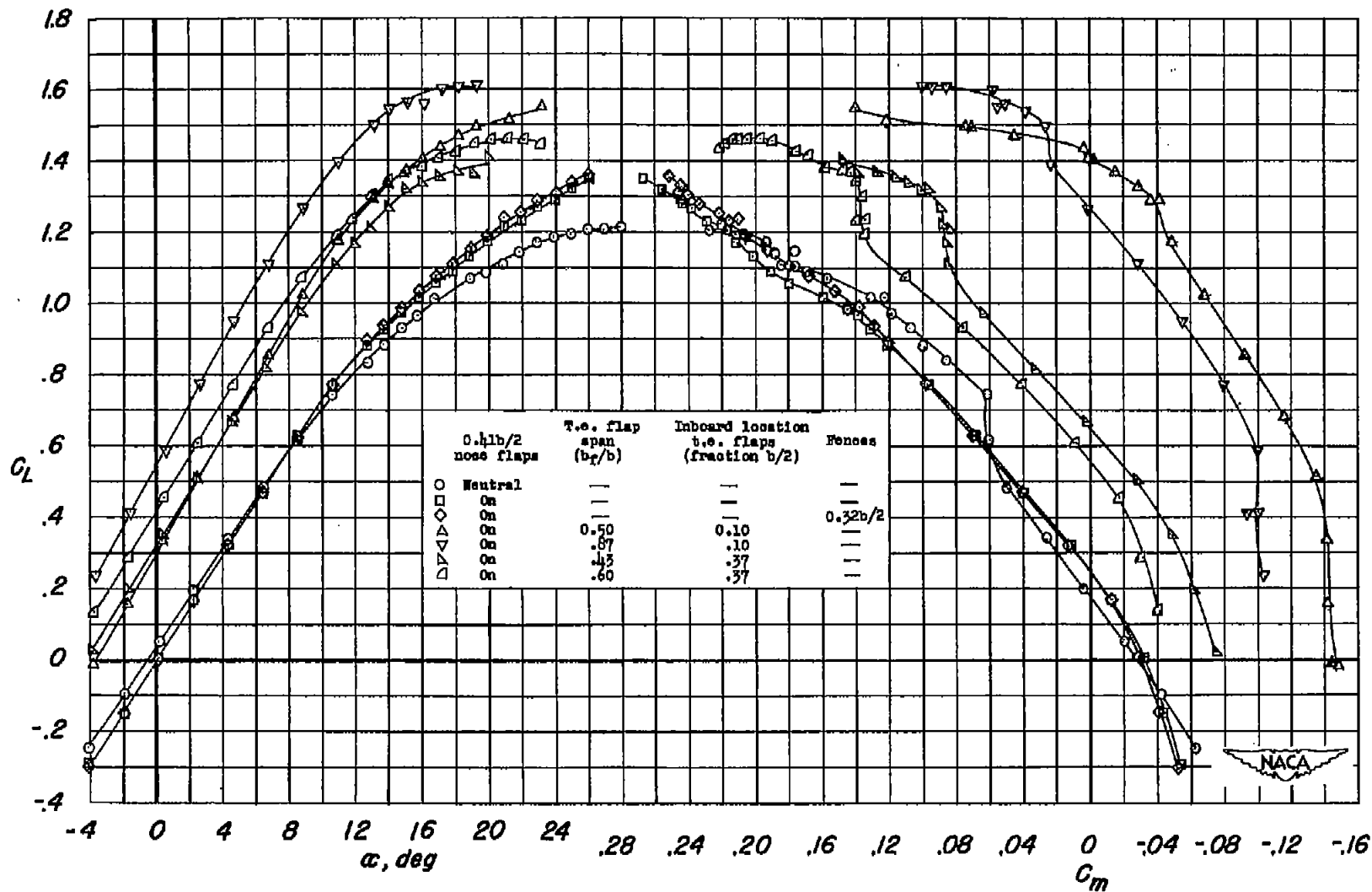
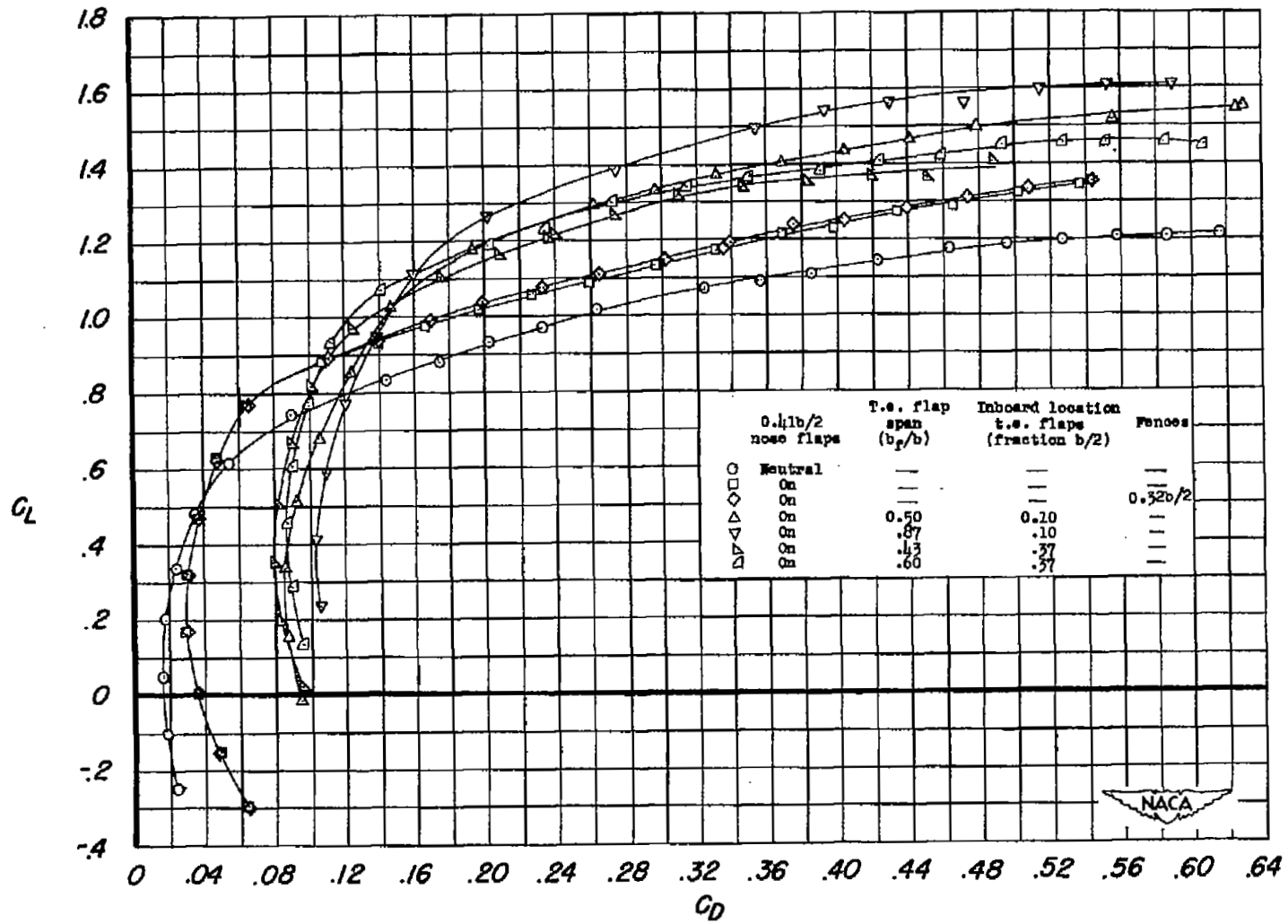
(c) C_L against C_D .

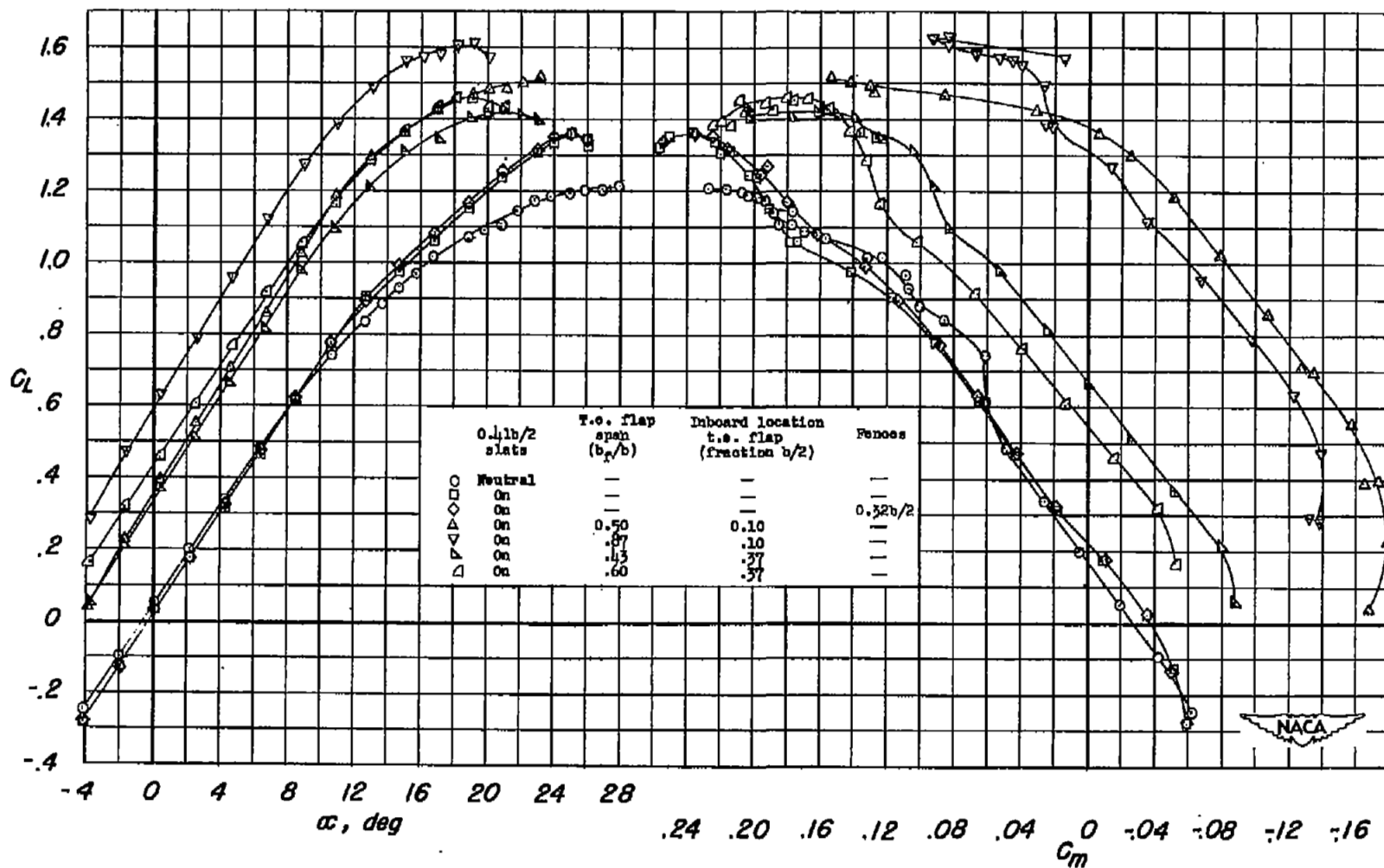
Figure 8.- Concluded.

(a) C_L against α and C_m .Figure 9.- Effects of extensible nose flaps and trailing-edge split flaps on aerodynamic characteristics of wing-fuselage combination. $R = 6.5 \times 10^6$.



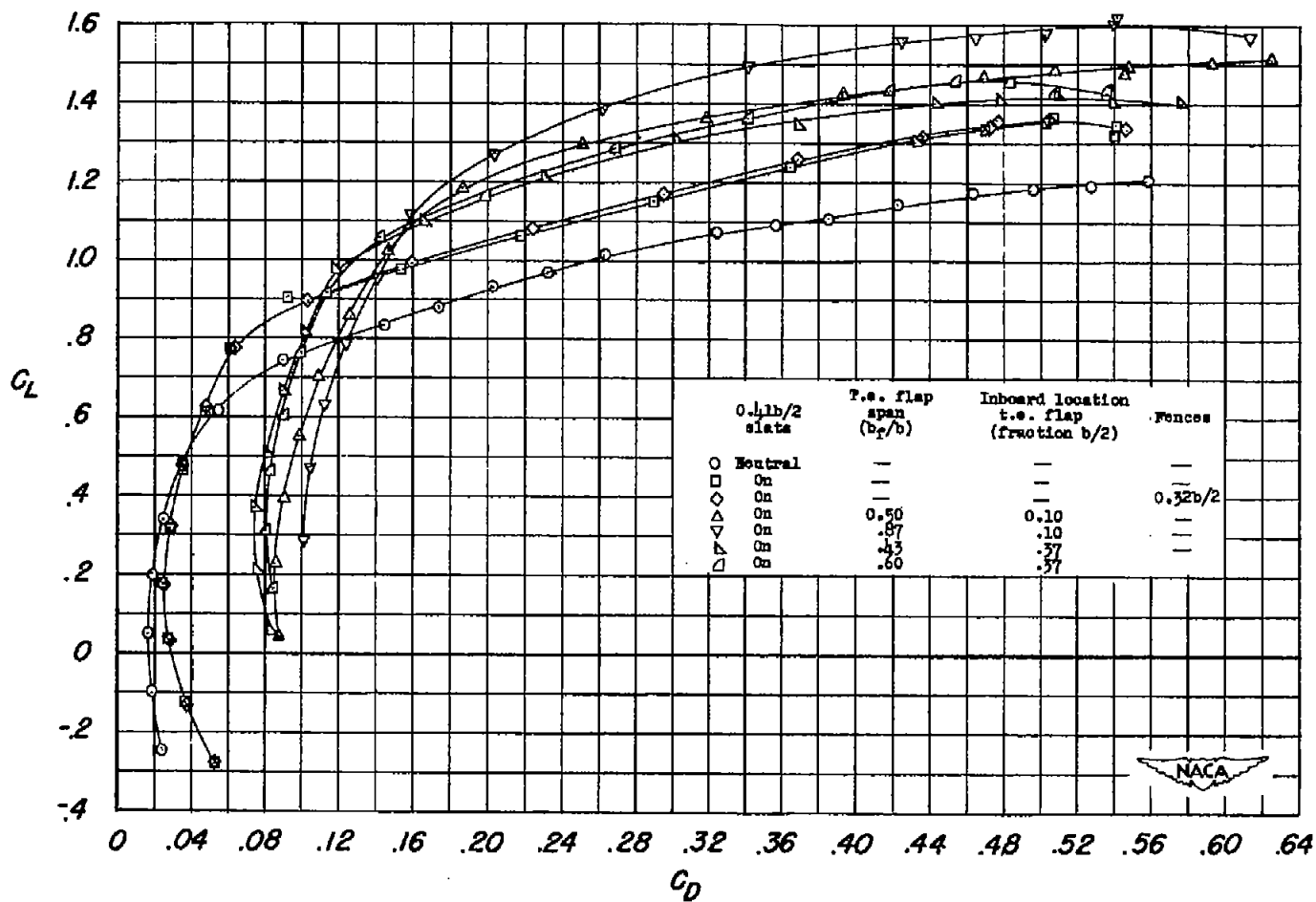
(b) C_L against C_D .

Figure 9.- Concluded.



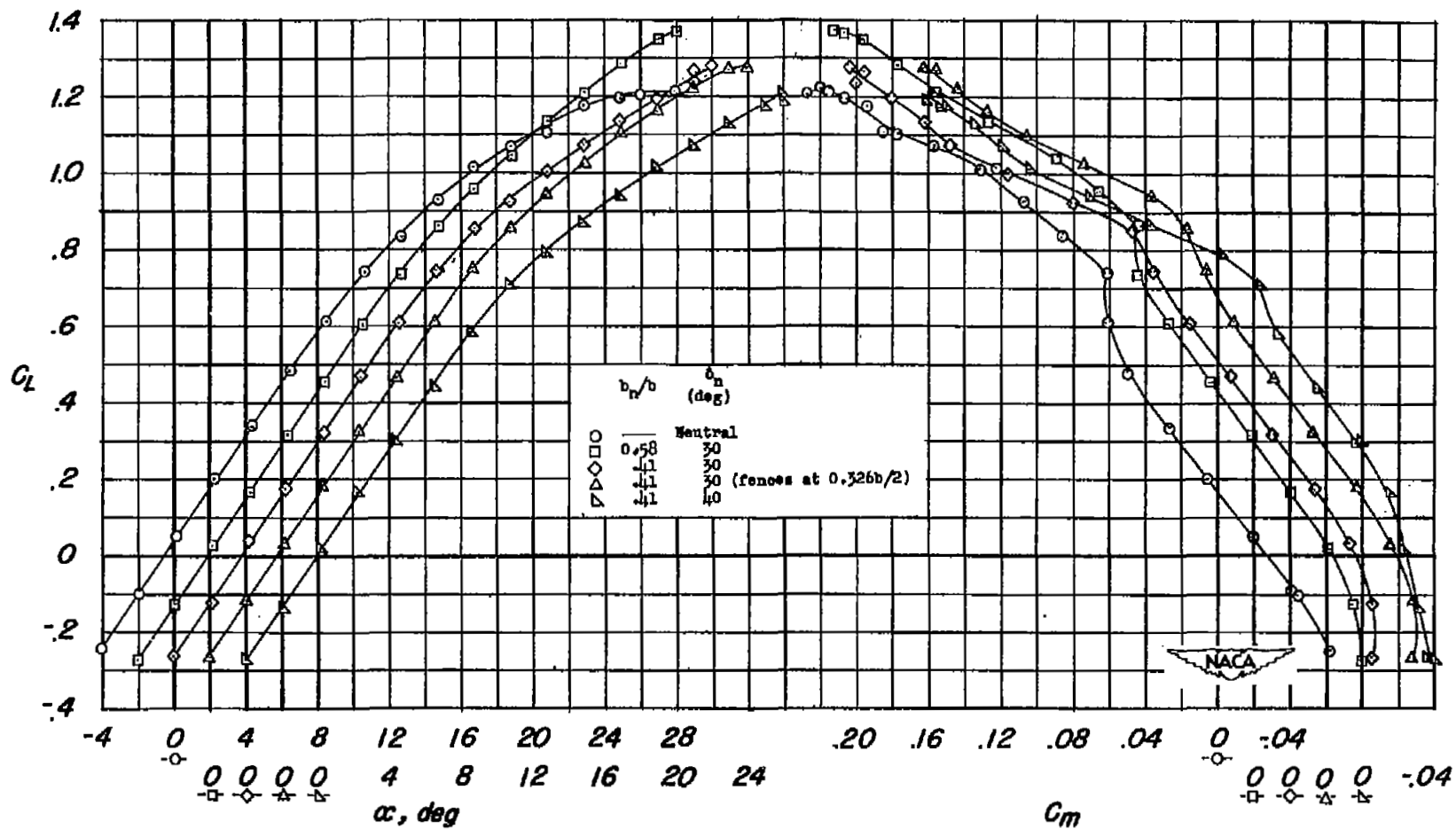
(a) C_L against α and C_m .

Figure 10.- Effects of slats and trailing-edge split flaps on aerodynamic characteristics of wing-fuselage combination. $R = 6.5 \times 10^6$.



(b) C_L against C_D .

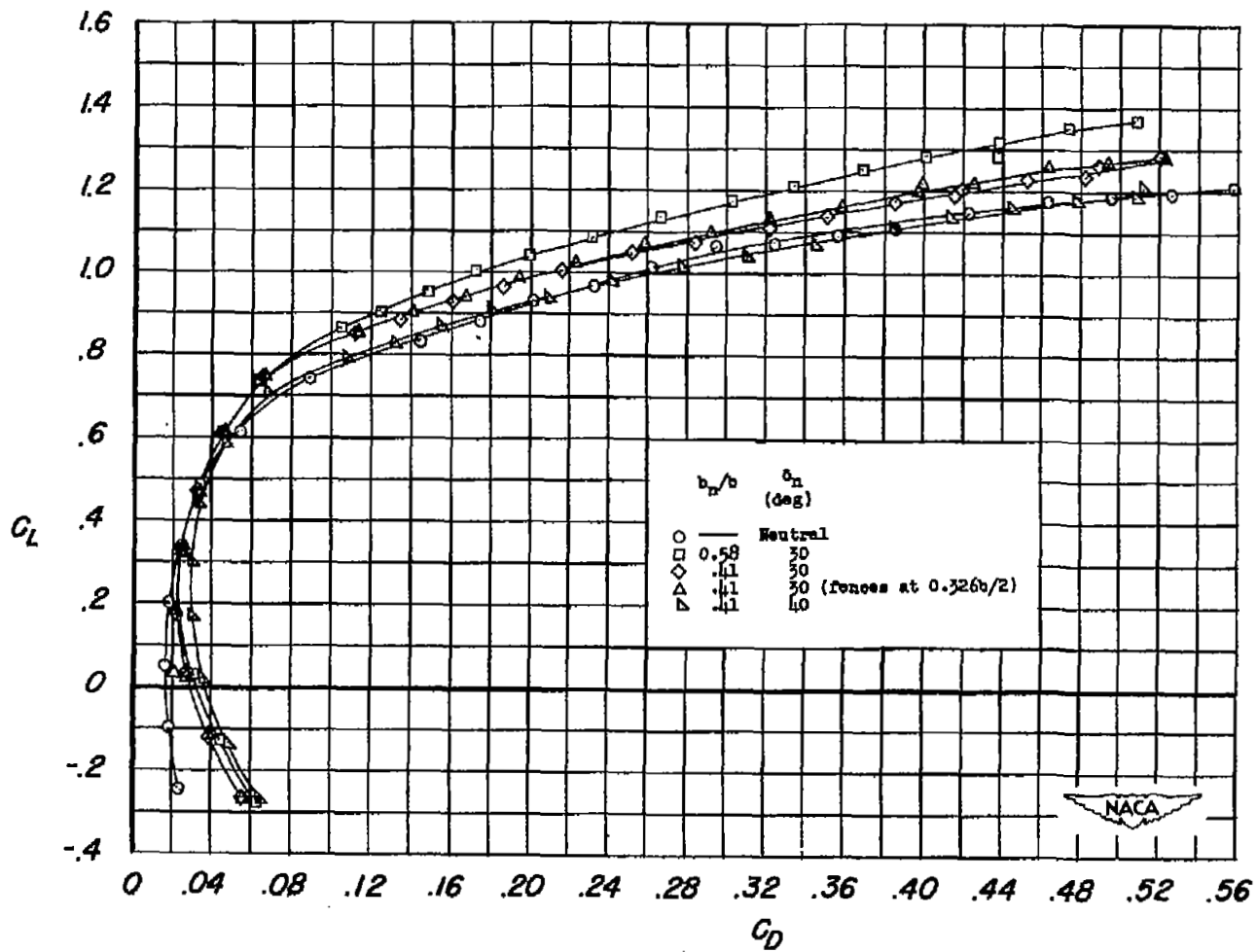
Figure 10.- Concluded.



(a) C_L against α and C_m .

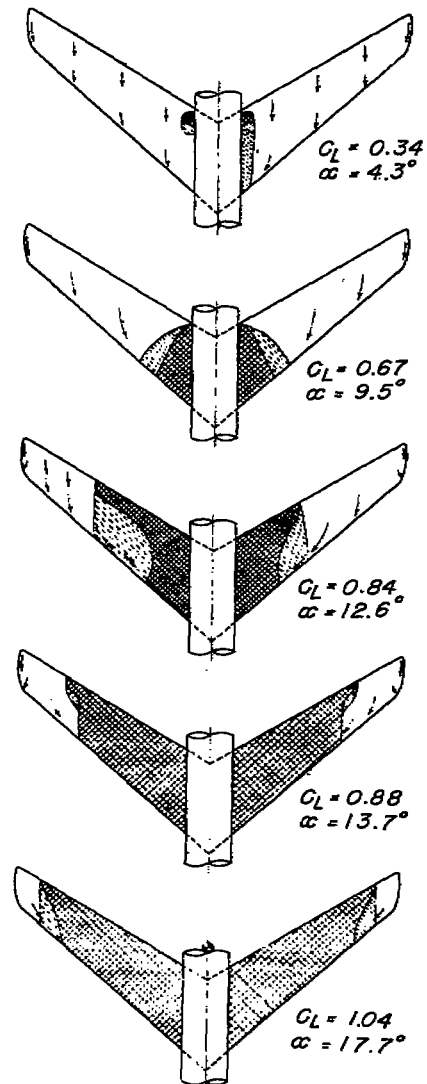
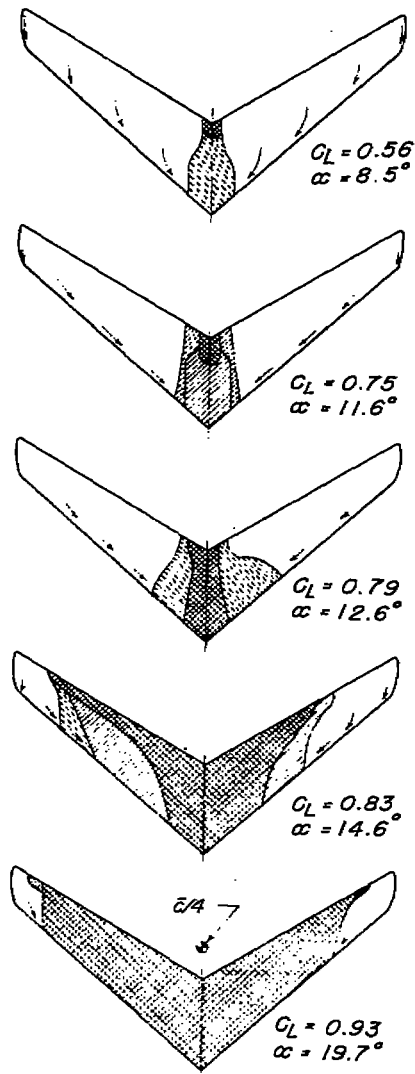
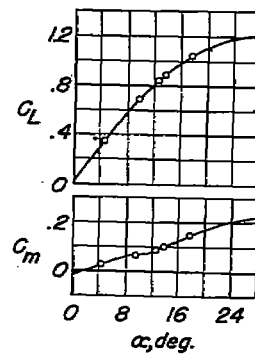
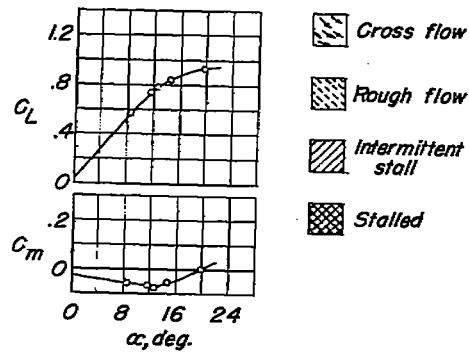
Figure 11.- Effects of drooped-nose flaps on aerodynamic characteristics of wing-fuselage combination.

$$R = 6.5 \times 10^6.$$



(b) C_L against C_D .

Figure 11.- Concluded.



(a) Fuselage off.

(b) Fuselage on.

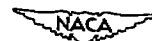


Figure 12.- Stalling characteristics of wing and wing with fuselage.

$R = 6.5 \times 10^6$.

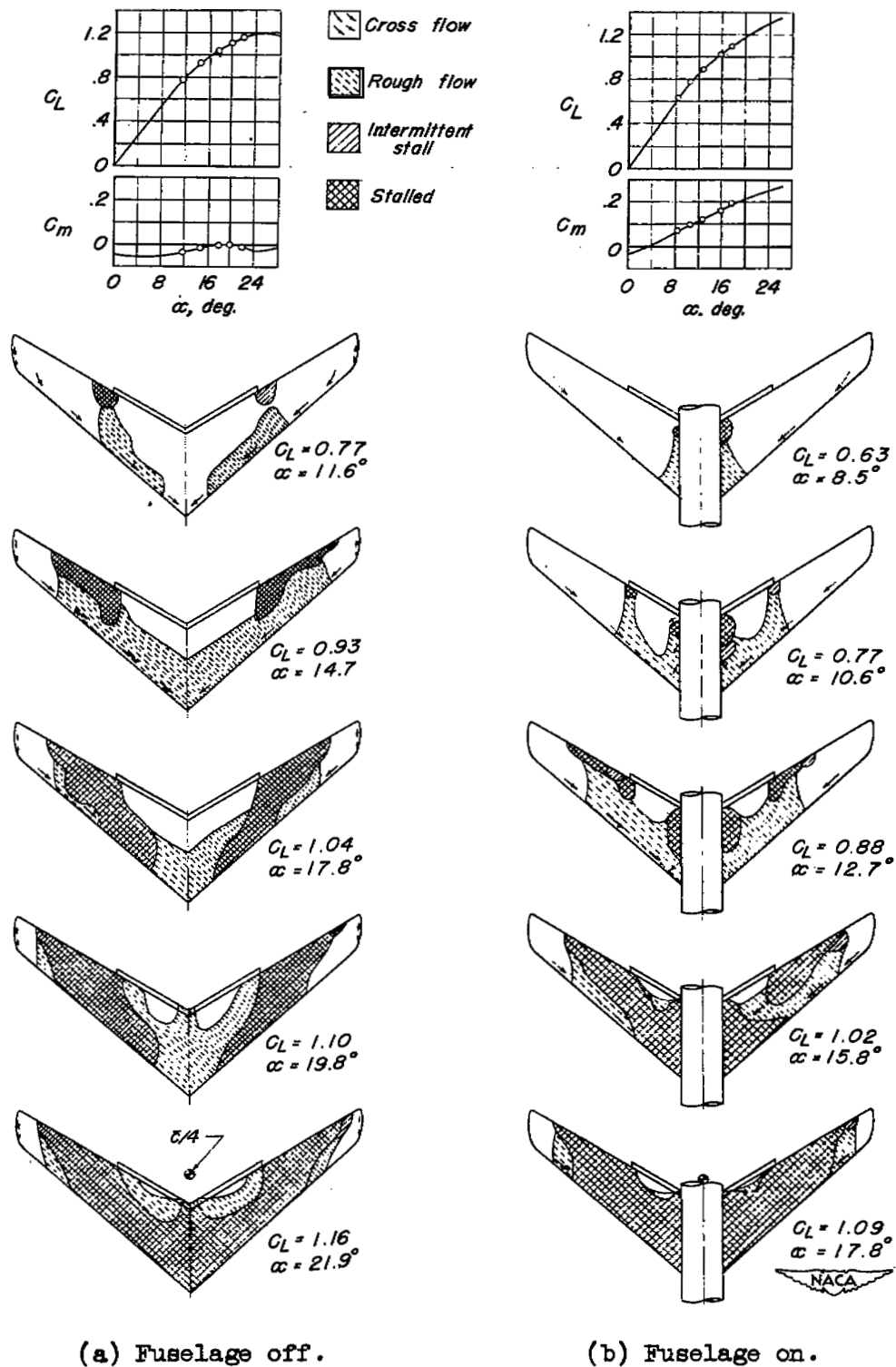
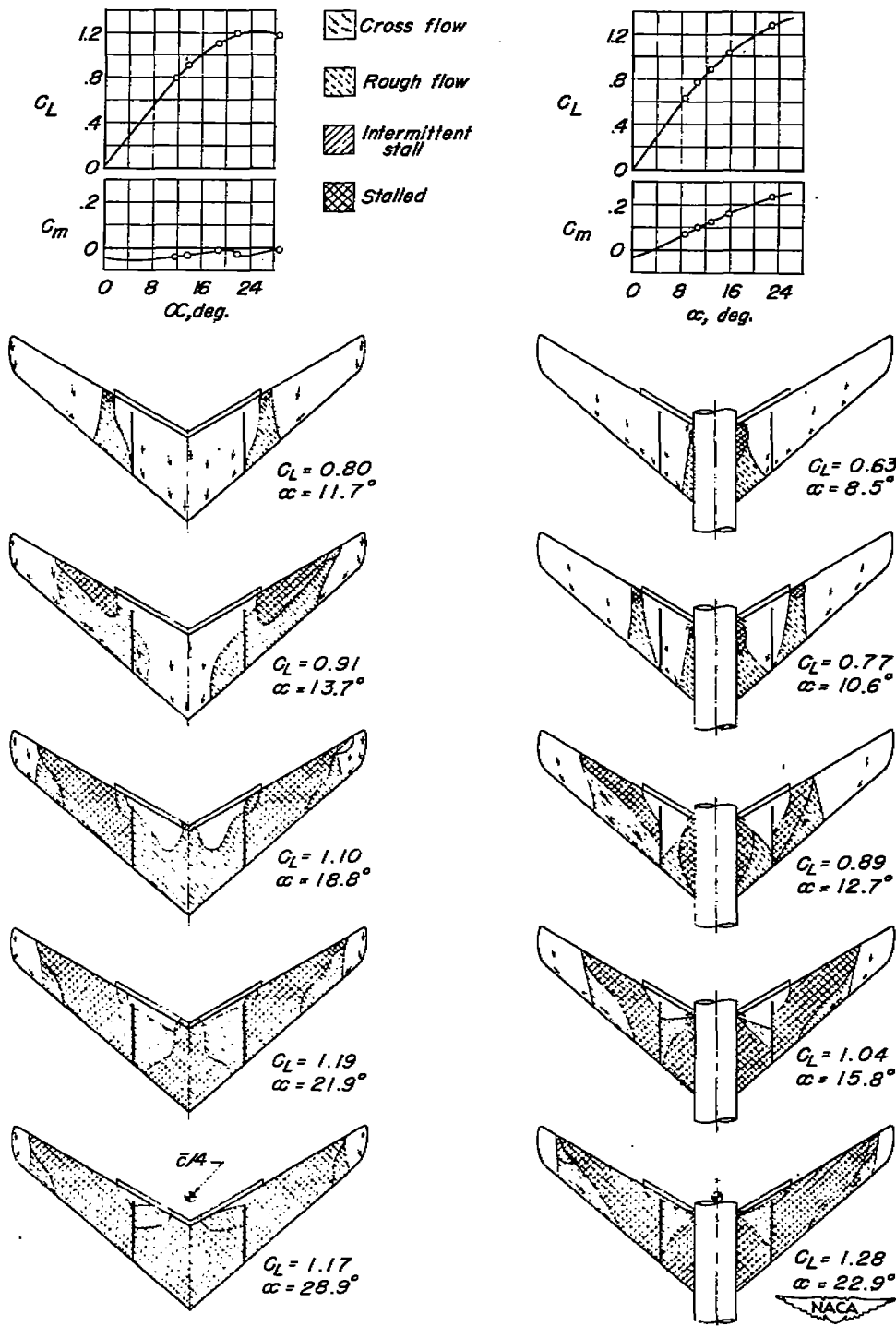


Figure 13.- Stalling characteristics of wing with $0.41\frac{b}{2}$ extensible nose flaps extended; fuselage on and off. $R = 6.5 \times 10^6$.



(a) Fuselage off.

(b) Fuselage on.

Figure 14.- Stalling characteristics of wing with $0.41\frac{b}{2}$ extensible nose flaps extended and fences at $0.32\frac{b}{2}$; fuselage on and off. $R = 6.5 \times 10^6$.

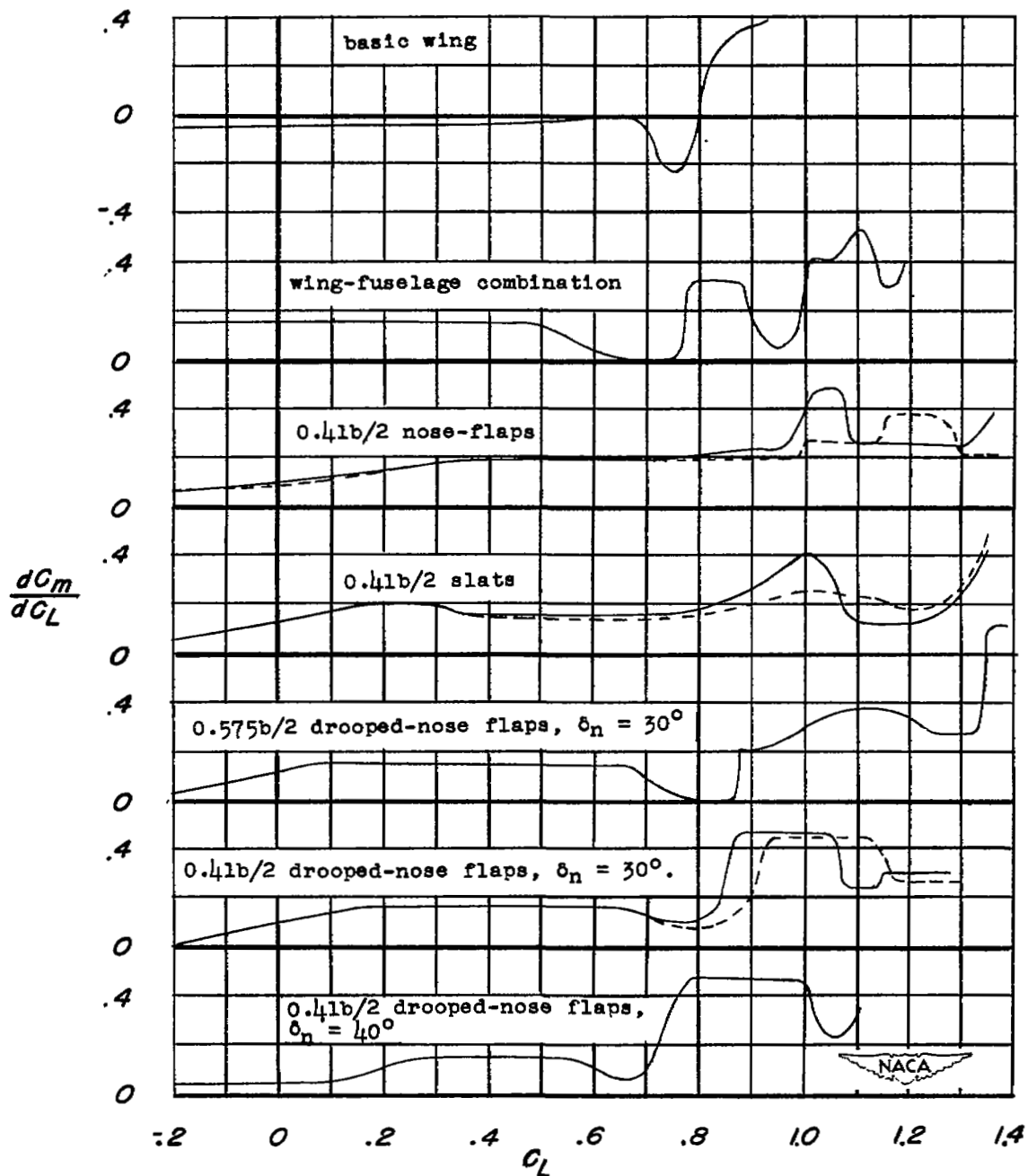
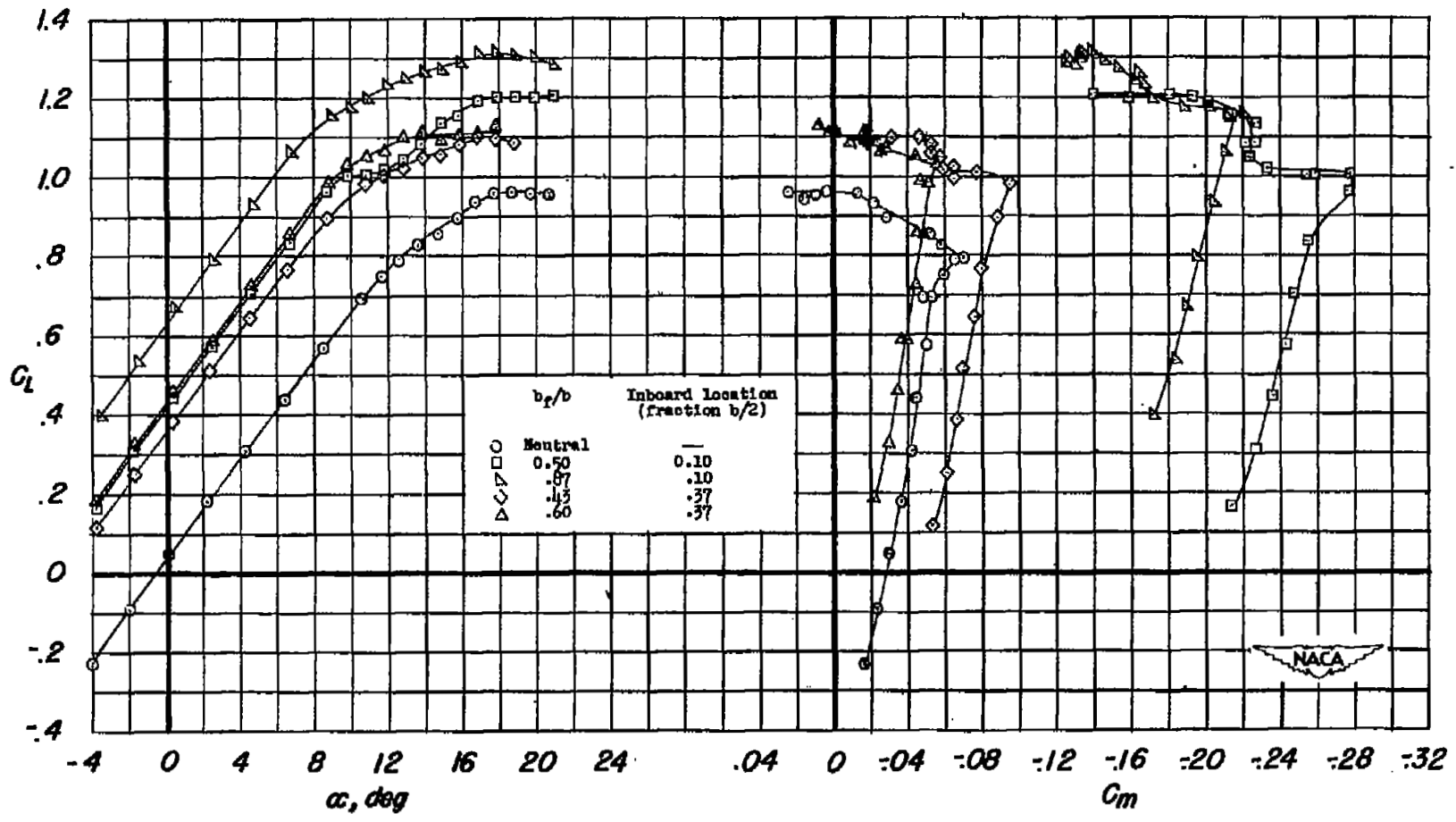


Figure 15.- Variation of total stability parameter with lift coefficient for wing-fuselage combination having several arrangements of leading-edge devices. Dotted curves indicate the addition of upper-surface fences at $0.32\frac{b}{2}$.



(a) C_L against α and C_m .

Figure 16.- Aerodynamic characteristics of basic wing with various spans of 0.20 normal-chord split flaps deflected 60° . $R = 6.5 \times 10^6$.

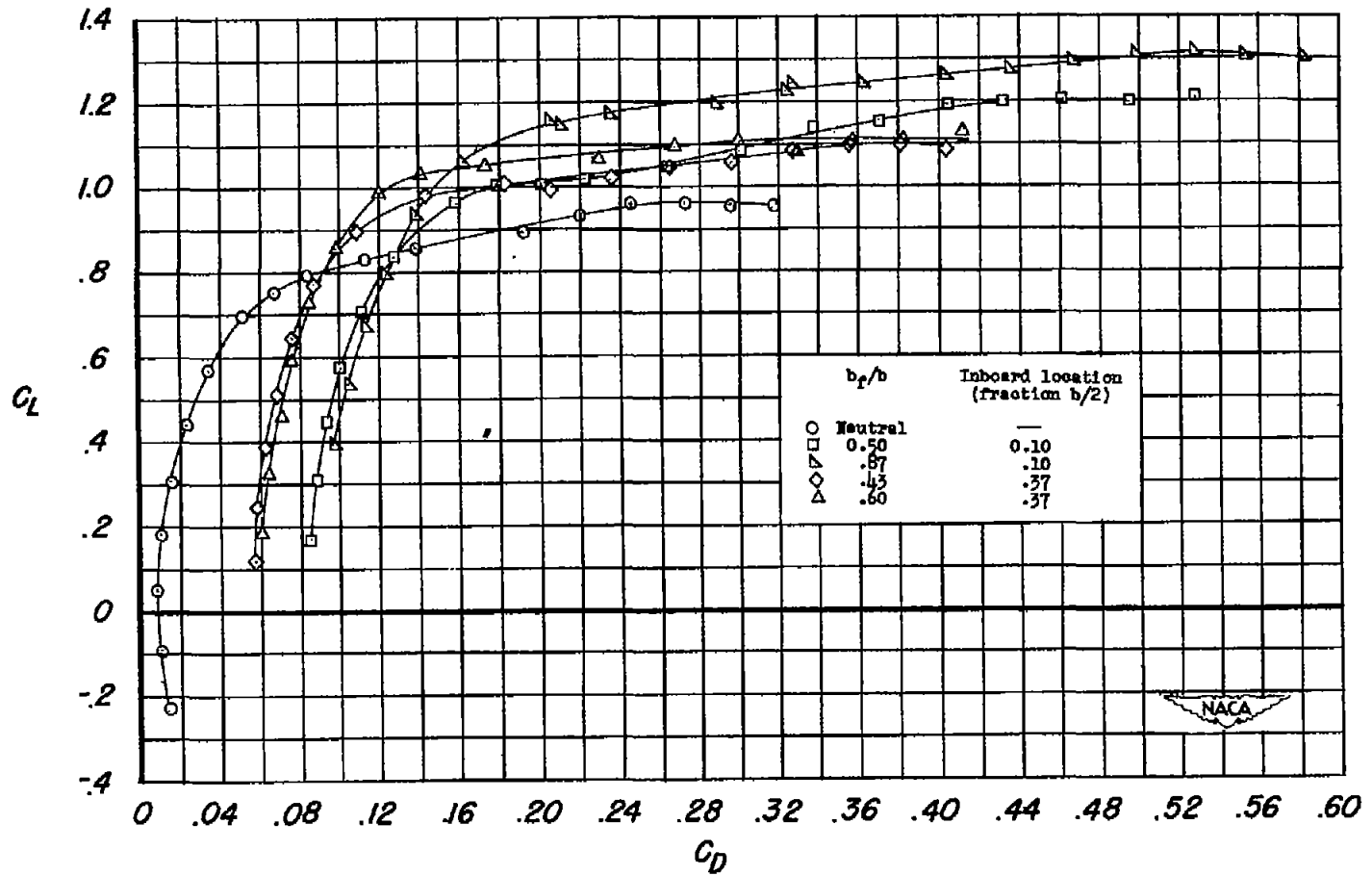
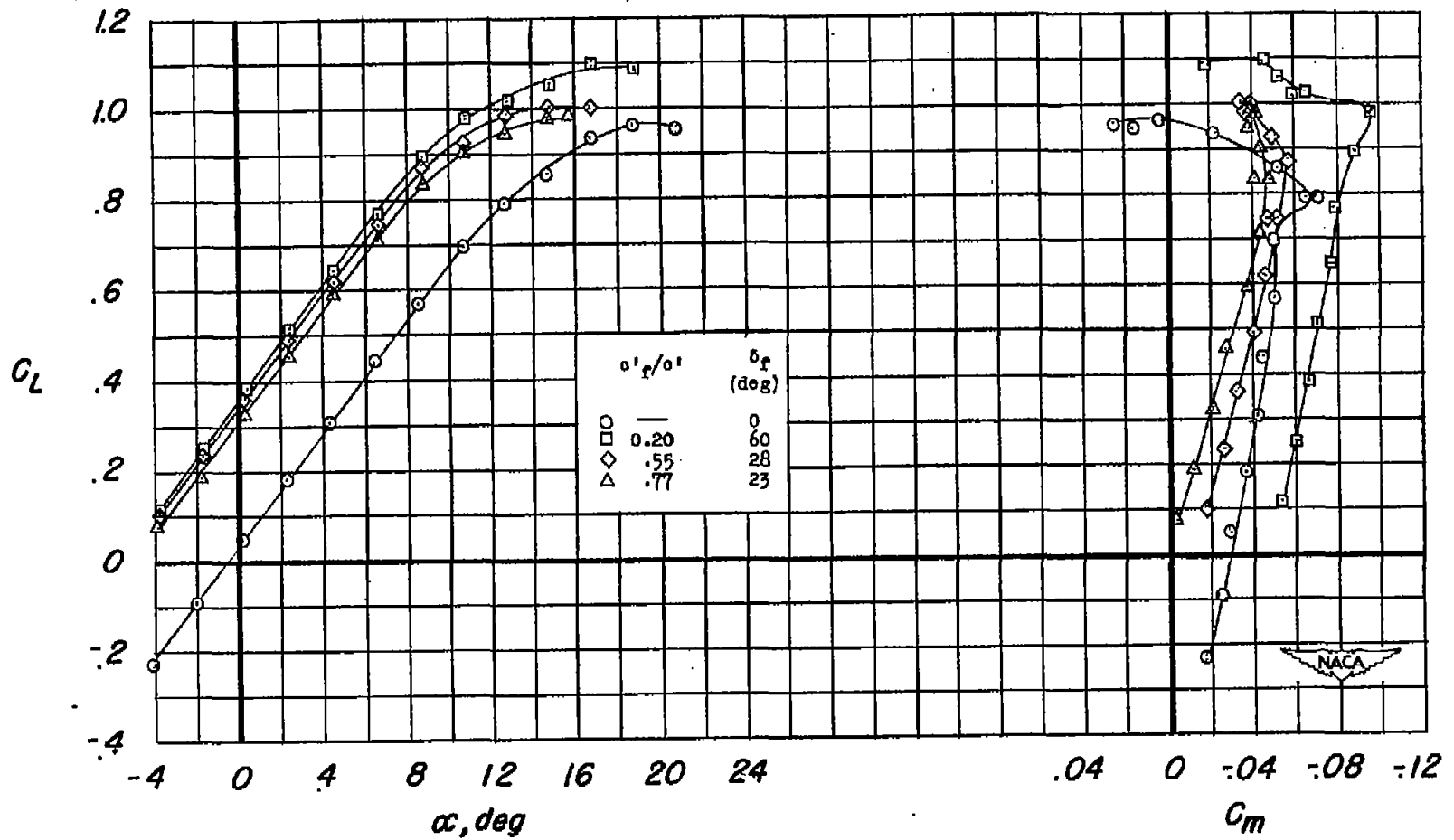
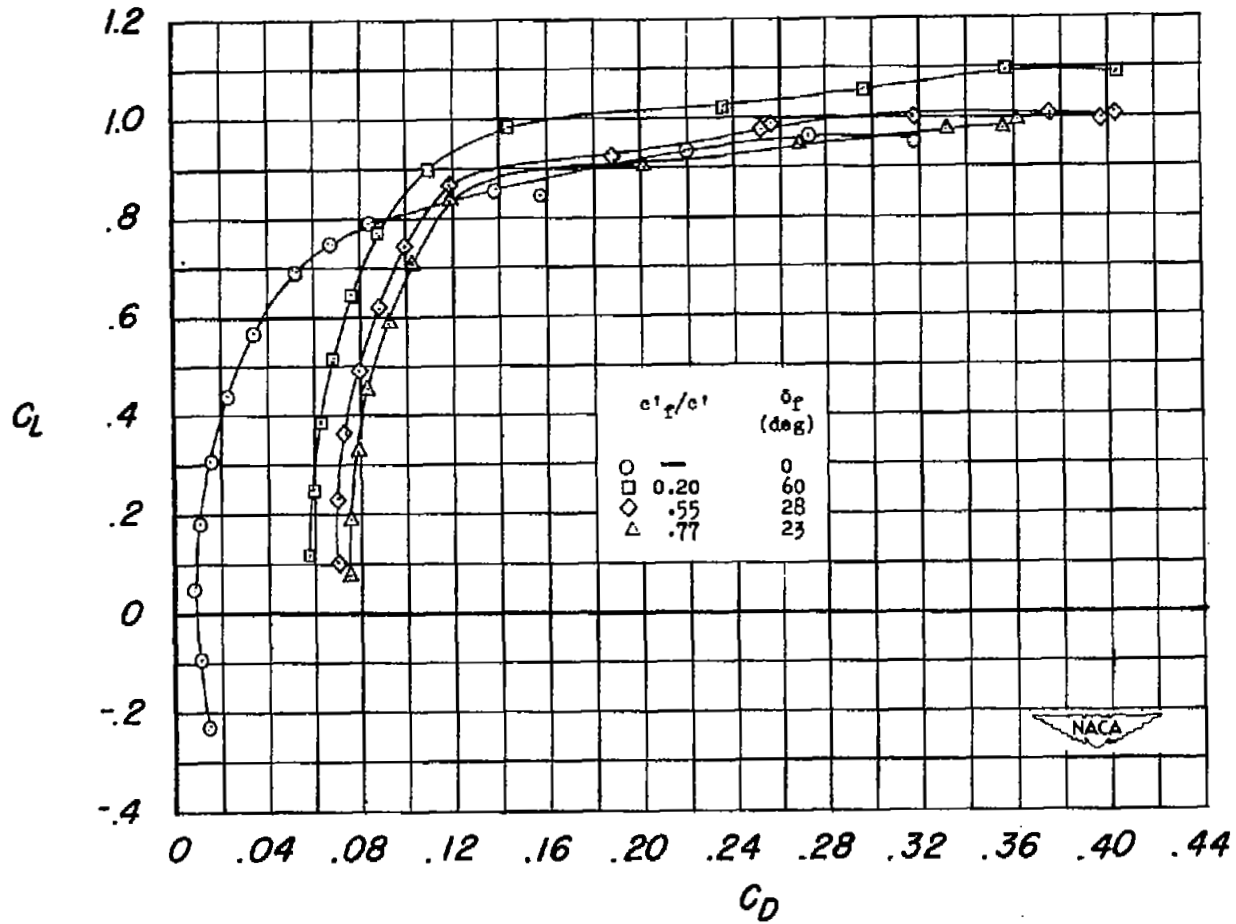
(b) C_L against C_D .

Figure 16.- Concluded.



(a) C_L against α and C_m .

Figure 17.- Aerodynamic characteristics of basic wing with several split trailing-edge flaps extending from $0.37\frac{b}{2}$ to $0.80\frac{b}{2}$. $R = 6.5 \times 10^6$.



(b) C_L against C_D .

Figure 17.- Concluded.

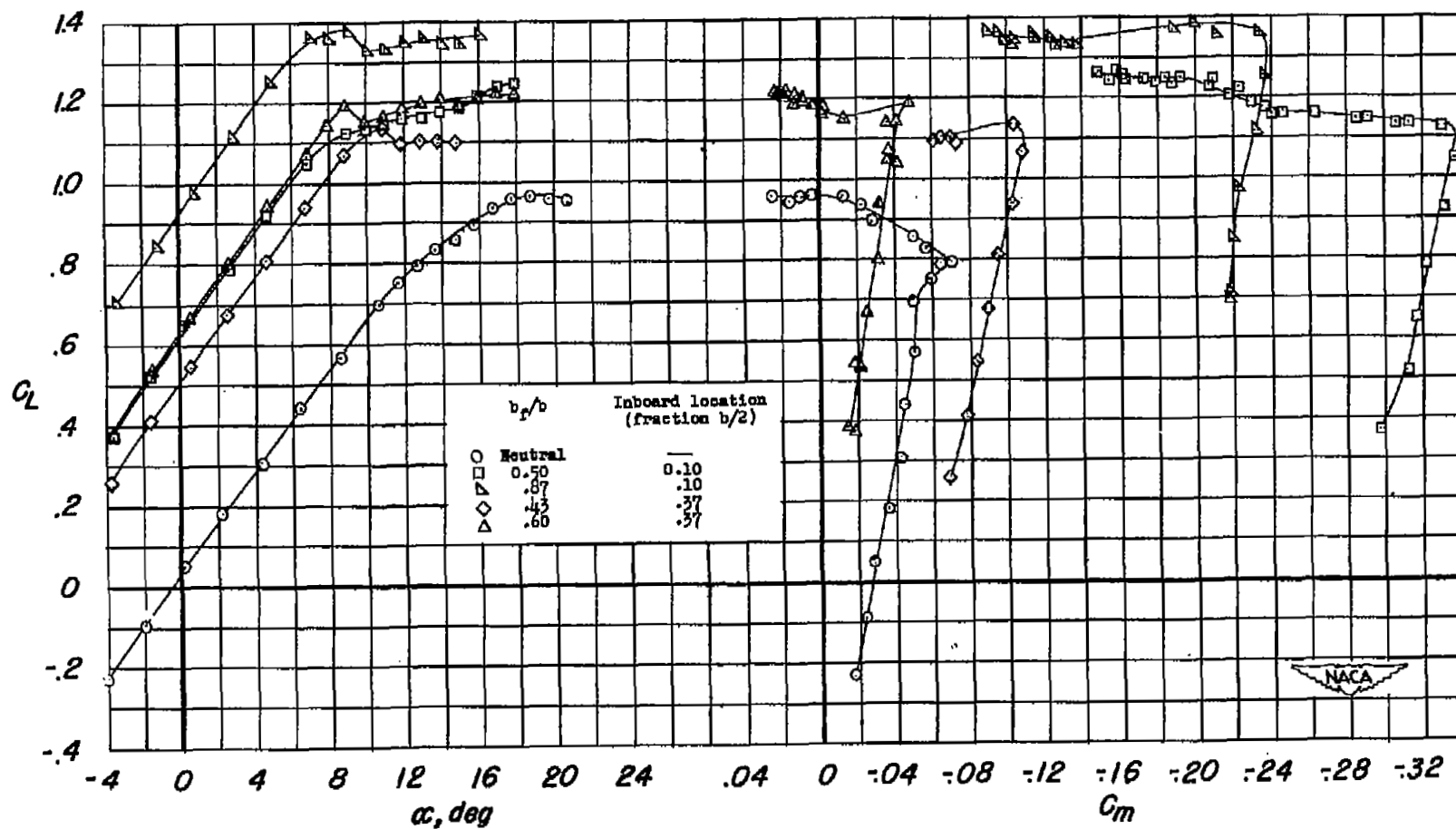
(a) C_L against α and C_m .

Figure 18.- Aerodynamic characteristics of basic wing with several spans of 0.25 normal-chord single slotted flaps deflected 45° . $R = 6.5 \times 10^6$.

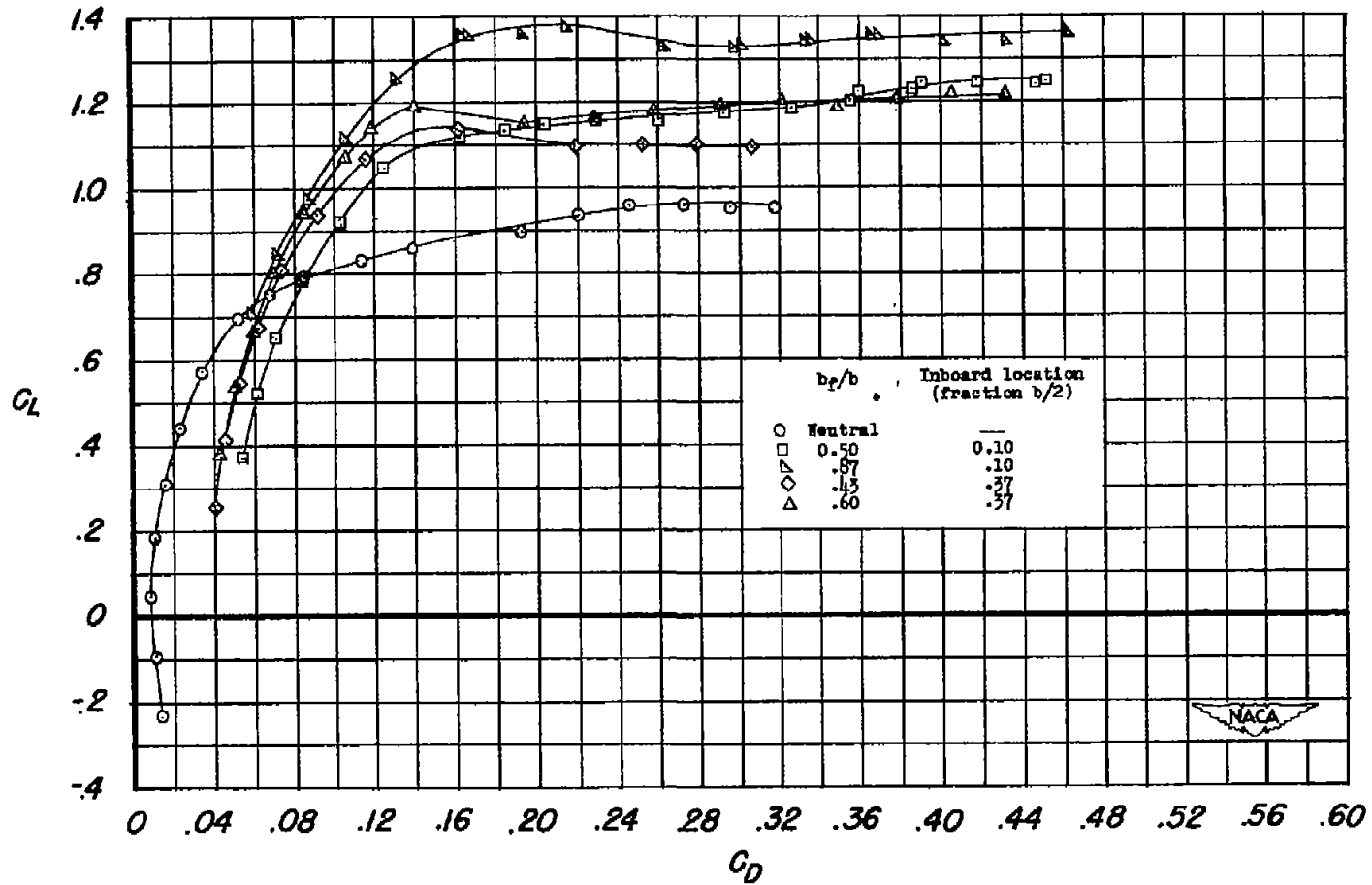
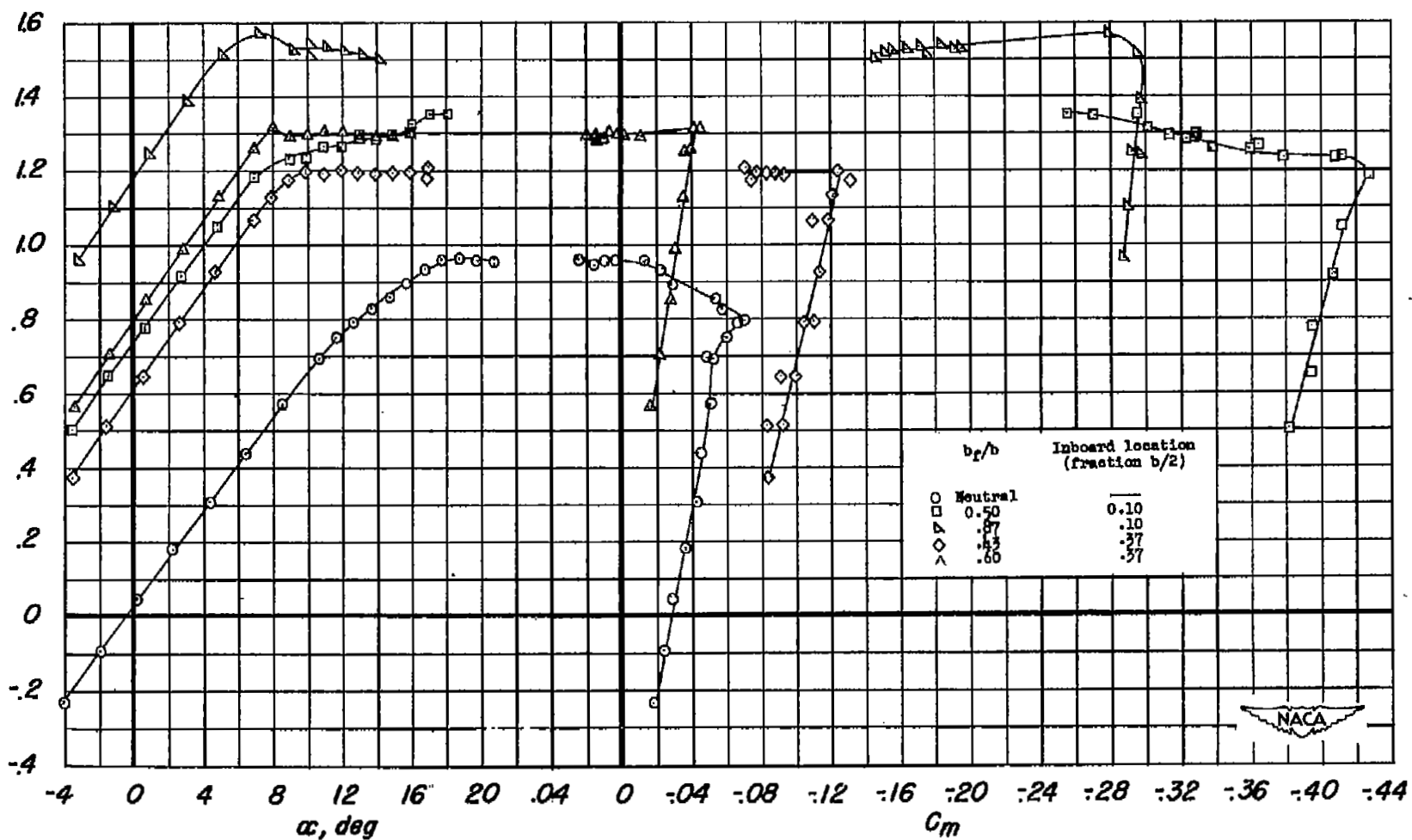
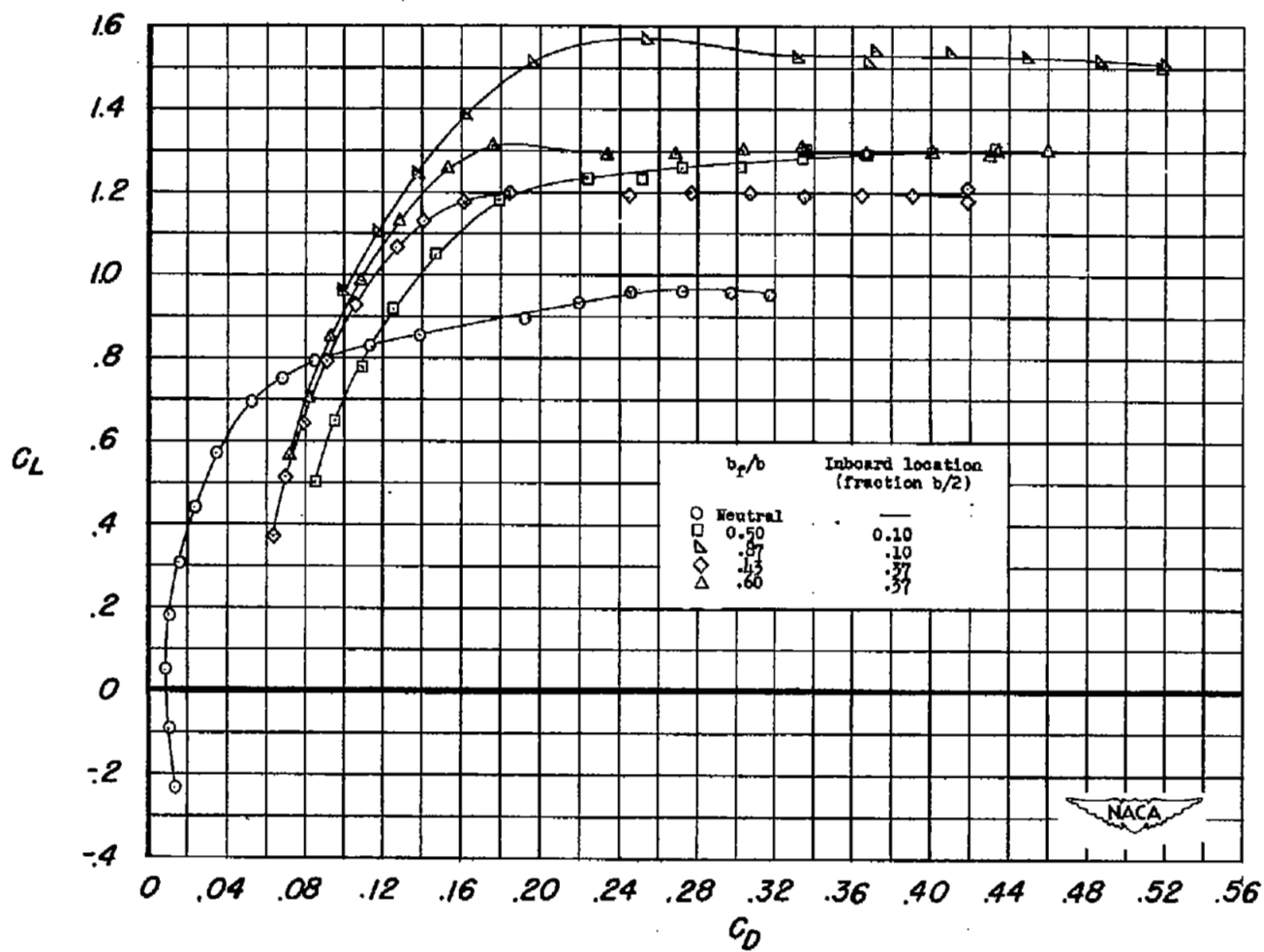
(b) C_L against C_D .

Figure 18.- Concluded.



(a) C_L against α and C_m .

Figure 19.- Aerodynamic characteristics of basic wing with several spans of 0.31 normal-chord double slotted flaps deflected 50° . $R = 6.5 \times 10^6$.



(b) C_L against C_D .

Figure 19.- Concluded.

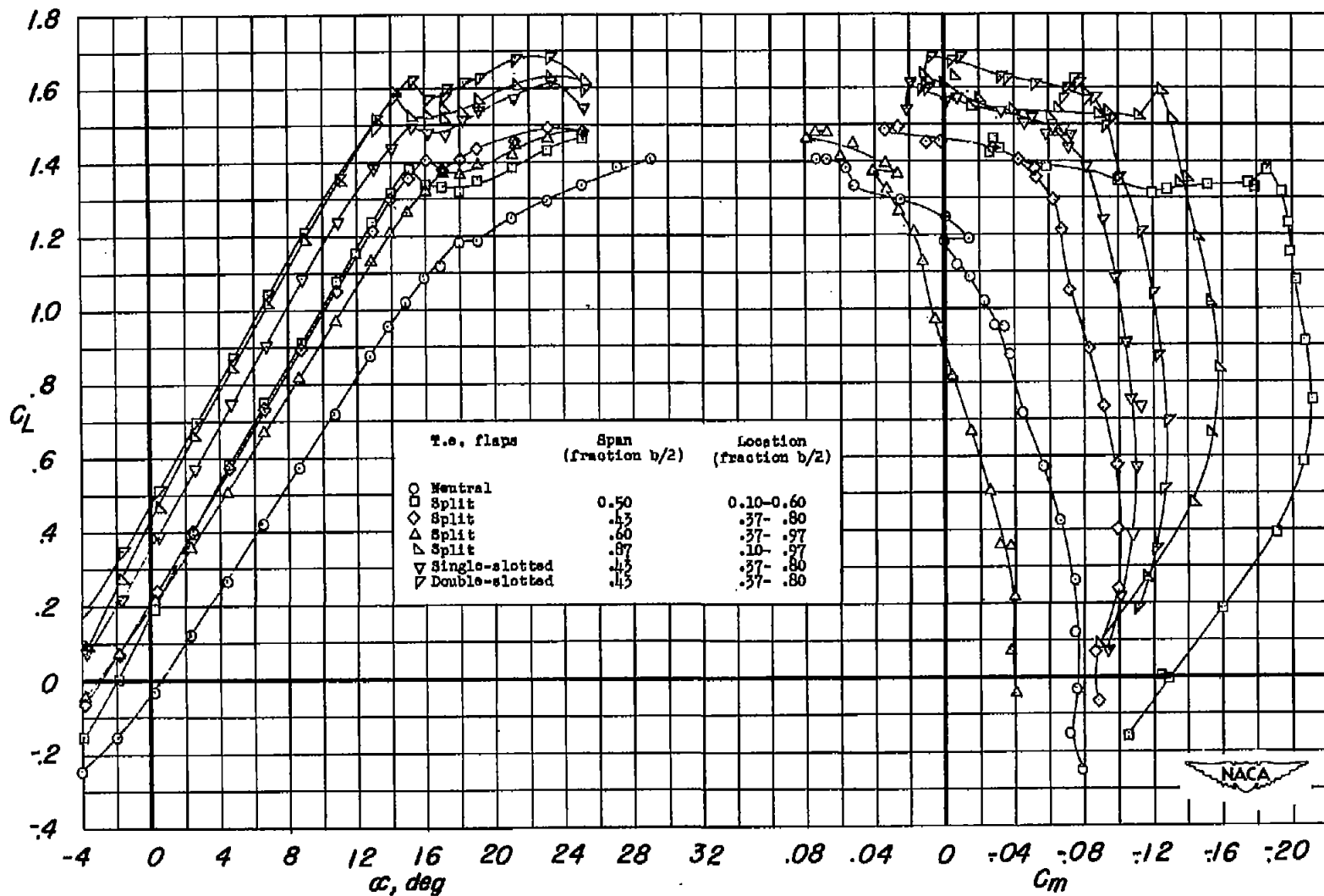
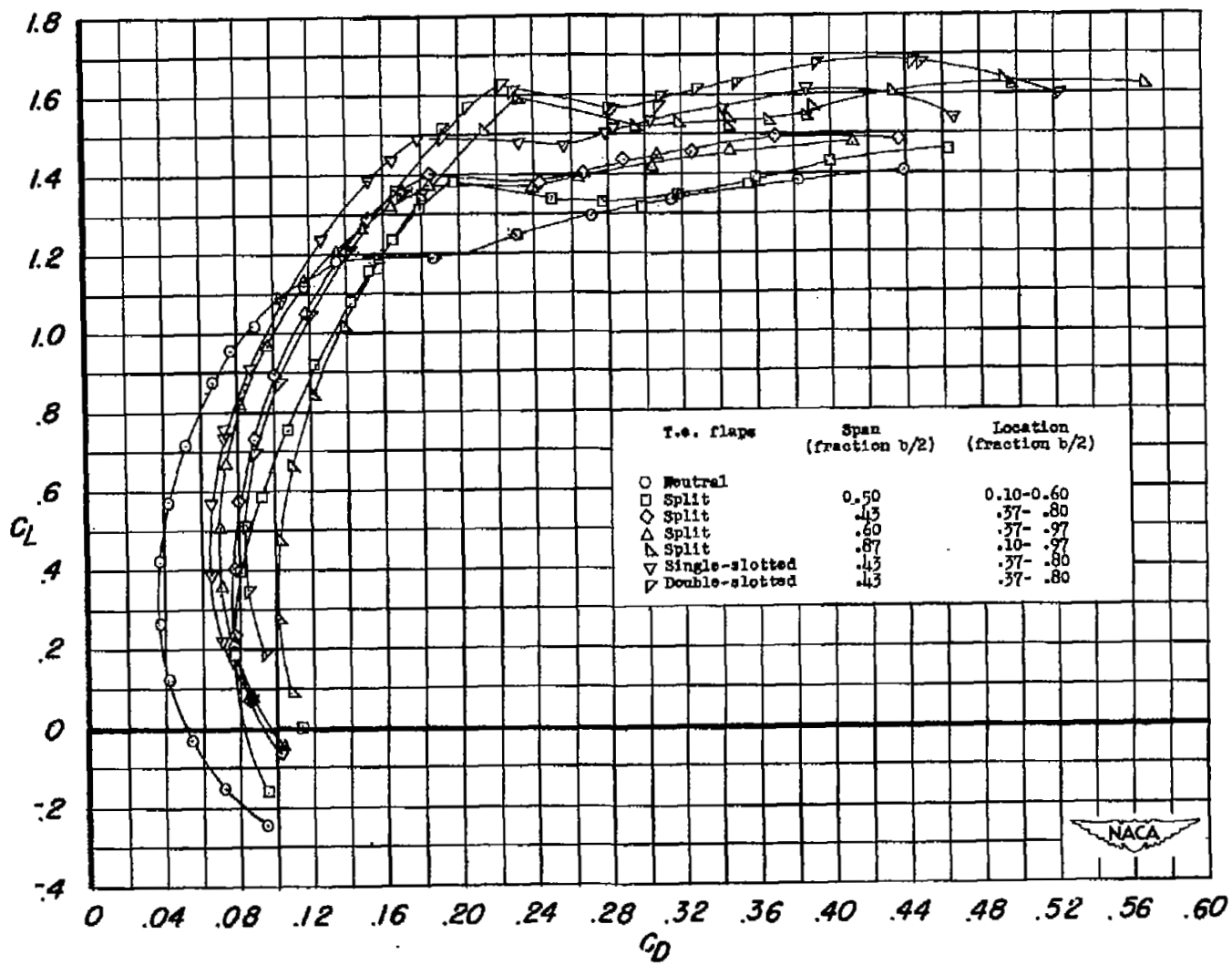
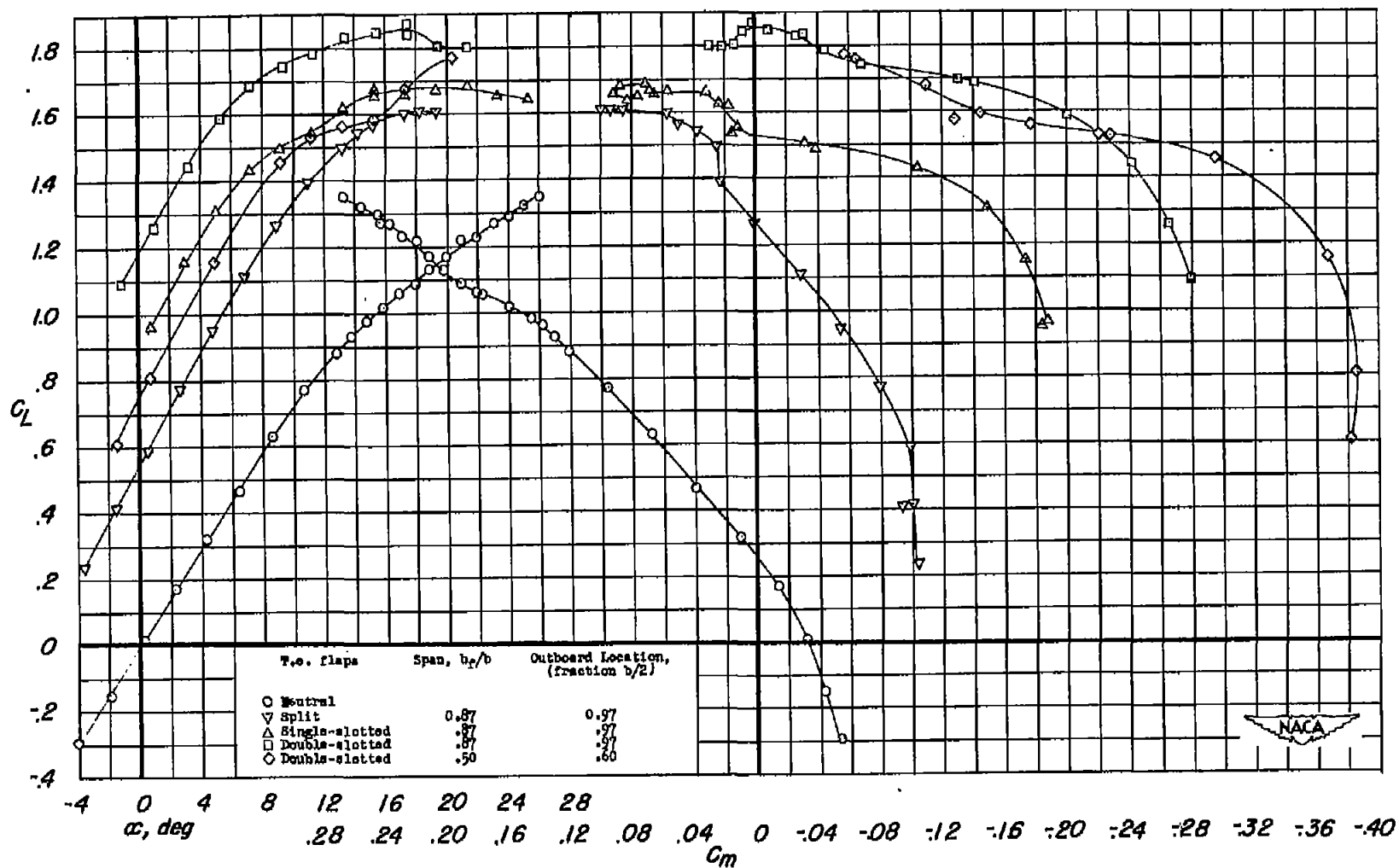
(a) C_L plotted against α and C_m .

Figure 20.- Aerodynamic characteristic of wing in combination with $0.75\frac{b}{2}$ extensible nose flaps and several trailing-edge flaps.



(b) C_L plotted against C_D .

Figure 20.- Concluded.



(a) C_L plotted against α and C_m .

Figure 21.- Aerodynamic characteristics of wing-fuselage combination with $0.41\frac{b}{2}$ nose flaps extended and various types of trailing-edge flaps. Inboard ends of trailing-edge flaps located at $0.10\frac{b}{2}$.

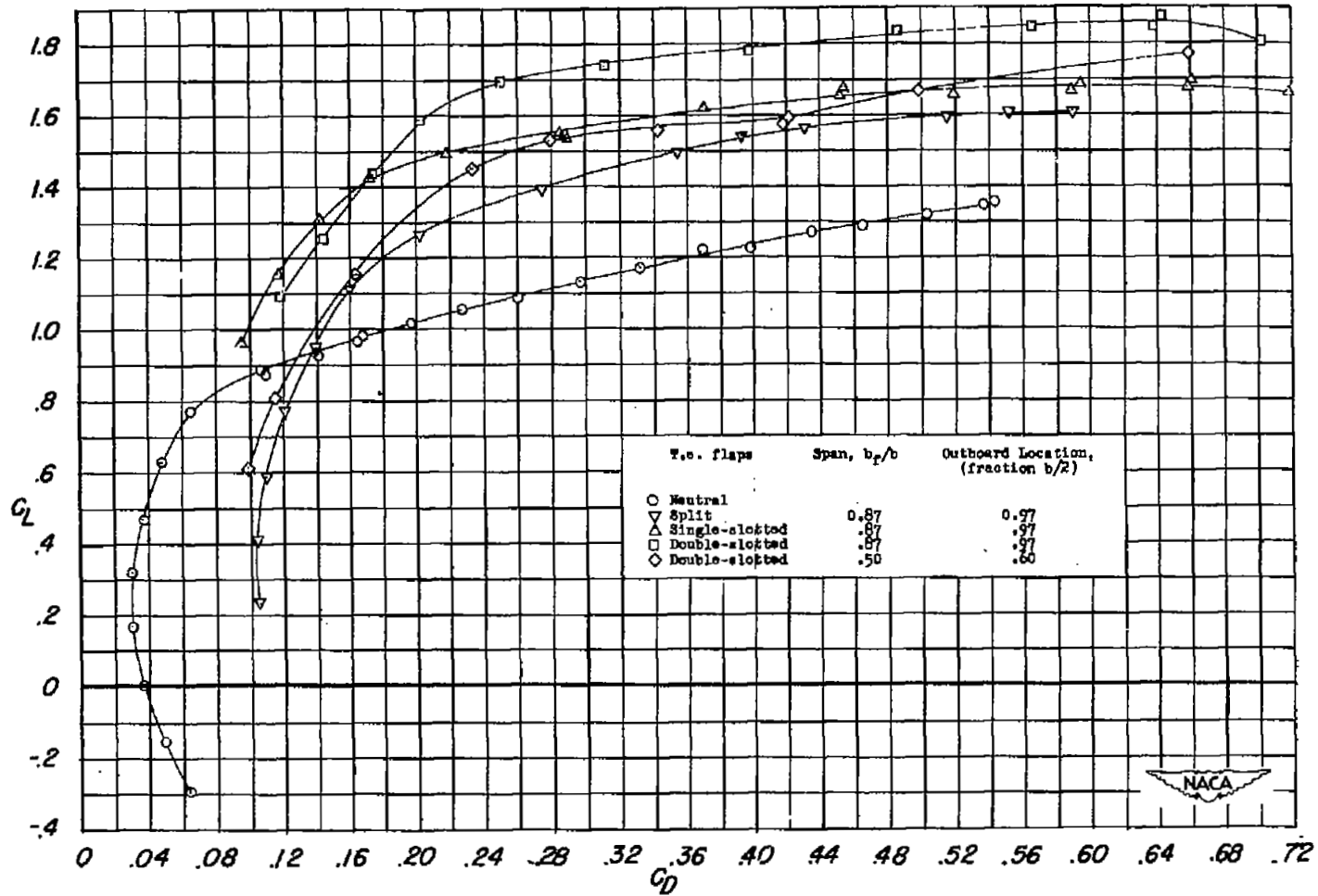
(b) C_L plotted against C_D .

Figure 21.- Concluded.

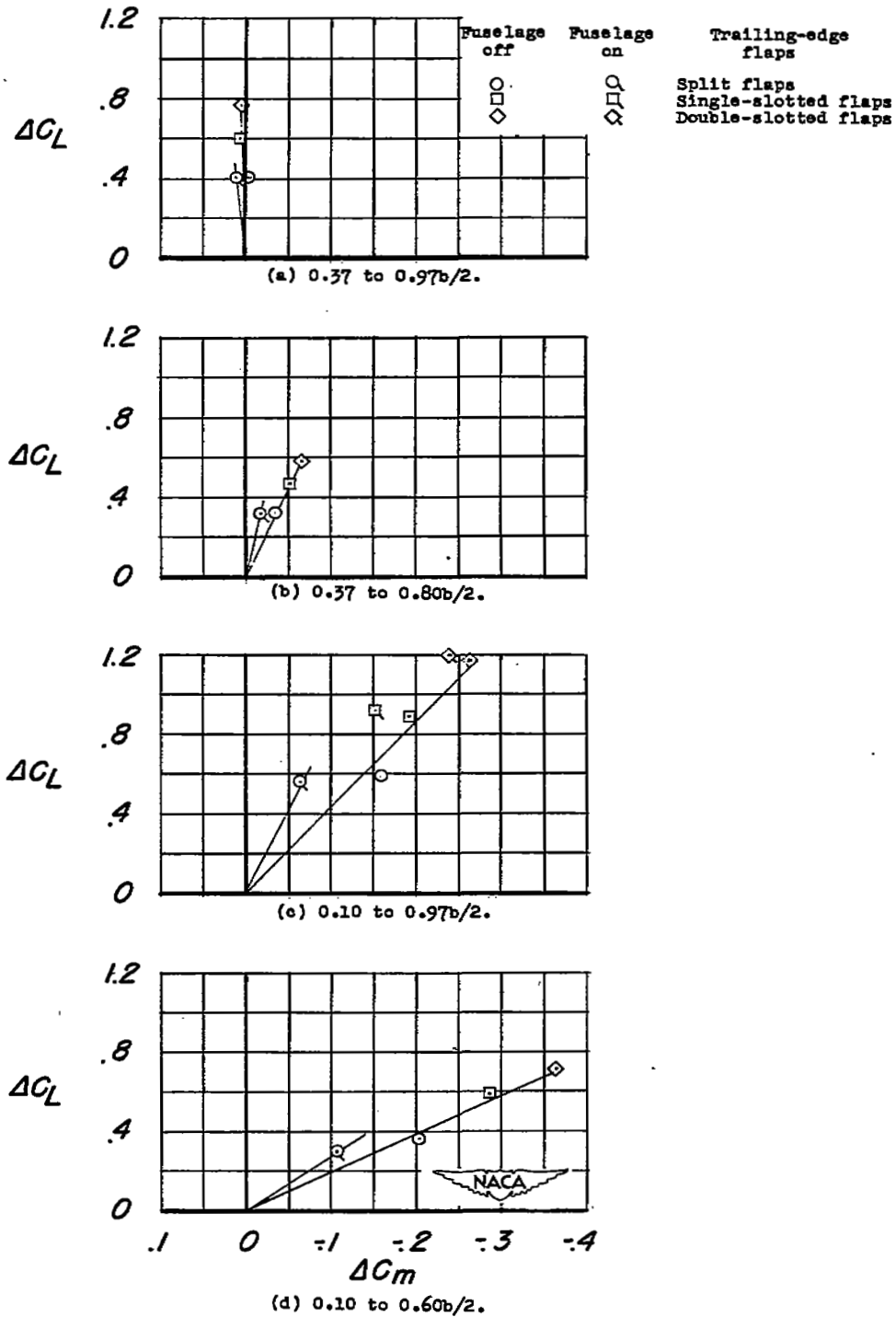


Figure 22.- Effects of span and spanwise locations of trailing-edge flaps and fuselage on pitching-moment increments due to flap deflection. $\alpha = -0.7^\circ$.

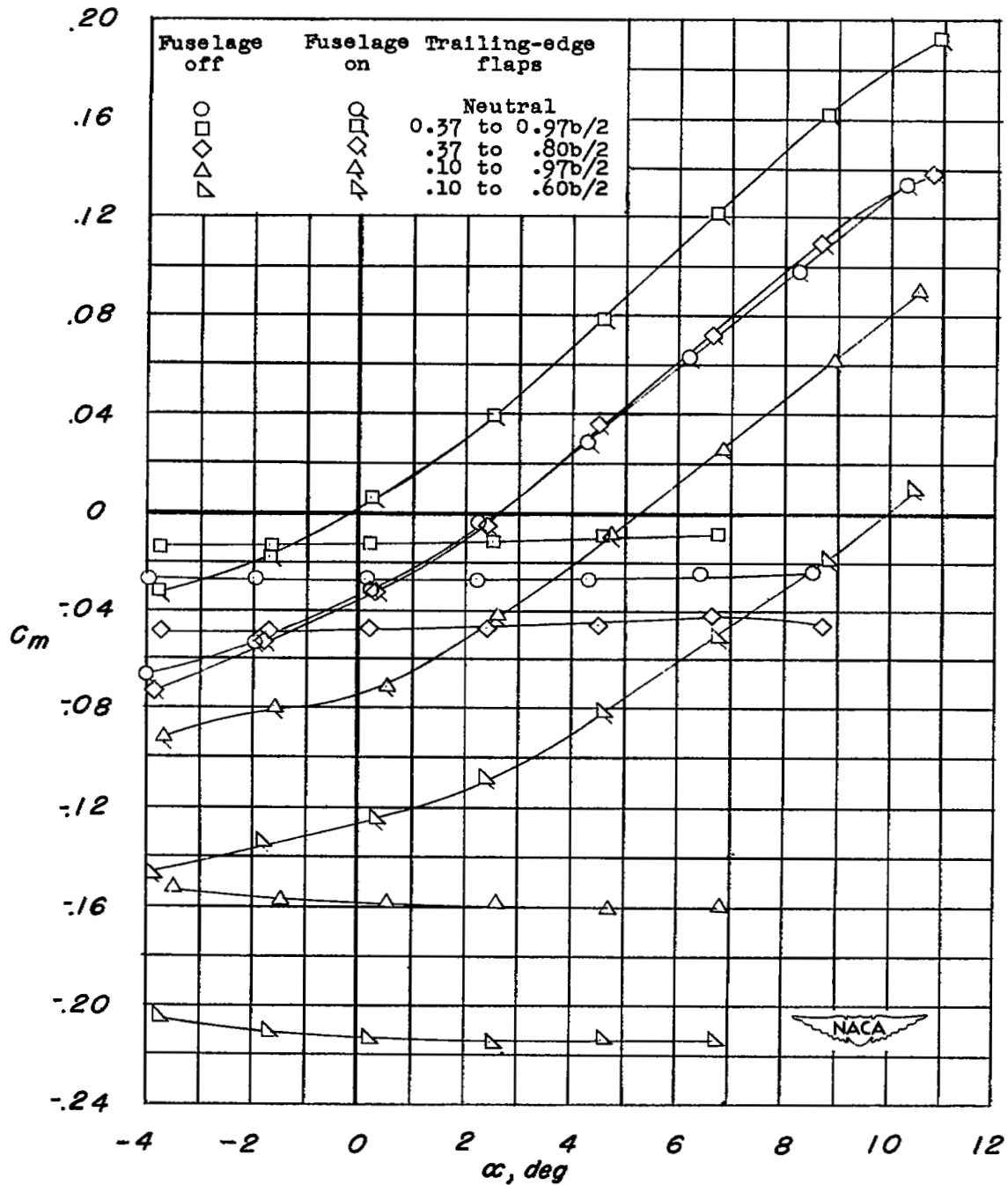
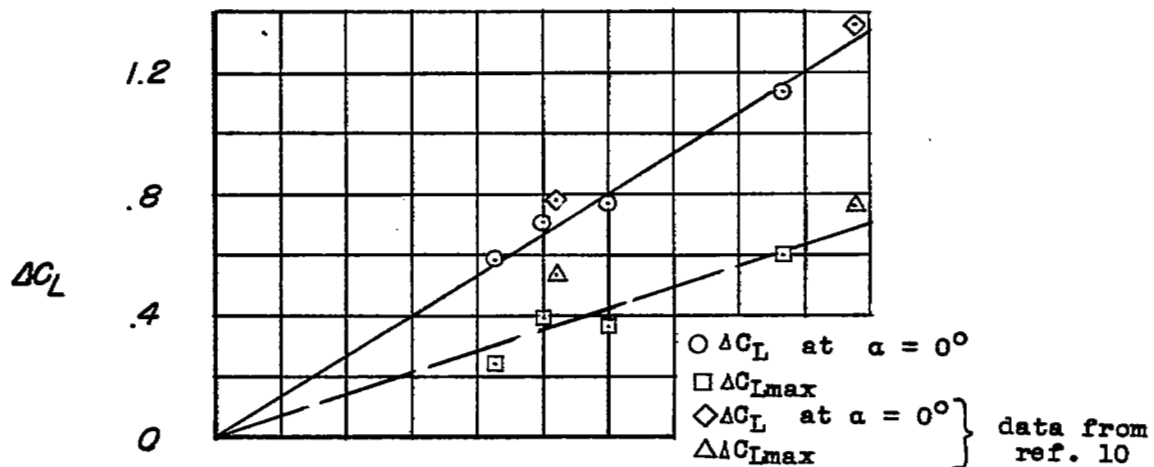
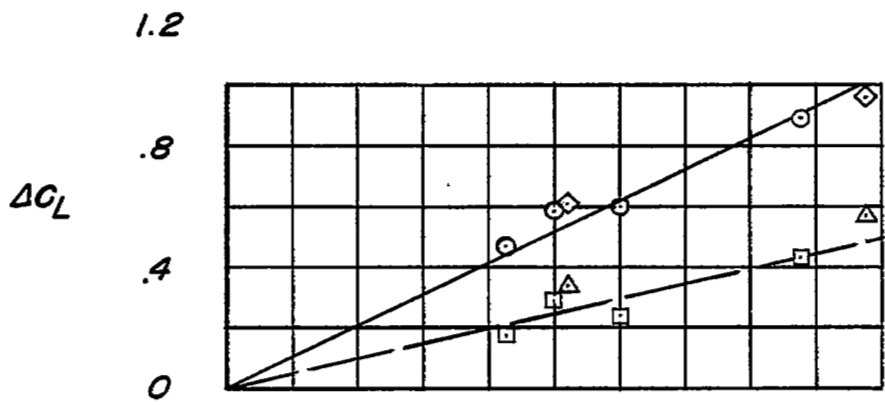


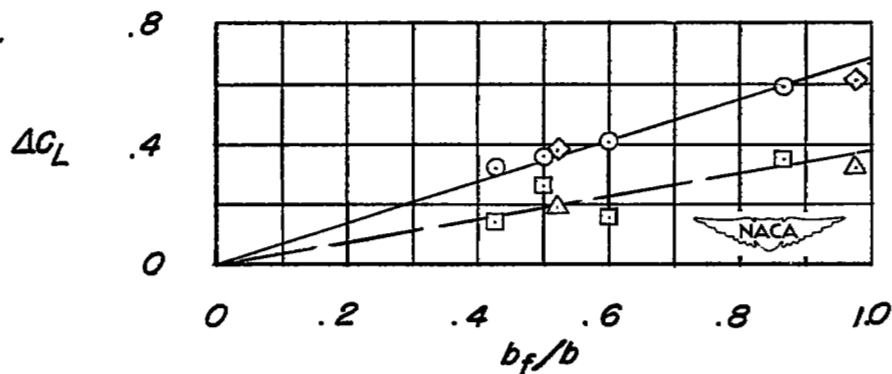
Figure 23.- Pitching-moment variation with angle of attack, fuselage on and off for various spans of split flaps. $0.41\frac{b}{2}$ nose flaps deflected with fuselage on. Center of gravity at 29.7 percent M.A.C.



(a) Double-slotted flaps.



(b) Single-slotted flaps.



(c) Split flaps.

Figure 24.- Summary of lift increments obtained with various types and spans of trailing-edge flaps.

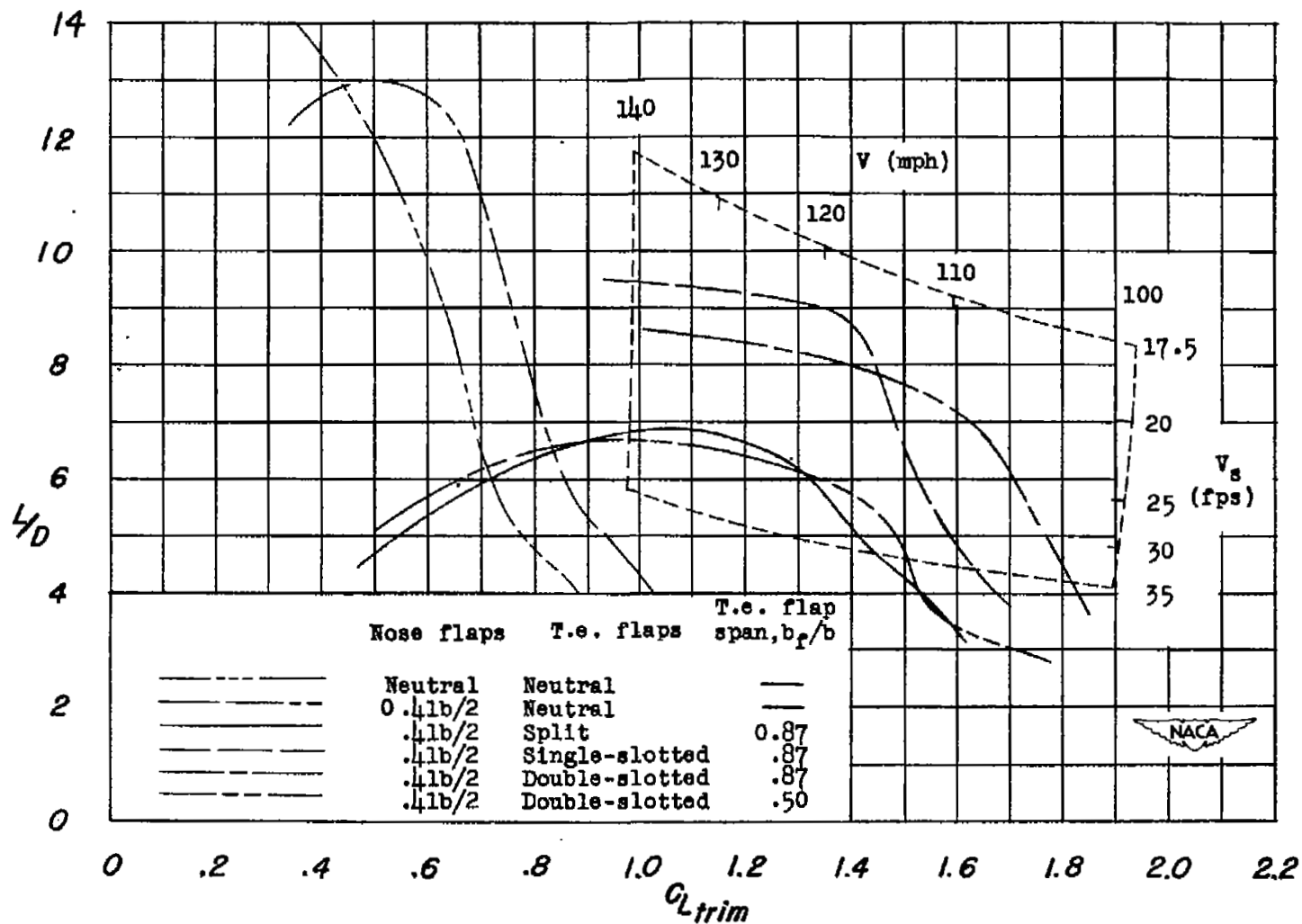


Figure 25.- Lift-drag ratios for wing and fuselage with several flap configurations. Glide and sinking-speed envelope for standard sea-level conditions and a wing loading of 50 pounds per square foot. Assumed tail length = 3.90 M.A.C.

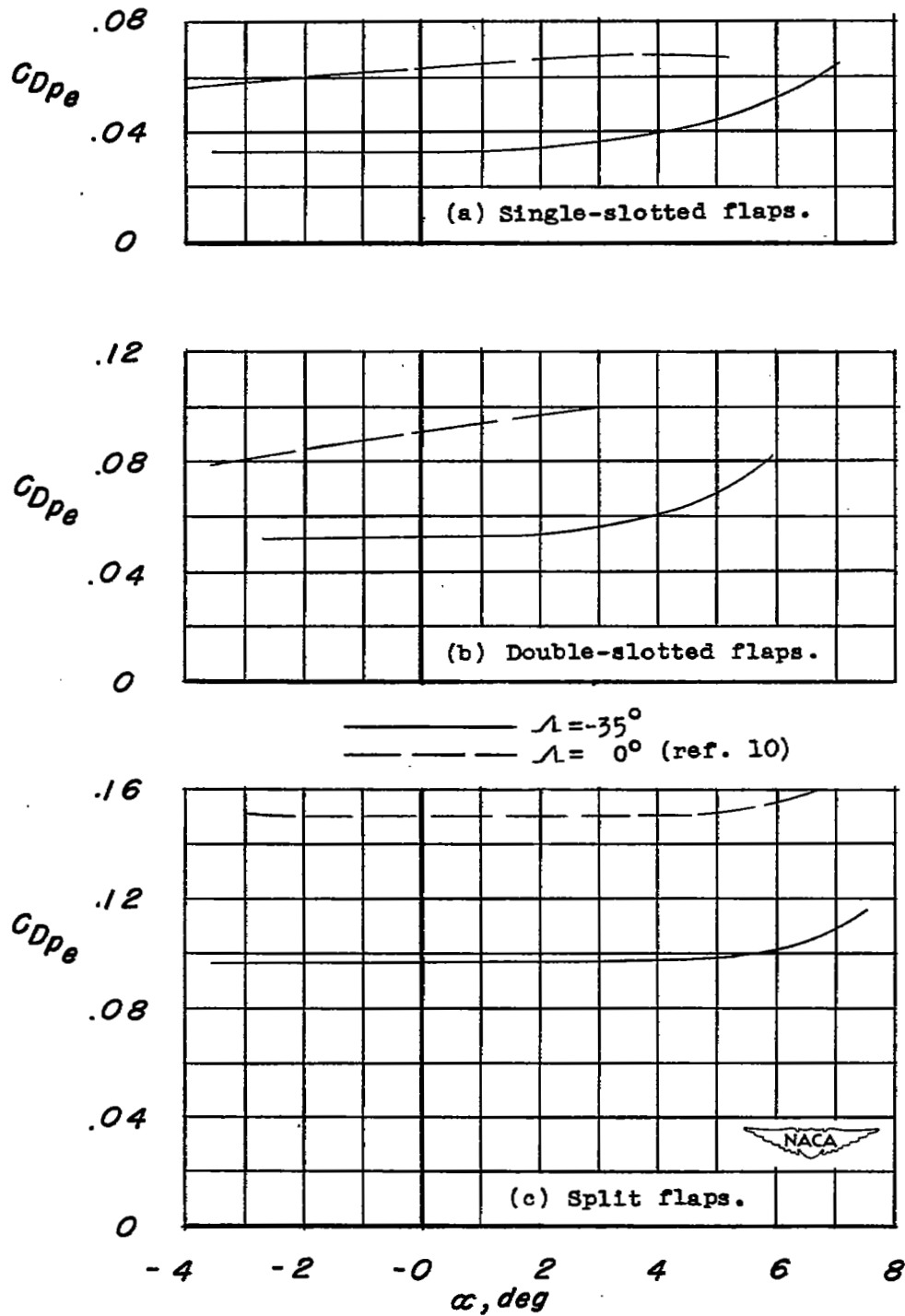
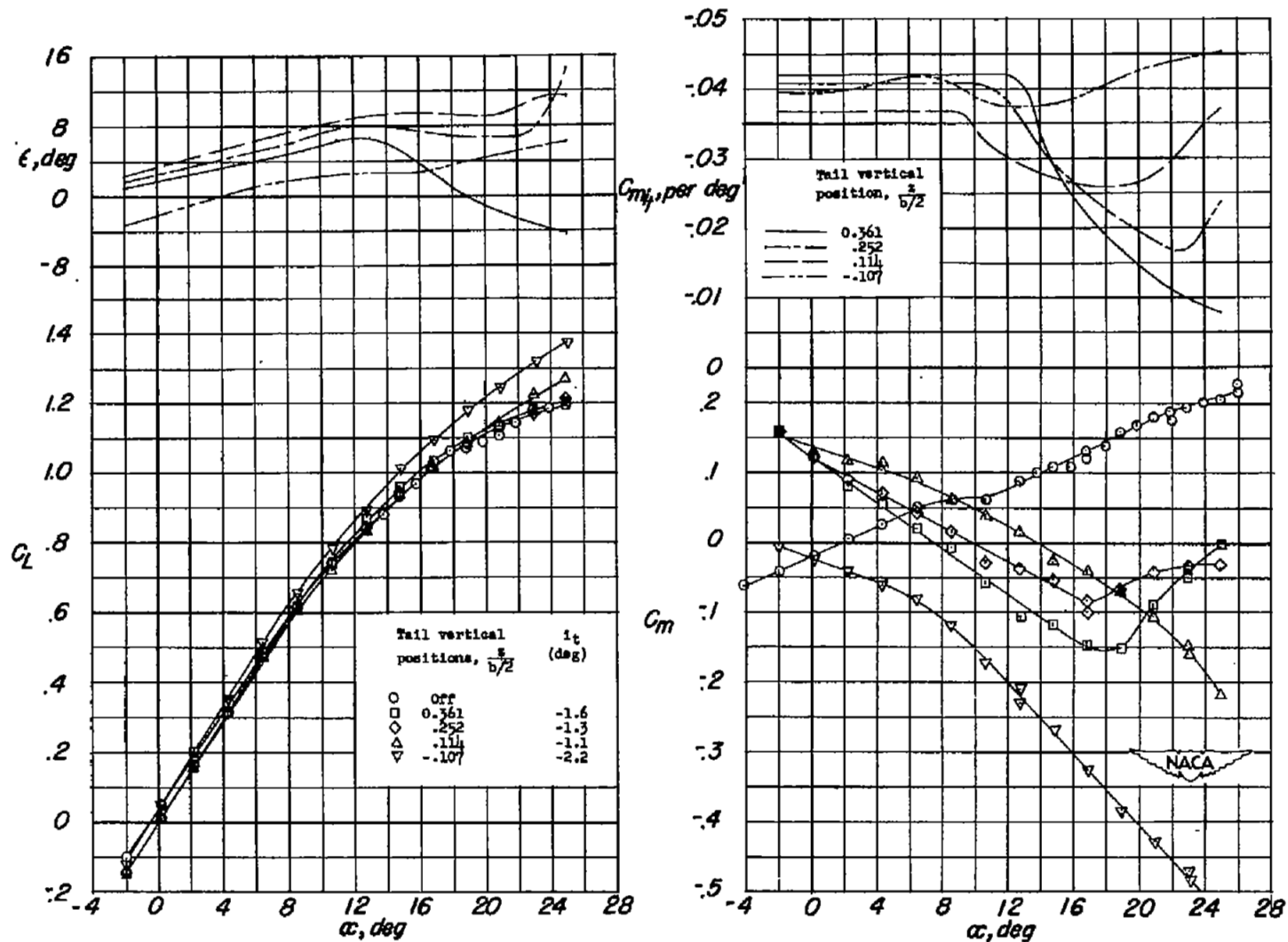
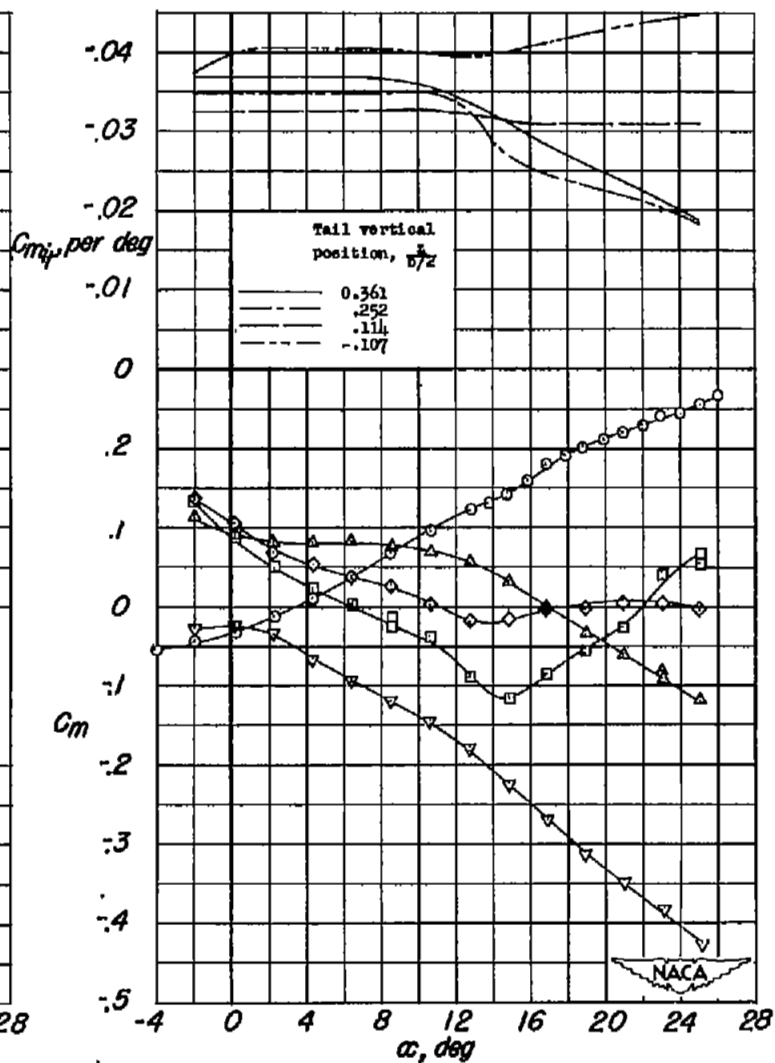
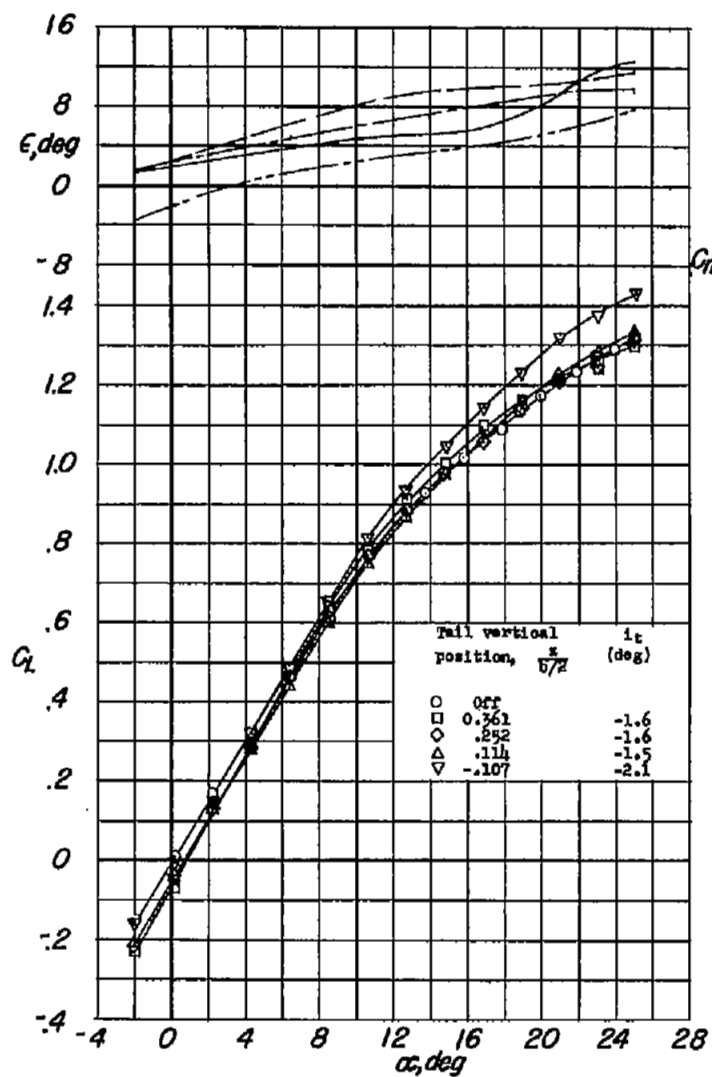


Figure 26.- Effects of sweepforward on effective profile drag coefficient for several full-span trailing-edge flaps.



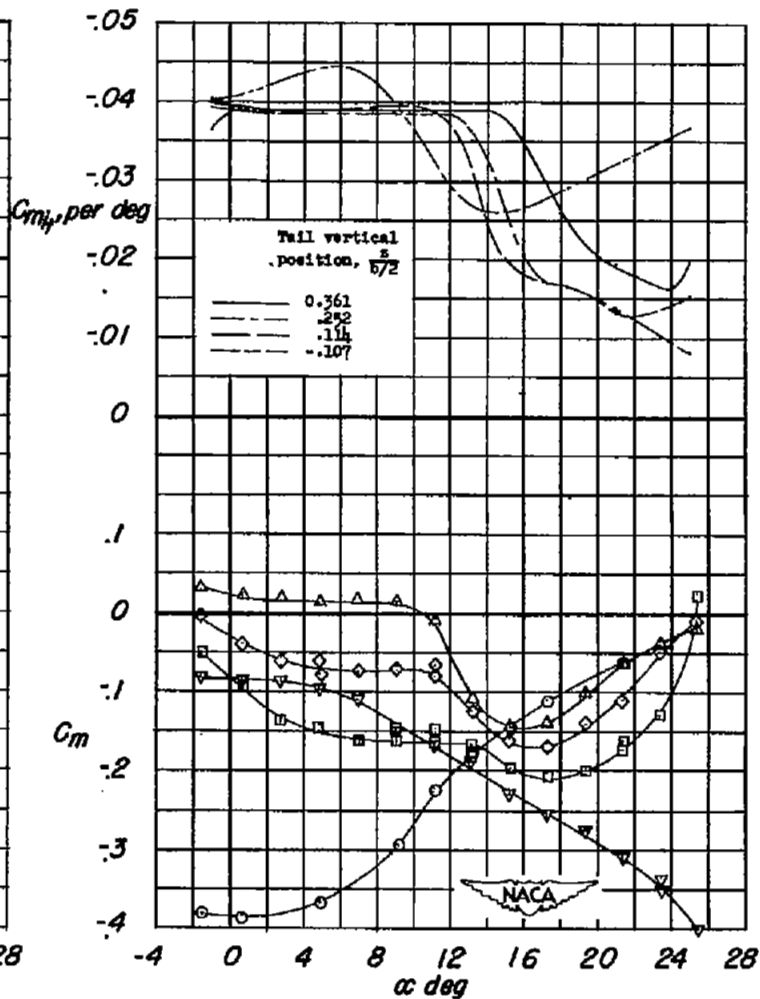
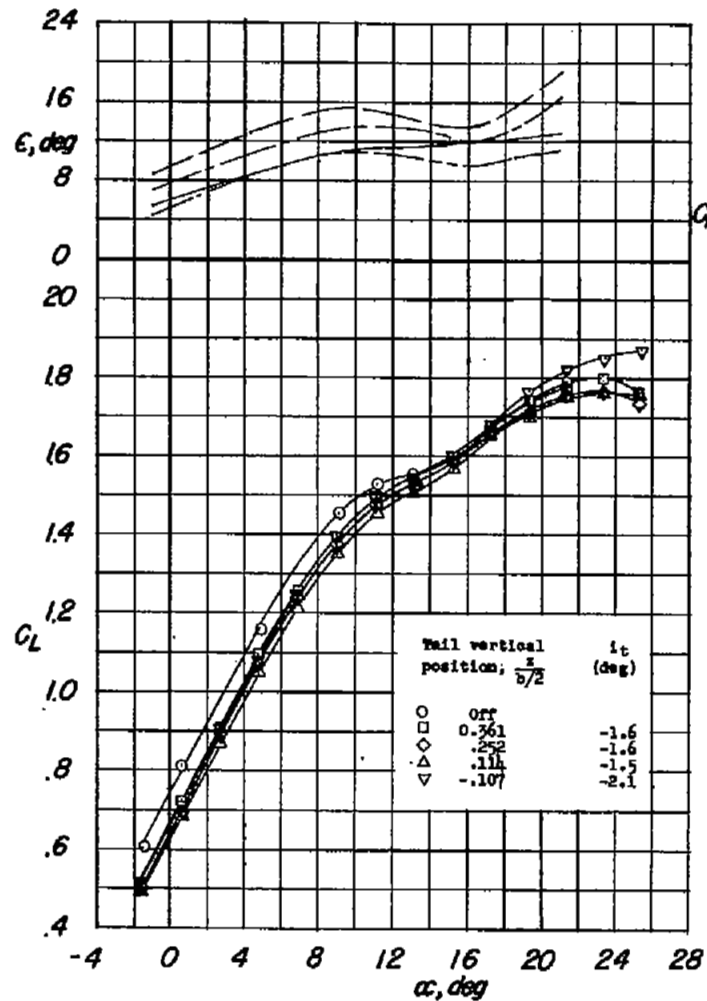
(a) Flaps neutral.

Figure 27.— Effects of a horizontal tail at several vertical positions on the aerodynamic characteristics of the wing-fuselage combination. $R = 5.0 \times 10^6$; $M \approx 0.15$.



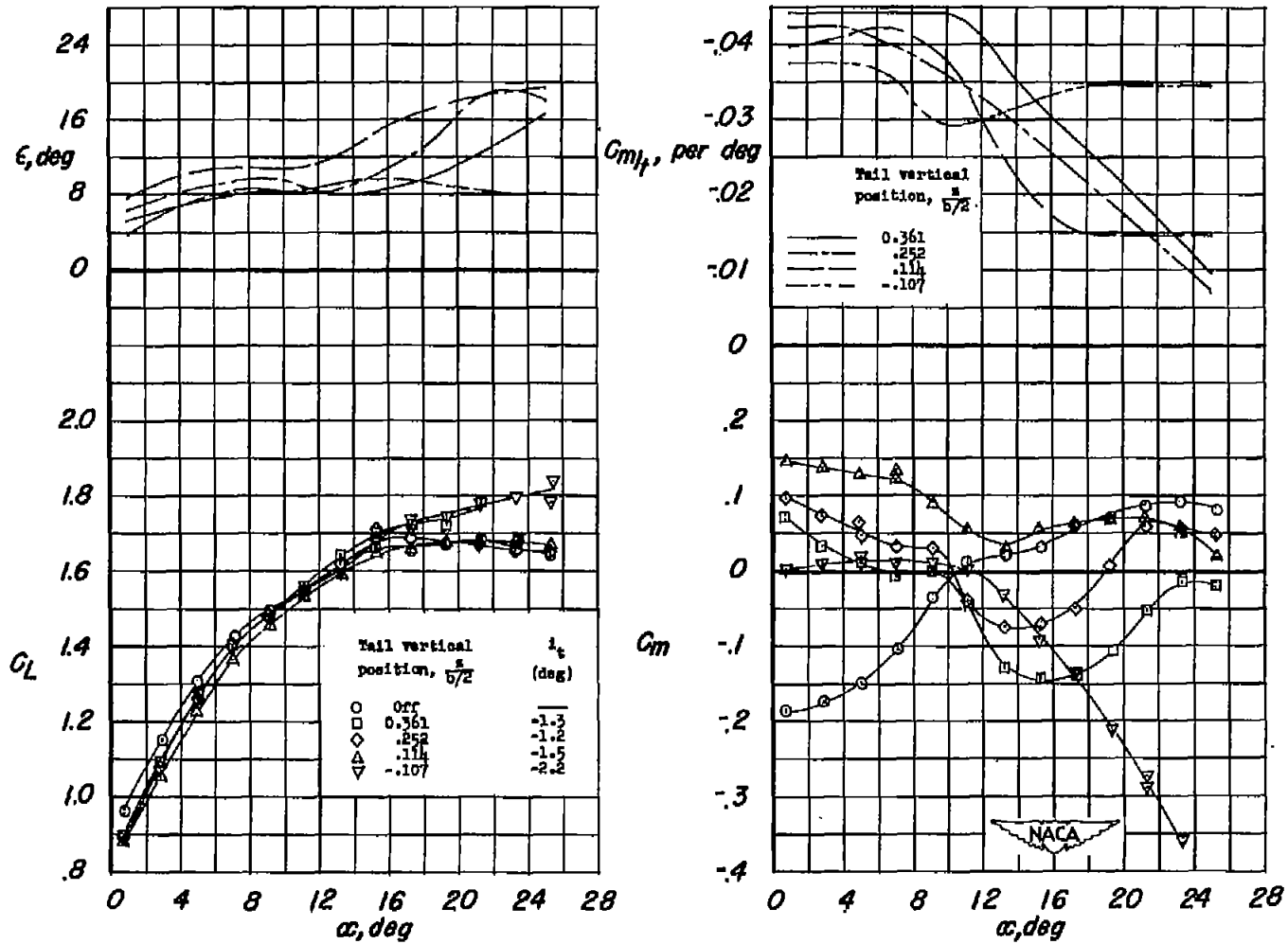
(b) $0.41\frac{b}{2}$ nose flaps.

Figure 27.- Continued.



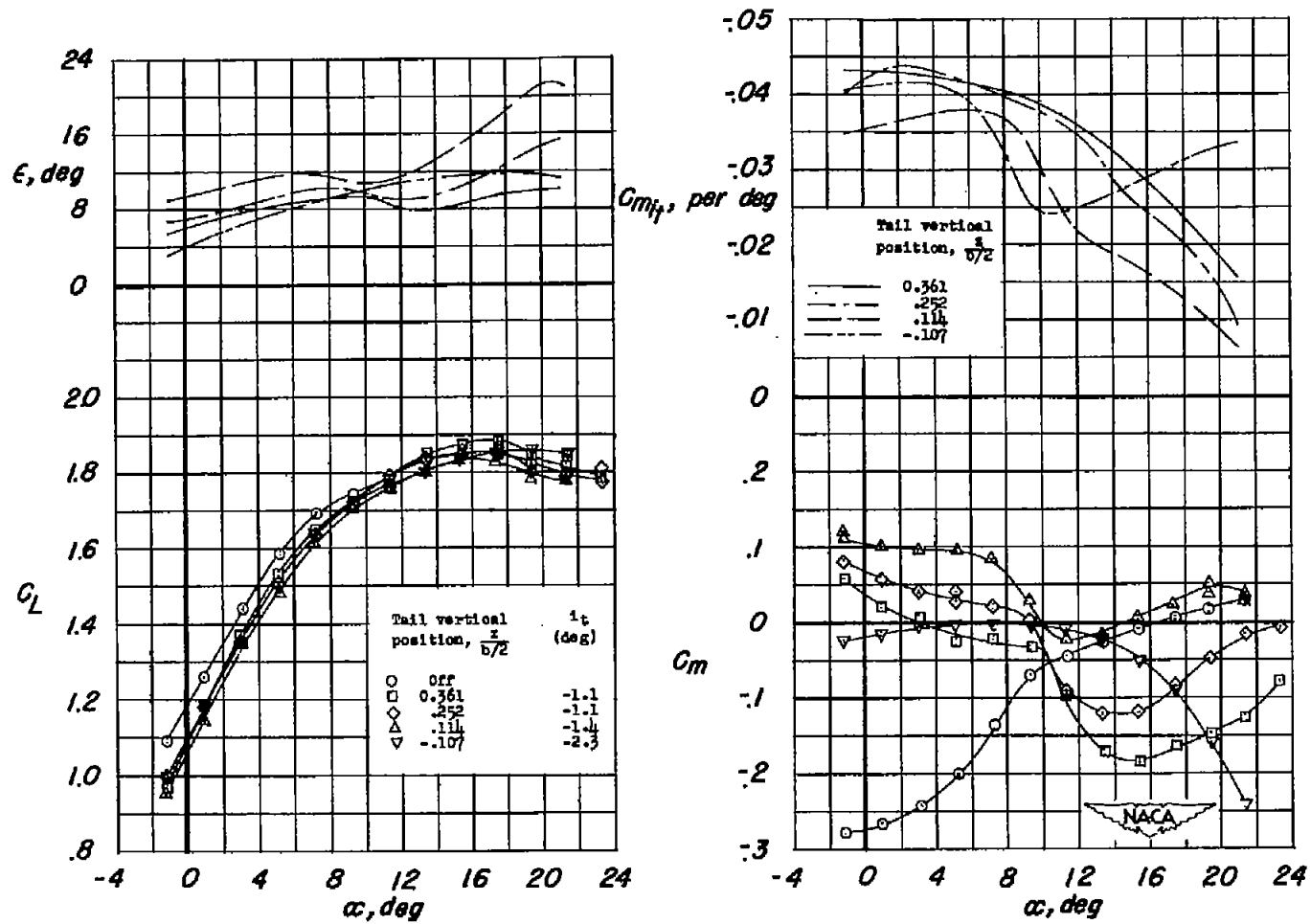
(c) $0.41\frac{b}{2}$ nose flaps and $0.50\frac{b}{2}$ double slotted flaps extending from $0.10\frac{b}{2}$ to $0.60\frac{b}{2}$.

Figure 27.- Continued.



(d) $0.41\frac{b}{2}$ nose flaps and $0.87\frac{b}{2}$ single slotted flaps deflected.

Figure 27.- Continued.



(e) $0.41\frac{b}{2}$ nose flaps and $0.87\frac{b}{2}$ double slotted flaps deflected.

Figure 27.- Concluded.

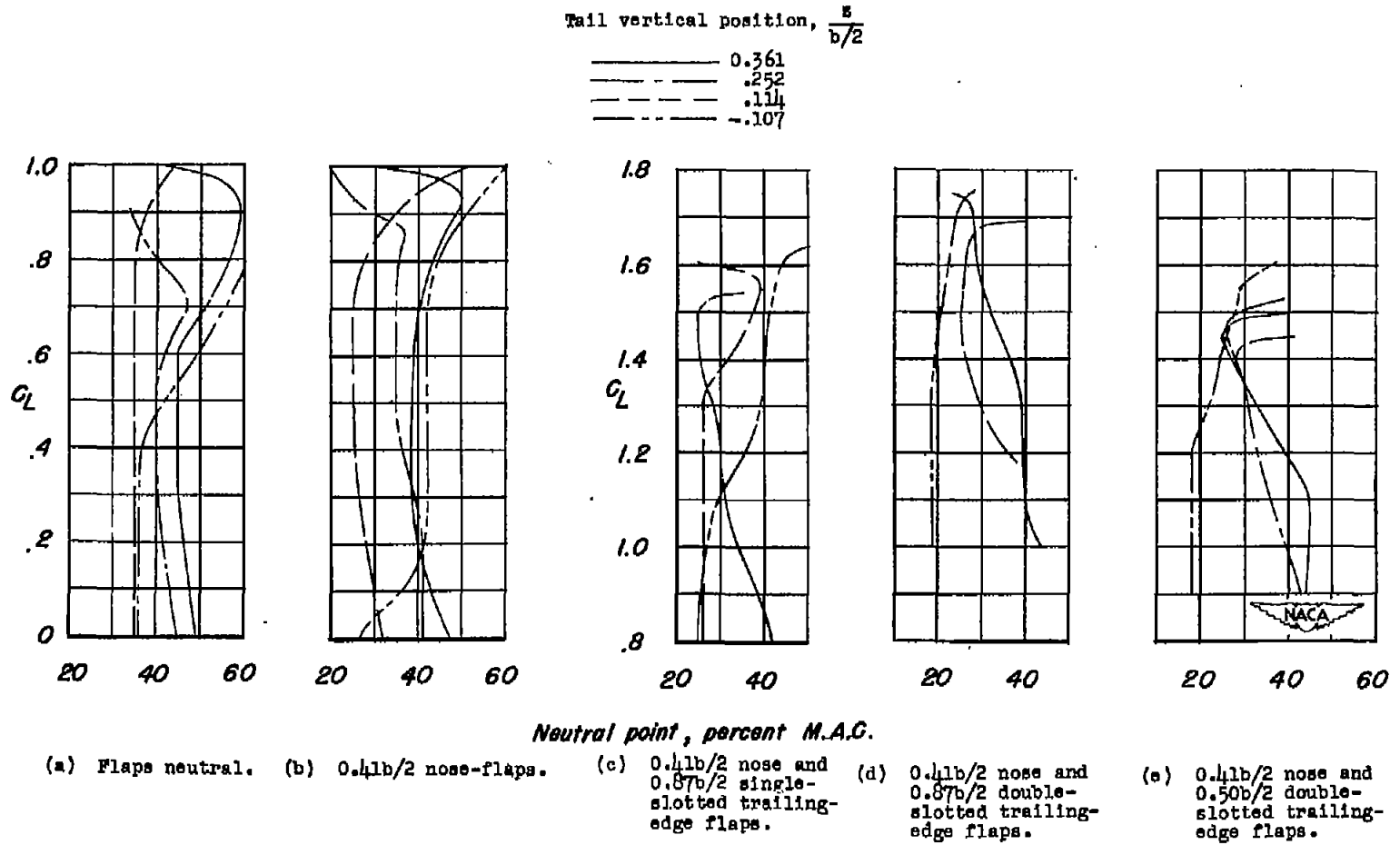


Figure 28.- Neutral point variation at several vertical locations of a horizontal tail.

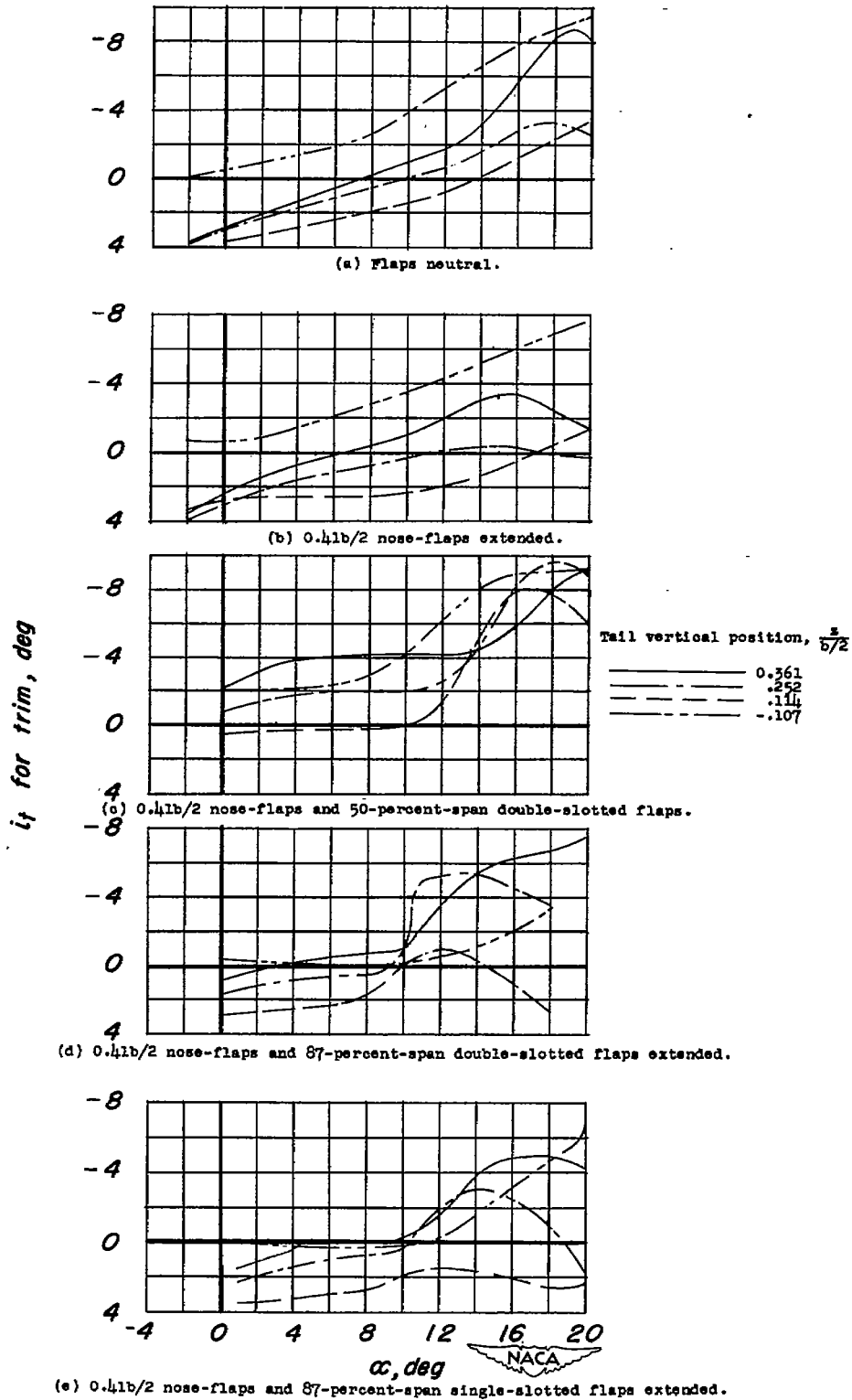


Figure 29.- Variation with angle of attack of the horizontal tail incidence required for trim as calculated by using the tail-effectiveness values of figure 27.